A COMPARISON OF FLUX-SPLITTING ALGORITHMS FOR THE EULER EQUATIONS WITH EQUILIBRIUM AIR CHEMISTRY

by

Joseph Lee Garrett

Thesis submitted to the Faculty of the

Virginia Polytechnic Institute and State University

in partial fulfillment of the requirements for the degree of

MASTER OF SCIENCE

in

Aerospace Engineering

APPROVED:

Bernard Grossman, Chairman

Joseph A. Schetz

Robert W. Walters

January 1989

Blacksburg, Virginia

A COMPARISON OF FLUX-SPLITTING ALGORITHMS FOR THE EULER EQUATIONS WITH EQUILIBRIUM AIR CHEMISTRY

by

Joseph Lee Garrett

Bernard Grossman, Chairman

Aerospace Engineering

(ABSTRACT)

The use of flux-splitting techniques on the Euler equations is considered for high Mach number, high temperature flows in which the fluid is assumed to be inviscid air in equilibrium. Three different versions of real gas extensions to the Steger-Warming and Van Leer flux-vector splitting, and four different versions of real gas extensions to the Roe flux-difference splitting, are compared with regard to general applicability and ease of implementation in existing perfect gas algorithms. Test computations are performed for the M = 5, high temperature flow over a 10-degree wedge and the M = 24.5 flow over a blunt body. Although there were minor differences between the computed results for the three types of flux-splitting algorithms considered, little variation is observed between different versions of the same algorithm.

Acknowledgements

The author wishes to express his sincere and deep appreciation to his advisor, Dr. Bernard Grossman, for the guidance, support, and encouragement that was given during the course of this study and to Dr. Robert Walters, for the support and insight that he also gave during this study.

The author would also like to thank Dr. Joseph Schetz for serving on his Advisory Committee.

Thanks and appreciation are also given to the author's friends for their support, suggestions, and help during this study.

Table of Contents

List of Illustrations

List of Symbols

A .....F-flux Jacobian matrix, $\frac{\partial F}{\partial Q}$

a .....speed of sound

B.....G-flux Jacobian matrix, $\frac{\partial G}{\partial Q}$

E.....total specific energy

e.....specific internal energy

$\vec{f}$ .....conservative flux vector

F, G .....components of flux vector in Cartesian coordinates

$\overline{F}, \overline{G}$ .....components of flux vector in curvilinear coordinates

H .....total specific enthalpy

$\hat{i}, \hat{j}, \hat{k}$.....Cartesian unit vectors

J .....Jacobian of a transformation matrix

M .....Mach number

$\hat{n}$ .....outward facing unit normal vector

p .....pressure at a point

Q .....vector of state variables

$\hat{Q}$ .....vector of conserved variables divided by the Jacobian

$<Q>$ .....vector of area-averaged state variables

q .....scalar velocity

S.....eigenvector matrix for Euler equations

s.....parameter produced by Van Albeda's limiter

T.....temperature

t.....time variable

Δt .....time step

$\vec{U}$ .....velocity vector in Cartesian coordiantes

u, v.....velocity component in Cartesian coordinates

$\bar{u}, \bar{v}$ .....velocity component in curvilinear coordinates

x, y .....Cartesian coodinate system

$x_\xi, x_\eta, y_\xi, y_\eta$....mapping metrics

$\Delta x, \Delta y$.....spatial step in Cartesian coodinate system

$\vec{\nabla}$.....gradient operator

$< >$ .....arithmetic mean, area average

Greek symbols

γ, Γ .....ratio of specific heats

Δ.....central difference operator in Cartesian coordinates

$\Delta(\bullet)$ .....$(\bullet)_R - (\bullet)_L$, difference between right and left states

$\Delta\xi, \Delta\eta$.....spatial step in curvilinear coodinate system

δ_ξ, δ_η.....central difference operator in curvilinear coordinates

ε.....small parameter

ϵ.....internal energy per unit volume

ξ, η .....curvilinear coordinates

$\xi_x, \xi_y, \eta_x, \eta_y$ ...mapping metrics

$\overline{\xi}, \overline{\eta}$ .....curvilinear direction cosines

κ.....partial derivative of p with respect to ϵ , ρ held constant

χ .....partial derivative of p with respect to ρ , ϵ held constant

Λ .....diagonal matrix of wave speeds

λ .....wave speed or eigenvalue of flux Jacobian matrix

ρ .....mass density at a point

σ .....parameter controlling accuracy of MUSCL-differencing

$d\tau$.....integration variable for volume

Subscripts

ij.....spatial indices

L.....left state

R.....right state

∞ .....freestream conditions

Superscripts

$(+)$.....non-negative value

$(-)$.....non-positive value

n.....time step level

$*$.....locally Cartesian

$\wedge$.....variable evaluated at a Roe-averaged state

$-$.....variable in generalized coordinates, dimensional quantity, arithmetic mean

$\sim$.....equivalent variable

I. INTRODUCTION

Computational fluid dynamics (CFD), which has been evolving for the past 25 years, has reached a point in maturity where it plays a significant role in the aerodynamic design process [1]. In particular, for hypersonic flows, a renewed interest in such high speed vehicles as the National Aerospace Plane, NASP, and the Aeroassisted Orbital Transfer Vehicle, AOTV, requires the use of CFD since experimental facilities presently available are unable to generate the high Mach number, temperature, and Reynolds number conditions necessary to accurately model the flow field around such craft. In general, such flows will require the solution of the Navier-Stokes equations with the inclusion of non-equilibrium chemistry to accurately predict the effects of dissociation and ionization produced by very strong shock-induced heating. However, over a large portion of the flight regime, inviscid flow in chemical equilibrium is a reasonable assumption since the shock and boundary layers will be confined to a small region close to the vehicle [2]. As a result, the Euler equations, with an equilibrium chemistry model for the

equation of state, will provide a reasonable first approximation for hypersonic flows. The success of CFD in simulating such high Mach number flows will largely depend on how well algorithms handle the generation and propagation of very strong shock waves.

In the 1960's and early 1970's, two approaches to numerical shock modeling were developed, shock fitting and shock capturing. Shock fitting procedures, normally applied to the non-conservative form of the Euler equations, specifically allow for discontinuties by tracking them and solving the appropriate jump relationships within their vicinity rather than solving the differential equations. Shock capturing methods, on the other hand, produce the correct weak solution of the governing differential equations as a natural consequence of solving them in conservation-law form, as proved by Lax [3] in 1954. Initially, shock capturing schemes had some practical success, but in regions where discontinuities should have been observed, the numerical solution would display a transition region of either a shallow slope or a steep slope with spurious oscillations [4]. These results are directly attributable to the fact that most early Euler solvers used central space derivatives, such as the MacCormack algorithm [5], which was considered to be the "workhorse" of the CFD aerodynamic community in the 1970's due to its ability to predict compressible, supersonic inviscid flowfields. These early algorithms were directly modified to account for real gas effects by the addition of a chemistry subroutine, which determined the pressure as a function of state at each mesh point [6]. The details of these modifications are discussed by Moretti

et al. [7] for shock-fitting procedures, and by Kutler et al. [8] for shock-capturing methods.

In the last decade, shock capturing methods attained mathematical respectability, due partly to the reinterpretation of the numerical equations as integral rather than differential laws, leading to what are referred to as finite-volume schemes, and partly to the incorporation of ideas drawn from the theory of characteristics, which form the foundation for upwind schemes. Upwind methods attempt to recognize the direction of information propagation in accordance with characteristic theory, and then form spatial derivatives biased in the signal direction. An advantage of one-sided spatial difference operators, as discussed by Beam and Warming [9], is that they are often desirable both along fixed external boundaries, and along moving internal boundaries (such as shocks), where a spatially centered scheme would require one or more points inside or across the boundary. The disadvantage of an upwind scheme is that it is more economical computationally to implement in non-conservative form, which requires the use of a shock-fitting algorithm. However, no sufficiently general shock-fitting approach able to efficiently handle complex shock wave interactions has been developed at present. A general discussion of recent work on shock fitting methods appears in Moretti [10]. In conservation form, upwind approaches generally require two to three times more arithmetic operations than central-difference methods. However, the increase in computational time per iteration can be offset by an improved steady state convergence rate as well as greater applicability to more

general problems without resorting to the use of adjustable parameters [11], such as artificial viscosity.

Lax [12] proposed a generic form for a finite difference approximation to the conservation law

$$U_t + F(U)_x = 0 \tag{1.1}$$

as

$$U_j^{n+1} = U_j^n - \frac{\Delta t}{\Delta x}[F_{j+1/2} - F_{j-1/2}] \tag{1.2}$$

where F can be evaluated with any number of differencing formulas utilizing points (..., j-1, j, j+1, ...) . Lax indicated that this form of the difference equation inherently satisfies certain physical properties. First, conservation is enforced since eq. (1.2) states that the amount of U in the jth cell at time n+1 is equal to the amount of U in the jth cell at time n plus the net change in U during the time period t due to the flux of U through the cell boundaries. Second, by evaluating the flux at j+1/2, eq. (1.2) guarantees that the flux out of cell j through the face at j+1/2 will exactly equal the flux into cell j+1 through the same face. Equation (1.2) is also the formulation for finite volume methods and may even be considered representative of upwind schemes, provided the fluxes at j+1/2 and j-1/2 are evaluated accordingly.

Upwind schemes were initially devised for explicit algorithms, a history of which is detailed by Steger and Warming [13]. Initially, only explicit schemes could be used because of hardware constraints on computer memory and speed. With the increased efficiency of hardware, implicit methods became more attractive since they are not constrained by the time restraint of explicit methods, and thus are able to achieve steady-state solutions more economically.

It is a well known fact that the characteristic wave speeds for the 1-D Euler equations are given by u, u + a, and u-a, where u is the local velocity and a is the local speed of sound. Thus, in subsonic flow, i.e. $u < a$, there will exist both left and right running characteristics associated with waves propagating with positive and negative speeds. In order to apply upwind methods to flows which contain subsonic regions, the flux terms (and their Jacobians for implicit time discretization) must be differentiated accordingly. The desire for more robust algorithms that incorporate the principles of characteristic theory led to the formation of flux-vector splitting and flux-difference splitting. The common goal of all flux splitting algorithms is to combine the two distinct sets of state quantities on either side of a cell interface into one set of normal fluxes through the interface [14].

Flux difference splitting constructs the cell interface fluxes by solving the associated Riemann problem, i.e. solving eq. (1.1) with piecewise uniform initial states on either side of the cell interface [11]. This approach was originally proposed by Godunov and was advanced by Roe, Van Leer, Harten, Osher, Chakavarthy,

Woodward and Collela, and others [15-22]. In each of these approaches, either an exact or an approximate solution to the Riemann problem at each cell is constructed. A physically correct value for the flux vector is found by solving the Riemann problem [14]. However, the exact solution of the Riemann problem is wasteful in two respects. First, it requires an iterative procedure. Second, it provides more accuracy than is needed to form the fluxes at cell interfaces. In practice, an approximation to the Riemann problem is sufficient. For the Euler equations, the solution to the Riemann problem consists of three waves centered at the cell interface, as shown in figure 1. The outer waves are either shock waves or rarefaction fans while the inner wave is a contact discontinuity [11]. The flux-difference splitting method of Roe [21] uses an approximation to the Riemann problem, the details of which are given in chapter 3.

The basic idea behind flux-vector splitting is to construct a stable upwind difference scheme for a set of hyperbolic conservation laws containing both positive and negative eigenvalues [11]. This is done by splitting the flux vector into two parts

$$F = F^+ + F^- \tag{1.3}$$

such that all the eigenvalues of $\partial F^+/\partial Q$ are non-negative and all the eigenvalues of $\partial F^-/\partial Q$ are non-positive. The most popular of these schemes are those of Steger and Warming [13] and Van Leer [23].

Initially, all flux splitting algorithms were formulated using the assumption of an ideal equation of state. Several comparisons of these formulations have been made, including those by Anderson et al. [24] and Van Leer et al. [14]. Anderson's results showed that, when applied to the Euler equations, the splittings of Van Leer and Steger-Warming generate essentially the same results, except for the appearance of a glitch in the Steger-Warming algorithm at sonic points. This is caused by the fact that the forward and backward fluxes are not differentiable when an eigenvalue changes sign. Also, the Van Leer splitting forms a shock structure over fewer interior points than the Steger-Warming splitting. The comparisons by Van Leer et al. show that Roe's method more accurately represents the shock and boundary layers formed by a Navier-Stokes flow than does Van Leer's flux-vector splitting.

In extending these methods towards the goal of accurate hypersonic predictions, several authors [6, 25-28] have derived real gas versions of the Steger-Warming and Van Leer flux-vector splittings and the Roe flux-difference splitting. As noted by Montagne [29], the absence of an analytical equation of state makes the use of upwind techniques more appealing since they require fewer thermodynamic computations than other methods.

The goal of this work is to compare these various formulations in conjunction with the two-dimensional Euler equations, with the intent of determing the general applicabilty as well as the programming effort required to implement these algorithms. Detailed analysis of the original perfect gas derivations and the real

gas formulations will be given in chapter 3. Comparisons of the real gas algorithms will be made using the test cases of a simple supersonic 10 degree inlet ramp and a hypersonic blunt body, with the equilibrium chemistry model provided by the curve-fits of Srinivasan, et al. [30]. A discussion of the solution algorithm is given in chapter 4 along with the computational results.

II. MATHEMATICAL FORMULATION

2.1 Euler Equations

The Euler equations are a coupled set of nonlinear equations which describe the motion of an unsteady, inviscid, adiabatic, compressible fluid flow. Physically, they represent the conservation of mass, momentum, and energy within the flow. Since they are derived for a continuum fluid, forms may be derived which are valid for both reacting and non-reacting flows. The differential vector form of the two dimensional Euler equations in a conservative, Cartesian reference frame is given as

$$\frac{\partial Q}{\partial t} + \frac{\partial F}{\partial x} + \frac{\partial G}{\partial y} = 0 \ , \tag{2.1a}$$

where Q is the vector of conserved variables

(2.1*b*)
$$Q = \begin{bmatrix} \rho \\ \rho u \\ \rho v \\ \rho E \end{bmatrix},$$

and F and G are the corresponding fluxes

(2.1*c*)
$$F = \begin{bmatrix} \rho u \\ \rho u^2 + p \\ \rho uv \\ u(\rho E + p) \end{bmatrix}, \qquad G = \begin{bmatrix} \rho v \\ \rho uv \\ \rho v^2 + p \\ v(\rho E + p) \end{bmatrix}.$$

The equations, presented in non-dimensional form, were done so by a reference length $\bar{L}$ and by freestream values of density $\bar{\rho}_\infty$ and velocity $\bar{u}_\infty$ such that

$$x = \frac{\bar{x}}{\bar{L}}\ ,\ y = \frac{\bar{y}}{\bar{L}}\ ,\ u = \frac{\bar{u}}{\bar{u}_\infty}\ ,\ v = \frac{\bar{v}}{\bar{u}_\infty}\ ,\ E = \frac{\bar{E}}{\bar{u}_\infty^2}\ ,\ \rho = \frac{\bar{\rho}}{\bar{\rho}_\infty}\ ,\ p = \frac{\bar{p}}{\bar{\rho}_\infty \bar{u}_\infty^2}\ ,$$

where the overbars represent dimensional quantities. Non-dimensionalization of the governing equations is important for various reasons. Non-dimensional variables will have roughly the same order of magnitude, thereby decreasing numerically induced round-off errors. In addition, non-dimensional variables eliminate the risk of using inconsistent units. The equations are presented in strong conservation law form (SCLF), rather than primitive variables, i.e. $[\rho, u, v, p]^T$, so that all flow discontinuities will evolve numerically as part of the solution process.

In order to close the system, an equation of state is defined as

$$p = p(\rho,e) \quad , \tag{2.2}$$

where the functional dependence of p can be determined from any real gas model such as an equilibrium air curve fit [30] or an equilibrium free-energy minimization [31].

2.2 Generalized Coordinates

Since eq. (2.1a) can only be used in conjunction with Cartesian grids, they are generally transformed from the physical (x,y) space to the curvilinear, computational (ξ, η) space by the mapping

$$\xi = \xi(x,y) \quad , \qquad \eta = \eta(x,y) \quad . \tag{2.3}$$

By applying the chain rule of differentiation, i.e.

$$\begin{aligned} \frac{\partial}{\partial x} &= \xi_x \frac{\partial}{\partial \xi} + \eta_x \frac{\partial}{\partial \eta} \quad , \\ \frac{\partial}{\partial y} &= \xi_y \frac{\partial}{\partial \xi} + \eta_y \frac{\partial}{\partial \eta} \quad , \end{aligned} \tag{2.4}$$

to eq. (2.1a), the governing equations in the (ξ, η) coordinate system become

$$\frac{\partial Q}{\partial t} + \xi_x \frac{\partial F}{\partial \xi} + \eta_x \frac{\partial F}{\partial \eta} + \xi_y \frac{\partial G}{\partial \xi} + \eta_y \frac{\partial G}{\partial \eta} = 0 \,, \tag{2.5a}$$

$$\begin{aligned} \xi_x &= \frac{\partial \xi}{\partial x} \,, \quad \xi_y = \frac{\partial \xi}{\partial y} \,, \\ \eta_x &= \frac{\partial \eta}{\partial x} \,, \quad \eta_y = \frac{\partial \eta}{\partial y} \,. \end{aligned} \tag{2.5b}$$

Equation (2.5a) can be simplified to yield:

$$\frac{\partial \overline{Q}}{\partial t} + \frac{\partial \overline{F}}{\partial \xi} + \frac{\partial \overline{G}}{\partial \eta} = 0 \,, \tag{2.6a}$$

where

$$\overline{Q} = \frac{1}{J} \begin{bmatrix} \rho \\ \rho u \\ \rho v \\ \rho E \end{bmatrix} , \tag{2.6b}$$

$$\overline{F} = \frac{\left|\vec{\nabla}\xi\right|}{J} \frac{\xi_x F + \xi_y G}{\left|\vec{\nabla}\xi\right|} = \frac{\left|\vec{\nabla}\xi\right|}{J} \begin{bmatrix} \rho \overline{u} \\ \rho u \overline{u} + \overline{\xi}_x p \\ \rho v \overline{u} + \overline{\xi}_y p \\ \overline{u}(\rho E + p) \end{bmatrix} , \tag{2.6c}$$

$$\overline{G} = \frac{\left|\vec{\nabla}\eta\right|}{J}\frac{\eta_x F + \eta_y G}{\left|\vec{\nabla}\eta\right|} = \frac{\left|\vec{\nabla}\eta\right|}{J}\begin{bmatrix} \rho\bar{v} \\ \rho u\bar{v} + \bar{\eta}_x p \\ \rho v\bar{v} + \bar{\eta}_y p \\ \bar{v}(\rho E + p) \end{bmatrix}, \tag{2.6d}$$

with the contravariant velocity components, $\bar{u}$ and $\bar{v}$, defined by

$$\bar{u} = \bar{\xi}_x u + \bar{\xi}_y v , \tag{2.7a}$$

$$\bar{v} = \bar{\eta}_x u + \bar{\eta}_y v , \tag{2.7b}$$

and the direction cosines defined by

$$\begin{aligned} \bar{\xi}_x &= \frac{\xi_x}{\left|\vec{\nabla}\xi\right|} , \quad \bar{\xi}_y = \frac{\xi_y}{\left|\vec{\nabla}\xi\right|} , \\ \bar{\eta}_x &= \frac{\eta_x}{\left|\vec{\nabla}\eta\right|} , \quad \bar{\eta}_y = \frac{\eta_y}{\left|\vec{\nabla}\eta\right|} . \end{aligned} \tag{2.7c}$$

This transformation, consistent with the work of Viviand [32], maintains the SCLF of the governing equation (2.1a). Note that in subsequent sections the overbars will refer to quantities in generalized coordinates, unless specifed otherwise.

2.3 Finite Volume Representation

In two-dimensional space, the integral conservation law can be written:

$$\frac{d}{dt}\iiint_R Q\,d\tau + \iint_S \vec{f}\cdot\hat{n}\,dS = 0 \tag{2.8a}$$

where Q is defined by eq. (2.1b), $\vec{f}$ is defined as:

$$\vec{f} = F\hat{i} + G\hat{j}\ , \tag{2.8b}$$

where F and G are given by eq. (2.1c), and $\hat{n}$ is defined as:

$$\hat{n} = n_x\hat{i} + n_y\hat{j}\ . \tag{2.8c}$$

Applying the integration in eq. (2.8a) to a quadrilateral mesh, the following discretization is obtained:

$$\frac{\partial}{\partial t}[<Q>\Delta V] + \sum_{\ell=1}^{4}[<Fn_x + Gn_y>\Delta S]_\ell = 0\ , \tag{2.9}$$
$$\ell = j \pm 1/2, k \pm 1/2\ ,$$

where

$<Q>$ represents the average Q in the cross-section (volume),

$<F, G>$ represent the average F, G on the cell edge (surface),

ΔV represents thecross-sectional area (volume) of the cell i, j,

ΔS represents the length (surface area) of edge ℓ, and

n_x, n_y represent the Cartesian components of outward facing surface normals.

This discretization corresponds to a cell-centered, finite volume formulation. The semi-discrete representation (2.9) may be rewritten in a form analogous to the differential form (2.6a) as:

$$\frac{\partial}{\partial t}(\overline{Q})_{jk} + \frac{(\overline{F}_{j+1/2} - \overline{F}_{j-1/2})}{\Delta\xi} + \frac{(\overline{G}_{k+1/2} - \overline{G}_{k-1/2})}{\Delta\eta} = 0 , \tag{2.10a}$$

where $\overline{F}$ and $\overline{G}$ are defined in a manner analogous to eqs. (2.6c) and (2.6d), respectively, and $\overline{Q}$ is defined as:

$$< \overline{Q} > = < Q > \frac{1}{\overline{J}} , \quad \text{with} \quad \frac{1}{\overline{J}} = \frac{\Delta V}{\Delta\xi\Delta\eta} . \tag{2.10b}$$

Eq. (2.10a) is equivalent to the expression:

$$\frac{\partial \overline{Q}_{jk}}{\partial t} + \frac{\delta_\xi \overline{F}_{jk}}{\Delta\xi} + \frac{\delta_\eta \overline{G}_{jk}}{\Delta\eta} = 0 , \tag{2.11}$$

which is similar to a finite difference formulation. Substituting eqs. (2.6c) and (2.6d) into (2.10a) results in an interpretation of the metric terms as the directed areas of the cell faces, i.e.

(2.12)

$$\left(\frac{|\vec{\nabla}\xi|}{J}\Delta\eta\right)_{j\pm1/2} = (\Delta S)_{j\pm1/2} = \left(x_\eta^2 + y_\eta^2\right)^{1/2}_{j\pm1/2}\Delta\eta = \left(\Delta x^2 + \Delta y^2\right)^{1/2}_{j\pm1/2}$$

$$\left(\frac{|\vec{\nabla}\eta|}{J}\Delta\xi\right)_{k\pm1/2} = (\Delta S)_{k\pm1/2} = \left(x_\xi^2 + y_\xi^2\right)^{1/2}_{k\pm1/2}\Delta\eta = \left(\Delta x^2 + \Delta y^2\right)^{1/2}_{k\pm1/2}$$

And the direction cosines of the $j \pm 1/2$ face normal to the ξ and η directions, as:

(2.13)

$$\left(\frac{\xi_x}{|\vec{\nabla}\xi|}\right)_{j\pm1/2} = (n_x)_{j\pm1/2} = \pm\frac{y_\eta\Delta\eta}{\left[x_\eta^2 + y_\eta^2\right]^{1/2}\Delta\eta} = \pm\frac{\Delta y}{\left[\Delta x^2 + \Delta y^2\right]^{1/2}}$$

$$\left(\frac{\xi_y}{|\vec{\nabla}\xi|}\right)_{j\pm1/2} = (n_y)_{j\pm1/2} = \mp\frac{x_\eta\Delta\eta}{\left[x_\eta^2 + y_\eta^2\right]^{1/2}}\Delta\eta = \mp\frac{\Delta x}{\left[\Delta x^2 + \Delta y^2\right]^{1/2}}$$

where the quantities above are evaluated at $j \pm 1/2$. The directon cosines of the $k \pm 1/2$ face normal to the ξ and η directions are, respectively:

(2.14)

$$\left(\frac{\eta_x}{|\vec{\nabla}\eta|}\right)_{k\pm1/2} = (n_x)_{k\pm1/2} = \pm\frac{y_\xi\Delta\xi}{\left[x_\xi^2 + y_\xi^2\right]^{1/2}\Delta\xi} = \pm\frac{\Delta y}{\left[\Delta x^2 + \Delta y^2\right]^{1/2}}$$

$$\left(\frac{\eta_y}{|\vec{\nabla}\eta|}\right)_{k\pm1/2} = (n_y)_{k\pm1/2} = \mp\frac{x_\xi\Delta\xi}{\left[x_\xi^2 + y_\xi^2\right]^{1/2}\Delta\xi} = \mp\frac{\Delta x}{\left[\Delta x^2 + \Delta y^2\right]^{1/2}} \quad ,$$

where the quantities above are evaluated at $k \pm 1/2$. The values of Δx and Δy in eqs. (2.12), (2.13) and (2.14) are obtained from the relations:

$$(\Delta x)_{j\pm1/2} = (x)_{j\pm1/2,\,k+1/2} - (x)_{j\pm1/2,\,k-1/2}$$
$$(\Delta y)_{j\pm1/2} = (y)_{j\pm1/2,\,k+1/2} - (y)_{j\pm1/2,\,k-1/2} \tag{2.15a}$$

and

$$(\Delta x)_{k\pm1/2} = (x)_{j\pm1/2,\,j+1/2} - (x)_{k\pm1/2,\,j-1/2}$$
$$(\Delta y)_{k\pm1/2} = (y)_{j\pm1/2,\,j+1/2} - (y)_{k\pm1/2,\,j-1/2} \cdot \tag{2.15b}$$

2.4 Flux-Splitting in Generalized Coordinates

Since flux splittings [13,21,23] are derived in a Cartesian reference frame, upwind schemes can only be applied to multidimensional curvilinear coordinates if the corresponding fluxes of eqs. (2.11c) and (2.11d) are transformed into a locally Cartesian coordinate system. Considering the ξ direction only, one must first find a rotation tensor T such that:

$$T\overline{F} \sim \begin{bmatrix} \rho\overline{u} \\ \rho\overline{u}^2 + p \\ \rho\overline{u}v^* \\ \overline{u}(\rho E + p) \end{bmatrix} . \tag{2.20}$$

Thus, it is necessary to transform from the ξ, η reference frame to a new frame ξ, η^*, defined as:

$$
\begin{aligned}
i^* &= \frac{\vec{\nabla}\xi}{\left|\vec{\nabla}\xi\right|} = \bar{\xi}_x\hat{i} + \bar{\xi}_y\hat{j} \ , \\
j^* &= \frac{\vec{\nabla}\eta^*}{\left|\vec{\nabla}\eta^*\right|} = \bar{\eta}_x^*\hat{i} + \bar{\eta}_y^*\hat{j} \ ,
\end{aligned}
\tag{2.21}
$$

By definition,

$$
\begin{aligned}
i^* \cdot j^* &= \bar{\xi}_x\bar{\eta}_x + \bar{\xi}_y\bar{\eta}_y = 0 \ , \\
i^* \times j^* &= (\bar{\xi}_x\bar{\eta}_y - \bar{\xi}_y\bar{\eta}_x)\hat{k} = \hat{k} \ ,
\end{aligned}
\tag{2.22a}
$$

which yield the system:

$$
\begin{bmatrix} \bar{\xi}_x & \bar{\xi}_y \\ -\bar{\xi}_y & \bar{\xi}_x \end{bmatrix} \begin{bmatrix} \bar{\eta}_x^* \\ \bar{\xi}_y^* \end{bmatrix} = \begin{bmatrix} 0 \\ 1 \end{bmatrix} \ ,
\tag{2.22b}
$$

with the solution

$$
\begin{aligned}
\bar{\eta}_x^* &= -\bar{\xi}_y \ , \\
\bar{\xi}_y^* &= \bar{\xi}_x \ .
\end{aligned}
\tag{2.22c}
$$

Thus, eq. (2.20) will be satisfied by choosing T such that:

$$T = \begin{bmatrix} 1 & 0 & 0 & 0 \\ 0 & \bar{\xi}_x & \bar{\xi}_y & 0 \\ 0 & \bar{\eta}_x^* & \bar{\eta}_y^* & 0 \\ 0 & 0 & 0 & 1 \end{bmatrix} = \begin{bmatrix} 1 & 0 & 0 & 0 \\ 0 & \bar{\xi}_x & \bar{\xi}_y & 0 \\ 0 & -\bar{\xi}_y & \bar{\xi}_x & 0 \\ 0 & 0 & 0 & 1 \end{bmatrix} , \tag{2.23}$$

which can be used to form the local Cartesian flux F^* :

$$F^* = T\bar{F} = \frac{|\vec{\nabla}\xi|}{J} \begin{bmatrix} \rho\bar{u} \\ \rho\bar{u}^2 + p \\ \rho\bar{u}v^* \\ \bar{u}(\rho E + p) \end{bmatrix} \tag{2.24}$$

where

$$v^* = u\bar{\eta}_x^* + v\bar{\eta}_y^* = -u\bar{\xi}_y + v\bar{\xi}_x \ . \tag{2.25}$$

Now that the rotation tensor T has been obtained, applying flux-splitting procedures to the Euler equations in generalized coordinates becomes straightforward. Multiplying eq. (2.11a) by the tensor T and incorporating the fact that

$$\delta_\xi(T\bar{F}) = T\delta_\xi\bar{F} + \bar{F}\delta_\xi T \ ,$$

the following expression is obtained:

$$\frac{\partial}{\partial t}(T\bar{Q}) + \frac{\delta_\xi}{\Delta\xi}(T\bar{F}) = -T\frac{\delta\bar{G}}{\Delta\eta} + \bar{F}\frac{\delta_\xi T}{\Delta\xi} \ , \tag{2.26}$$

which can be written as:

$$\frac{\partial Q^*}{\partial t} + \frac{\delta_\xi F^*}{\Delta\xi} = RHS \ , \tag{2.27}$$

where F^* is defined by eq. (2.24) and Q^* can be defined by:

$$Q^* = T\overline{Q} = TQ\frac{1}{\overline{J}} = \frac{1}{\overline{J}}\begin{bmatrix} \rho \\ \rho\overline{u} \\ \rho v^* \\ \rho E \end{bmatrix} . \tag{2.28}$$

Eq. (2.27) can now be split in the usual manner:

$$F^* = F^{*+} + F^{*-} \ , \tag{2.29}$$

yielding the expression

$$\frac{\partial Q^*}{\partial t} + \frac{\delta_\xi}{\Delta\xi}\left(F^{*+} + F^{*-}\right) = RHS \ , \tag{2.30}$$

After obtaining the split fluxes $F^{*\pm}$, it is possible to transform eq. (2.30) back to:

$$\frac{\partial \overline{Q}}{\partial t} + \frac{\delta_\xi}{\Delta\xi}\left(\overline{F}^+ + \overline{F}^-\right) + \frac{\delta_\eta}{\Delta\eta}\overline{G} = 0 \ , \tag{2.31}$$

where

$$\overline{F}^{\pm} = T^{-1}F^{*\pm} \ . \tag{2.32}$$

Thus, the flux vector $\overline{F}$ has been split by applying the transformation matrix T^{-1} to the locally Cartesian flux vector F^*. A similar procedure is employed to split the flux vector $\overline{G}$.

III. FLUX SPLITTINGS

For clarity, the following nomenclature is used in the discussion of the ten flux-splitting algorithms considered:

SW1 Steger-Warming-type flux-vector splitting of Grossman and Walters [6,25]

SW2 Steger-Warming-type flux-vector splitting of Liou et al. [26]

SW3 Steger-Warming-type flux-vector splitting of Vinokur and Liu [27]

VL1 Van Leer-type flux-vector splitting of Grossman and Walters [6,25]

VL2 Van Leer-type flux-vector splitting of Liou et al. [26]

VL3 Van Leer-type flux-vector splitting of Vinokur and Liu [27]

Roe1 Roe-type flux-difference splitting of Grossman and Walters [6,25]

Roe2 Roe-type flux-difference splitting of Liou et al. [26]

Roe3 Roe-type flux-difference splitting of Vinokur and Liu [27]

Roe4 Roe-type flux-difference splitting of Glaister [27]

3.1 *Steger-Warming Flux-Vector Splitting*

Steger and Warming [13] developed a flux-vector splitting for the Euler equations assuming a perfect gas law for the equation of state, i.e.

$$p = (\gamma - 1)\rho\left[E - \frac{(u^2 + v^2)}{2}\right], \tag{3.1}$$

in terms of the conserved variables Q. With this form of the state equation, it can be shown that the flux vectors are homogeneous of degree one, i.e.

$$F = AQ \quad \text{and} \quad G = BQ\ , \tag{3.2}$$

where A and B, the Jacobians of eqs. (2.1a)-(2.1c), are defined as:

$$A = \frac{\partial F}{\partial Q} \quad \text{and} \quad B = \frac{\partial G}{\partial Q}\ . \tag{3.3}$$

In the following discussion, only the A Jacobian will be considered since similar results can be obtained for the B Jacobian. In their derivation, Steger and Warming utilized the homogeneity property in splitting the fluxes by diagonalizing the Jacobian A :

$$A = S\Lambda S^{-1}\ , \tag{3.4a}$$

where S is the similarity matrix whose columns are composed of the right eigenvectors of A :

$$S = \begin{bmatrix} 1 & 0 & 1 & 1 \\ u & 1 & u+a & u-a \\ v & 1 & v & v \\ \frac{q^2}{2} & v & H+au & H-au \end{bmatrix} , \tag{3.4b}$$

and Λ is the diagonal matrix of the wave speeds of A :

$$\Lambda = \begin{bmatrix} \lambda_1 & 0 & 0 & 0 \\ 0 & \lambda_2 & 0 & 0 \\ 0 & 0 & \lambda_3 & 0 \\ 0 & 0 & 0 & \lambda_4 \end{bmatrix} = \begin{bmatrix} u & 0 & 0 & 0 \\ 0 & u & 0 & 0 \\ 0 & 0 & u+a & 0 \\ 0 & 0 & 0 & u-a \end{bmatrix} , \tag{3.4c}$$

with a, the speed of sound, defined as:

$$a^2 = \frac{\gamma p}{\rho} = \gamma(\gamma - 1)e \ . \tag{3.5}$$

They then split the matrix Λ into positive and negative contributions such that:

$$\Lambda = \Lambda^+ + \Lambda^- , \tag{3.6a}$$

by splitting the individual wave speeds, λ_i :

$$\lambda_i^{\pm} = \frac{\lambda_i \pm |\lambda_i|}{2} \ . \tag{3.6b}$$

The split fluxes are then formed such that:

(3.7a)
$$\begin{aligned} F^{\pm} &= S\Lambda^{\pm}S^{-1}Q \\ &= F_1\lambda_1^{\pm} + F_3\lambda_3^{\pm} + F_4\lambda_4^{\pm} \ , \end{aligned}$$

where

(3.7b)
$$F_1 = \frac{(\gamma-1)}{\gamma}\rho\begin{bmatrix} 1 \\ u \\ v \\ \frac{q^2}{2} \end{bmatrix} , \qquad F_{3,4} = \frac{\rho}{2\gamma}\begin{bmatrix} 1 \\ u \pm a \\ v \\ H \pm ua \end{bmatrix} ,$$

and the $\lambda_i^{\pm}$ are given by eq. (3.6b) with

(3.7c)
$$\lambda_1 = u \ , \quad \lambda_3 = u + a \ , \quad \lambda_4 = u - a \ .$$

The Jacobian A for a real gas in equilibrium, derived in appendix A, is given by:

(3.8)
$$A = \begin{bmatrix} 0 & 1 & 0 & 0 \\ p_\rho - u^2 + \frac{p_e}{\rho}(\frac{q^2}{2} - e) & u(2 - \frac{p_e}{\rho}) & -v\frac{p_e}{\rho} & \frac{p_e}{\rho} \\ -uv & v & u & 0 \\ u[p_\rho - H + \frac{p_e}{\rho}(\frac{q^2}{2} - e)] & H - u^2\frac{p_e}{\rho} & -uv\frac{p_e}{\rho} & u(1 + \frac{p_e}{\rho}) \end{bmatrix}$$

where

(3.9)
$$p_e = \frac{\partial p}{\partial e}\Big|_\rho \quad \text{and} \quad p_\rho = \frac{\partial p}{\partial \rho}\Big|_e \ .$$

The terms p_ρ and p_e appear because the equation of state is no longer a simple analytical function of ρ and e. As a result, the Euler equations no longer remain homogeneous of degree one for a real gas, and thus the equalities of eq. (3.2) are invalid. In order to utilize flux-splitting for a real gas, an alternative to eq. (3.2) is required.

3.1.1 SW1 - Splitting by Grossman and Walters

Grossman and Walters [6, 25] sought a splitting that could be readily applied to existing perfect gas algorithms. Based on the local parameterization of the state equation by Colella and Glaz [34], they introduced an equivalent $\tilde{\gamma}$ defined as:

$$\tilde{\gamma} = \tilde{\gamma}(\rho,e) = 1 + \frac{p(\rho,e)}{\rho e} \quad . \tag{3.10}$$

In terms of $\tilde{\gamma}$ and its derivatives, the sound speed a can be expressed as:

$$a^2 = \frac{\tilde{\gamma} p}{\rho} + \rho e \left[\tilde{\gamma}_\rho + \frac{p}{\rho^2} \tilde{\gamma}_e \right] \quad , \tag{3.11}$$

and the Jacobian matrix A, as:

$$A = \tilde{A} + \rho e \tilde{\gamma}_\rho \begin{bmatrix} 0 & 0 & 0 & 0 \\ 1 & 0 & 0 & 0 \\ 0 & 0 & 0 & 0 \\ u & 0 & 0 & 0 \end{bmatrix} - e\tilde{\gamma}_e \begin{bmatrix} 0 & 0 & 0 & 0 \\ E - q^2 & u & v & -1 \\ 0 & 0 & 0 & 0 \\ u(E - q^2) & u^2 & uv & -u \end{bmatrix}, \tag{3.12}$$

where $\tilde{\gamma}_\rho = \frac{\partial \tilde{\gamma}}{\partial \rho} \Big|_e$, $\tilde{\gamma}_e = \frac{\partial \tilde{\gamma}}{\partial e} \Big|_\rho$, and

$$\tilde{A} = \begin{bmatrix} 0 & 1 & 0 & 0 \\ (\tilde{\gamma} - 1)\frac{q^2}{2} - u^2 & (3 - \tilde{\gamma})u & (1 - \tilde{\gamma})v & \tilde{\gamma} - 1 \\ -uv & v & u & 0 \\ u[(\tilde{\gamma} - 1)q^2 - \tilde{\gamma}E] & H + (1 - \tilde{\gamma})u^2 & (1 - \tilde{\gamma})uv & \tilde{\gamma}u \end{bmatrix}. \tag{3.13}$$

The eigenvalues of the matrix $\tilde{A}$ are:

$$\tilde{\lambda}(\tilde{A}) = u, \; u, \; u + \tilde{a}, \; u - \tilde{a} \; , \tag{3.14}$$

where

$$\tilde{a}^2 = \frac{\tilde{\gamma} p}{\rho} \; . \tag{3.15}$$

Grossman and Walters determine that $\tilde{A}$ satisfies the following property:

$$F = \tilde{A} Q \; . \tag{3.16}$$

Although eq. (3.16) is an accurate representation of the flux F, the matrix $\tilde{A}$ is not the flux Jacobian $\partial F / \partial Q$. Thus, splittings based on the sign of $\tilde{\lambda}$ may not

physically agree with splittings based on the true wave speeds, λ. A discussion on the effects of this approximation are given in chapter 4. The matrix $\tilde{A}$ can be diagonalized:

$$\tilde{A} = \tilde{S}\tilde{\Lambda}\tilde{S}^{-1} \quad , \tag{3.17}$$

where $\tilde{S}$ and $\tilde{\Lambda}$ are defined by eqs. (3.4b) and (3.4c), respectively, with two exceptions. The sound speed, a, is replaced by $\tilde{a}$ and the total enthalpy, H, is replaced by $\tilde{H}$, defined as:

$$\tilde{H} = \frac{\tilde{a}^2}{\tilde{\gamma}-1} + \frac{q^2}{2} \quad . \tag{3.18a}$$

where

$$q^2 = u^2 + v^2 \quad . \tag{3.18b}$$

The resulting split fluxes are expressed as:

$$\begin{aligned} F^{\pm} &= \tilde{S}\tilde{\Lambda}^{\pm}\tilde{S}^{-1}Q \\ &= \tilde{F}_1\tilde{\lambda}_1^{\pm} + \tilde{F}_3\tilde{\lambda}_3^{\pm} + \tilde{F}_4\tilde{\lambda}_4^{\pm} \quad , \end{aligned} \tag{3.19a}$$

where

$$(3.19b) \qquad \tilde{F}_1 = \frac{(\tilde{\gamma}-1)}{\tilde{\gamma}}\rho\begin{bmatrix} 1 \\ u \\ v \\ \frac{q^2}{2} \end{bmatrix}, \qquad \tilde{F}_{3,4} = \frac{\rho}{2\tilde{\gamma}}\begin{bmatrix} 1 \\ u \pm \tilde{a} \\ v \\ \tilde{H} \pm u\tilde{a} \end{bmatrix},$$

and the $\tilde{\lambda}_i^{\pm}$ are given by eq. (3.6b) with

$$(3.19c) \qquad \tilde{\lambda}_1 = u\,, \quad \tilde{\lambda}_3 = u + \tilde{a}\,, \quad \tilde{\lambda}_4 = u - \tilde{a}\,.$$

This form is identical to the perfect gas form, eq. (3.7b), with a modified definition of $\tilde{a}$ and $\tilde{\gamma}$.

3.1.2 *SW2 - Splitting by Liou, Van Leer, and Shuen*

Liou et al. [26] factored the Jacobian A into two matrices, each containing only derivatives with respect to ρ or e such that:

$$(3.20a) \qquad A = A_e + A_\rho\,,$$

where

(3.20*b*)

$$A_e = \begin{bmatrix} 0 & 1 & 0 & 0 \\ \frac{p}{\rho} - u^2 + \frac{p_e}{\rho}(\frac{q^2}{2} - e) & u(2 - \frac{p_e}{\rho}) & -v\frac{p_e}{\rho} & \frac{p_e}{\rho} \\ -uv & v & u & 0 \\ u[\frac{p}{\rho} - H + \frac{p_e}{\rho}(\frac{q^2}{2} - e)] & H - u^2\frac{p_e}{\rho} & -uv\frac{p_e}{\rho} & u(1 + \frac{p_e}{\rho}) \end{bmatrix}$$

contains the derivative p_e, and

(3.20c)
$$A_\rho = \begin{bmatrix} 0 & 0 & 0 & 0 \\ p_\rho - \frac{p}{\rho} & 0 & 0 & 0 \\ 0 & 0 & 0 & 0 \\ u[p_\rho - \frac{p}{\rho}] & 0 & 0 & 0 \end{bmatrix}$$

contains the derivative p_ρ, where p_e and p_ρ are defined by eq. (3.9). The eigenvalues of these matrices are :

(3.21a)
$$\lambda(A) = u,\ u,\ u+a,\ u-a,$$

(3.21b)
$$\lambda(A_e) = u,\ u,\ u+a_e,\ u-a_e,$$

(3.21c)
$$\lambda(A_\rho) = 0,\ 0,\ 0,\ 0,$$

where the speeds of sound, a and a_e, are now defined as:

(3.22a)
$$a^2 = \frac{\partial p}{\partial \rho}\Big|_s = p_\rho + \frac{pp_e}{\rho^2},$$

(3.22*b*) $$a_e^2 = \frac{p}{\rho}\left(\frac{p_e}{\rho} + 1\right) = a^2 - \left(p_\rho - \frac{p}{\rho}\right) .$$

They then define F to be the sum of homogeneous and inhomogeneous parts :

(3.23*a*) $$F = F_h + F' ,$$

(3.23*b*) $$F_h = AQ , \quad F' = - A_\rho Q .$$

Since A has a complete set of eigenvectors, it can be diagonalized by eq (3.4a) with S now given by:

(3.24) $$S = \begin{bmatrix} 1 & 0 & 1 & 1 \\ u & 1 & u+a & u-a \\ v & 1 & v & v \\ \frac{q^2}{2} + \left(e - \frac{\rho p_\rho}{p_e}\right) & v & H + au & H - au \end{bmatrix} ,$$

and Λ still defined by eq. (3.4c). For a perfect gas, the term $\left(e - \frac{\rho p_\rho}{p_e}\right)$ is zero and eq. (3.24) reduces to eq. (3.4b), as expected. Utilizing eqs. (3.6), the homogeneous flux-splitting is found to be:

(3.25*a*) $$\begin{aligned} F_h^\pm &= S\Lambda^\pm S^{-1} Q \\ &= F_{1h}\lambda_1^\pm + F_{3h}\lambda_3^\pm + F_{4h}\lambda_4^\pm , \end{aligned}$$

where

$$(3.25b)\quad F_{1h} = (1 - \frac{p_\rho}{a^2})\rho \begin{bmatrix} 1 \\ u \\ v \\ E - \frac{\rho p_\rho}{p_e} \end{bmatrix}, \qquad F_{3h,4h} = \frac{\rho}{2}(\frac{p_\rho}{a^2}) \begin{bmatrix} 1 \\ u \pm a \\ v \\ H \pm ua \end{bmatrix},$$

and the $\lambda_i^{\pm}$ are defind by eqs. (3.6b), (3.7c), and (3.22a).

Since A_ρ does not have a complete set of eigenvectors, the flux F' cannot be split. As a result, Liou et al. proposed that the F' flux be included using central differencing, resulting in the pseudo-splitting:

$$(3.26)\qquad F^{\pm} = F_h^{\pm} + \frac{1}{2}F' \ .$$

3.1.3 SW3 - Splitting by Vinokur and Liu

Vinokur and Liu [27] expressed the state equation in a slightly different form as:

$$(3.27a)\qquad p = p(\rho, \rho e) = p(\rho, \epsilon) \ ,$$

with its derivatives defined as:

$$(3.27b)\qquad \chi = \frac{\partial p}{\partial \rho}\Big|_{\epsilon} = p_\rho - \frac{e}{\rho}p_e \ ,$$

$$\kappa = \frac{\partial p}{\partial \epsilon}\Big|_{\rho} = \frac{1}{\rho} p_e \ , \tag{3.27c}$$

where p_e and p_ρ are defined by eq. (3.9). The derivatives κ and χ must be evaluated with e rather than ϵ, since that is how p is determined in the equilibrium air curve fit [30]. Defining the specific enthalpy as:

$$h = \frac{\epsilon + p}{\rho} \ , \tag{3.28}$$

the speed of sound can be expressed as:

$$a^2 = \chi + \kappa h \ . \tag{3.29}$$

Algebraic manipulation indicates that eq. (3.29) is equivalent to eq. (3.22a). Vinokur and Liu also introduced the variable Γ, defined now as:

$$\Gamma = \frac{\rho a^2}{p} \ . \tag{3.30}$$

Ref. 27 used the notation γ for this variable. In our notation, the Jacobian matrix A is given by:

$$A = \begin{bmatrix} 0 & 1 & 0 & 0 \\ \chi - u^2 + \kappa \dfrac{q^2}{2} & u(2-\kappa) & -v\kappa & \kappa \\ -uv & v & u & 0 \\ u[\chi - H + \kappa \dfrac{q^2}{2}] & H - u^2\kappa & -uv\kappa & u(1+\kappa) \end{bmatrix} , \tag{3.31a}$$

with the corresponding right eigenvector matrix S:

$$(3.31b) \qquad S = \begin{bmatrix} 1 & 0 & 1 & 1 \\ u & 1 & u+a & u-a \\ v & 1 & v & v \\ \frac{q^2}{2} - \frac{\chi}{\kappa} & v & H+au & H-au \end{bmatrix},$$

In a previous derivation by Vinokur [35], the left and right eigenvector matrices, S^{-1} and S, were used to form projection operators, P_i :

$$(3.32) \quad S^{-1}P_1S = \begin{bmatrix} 1 & 0 & 0 \\ 0 & 0 & 0 \\ 0 & 0 & 0 \end{bmatrix}, \quad S^{-1}P_3S = \begin{bmatrix} 0 & 0 & 0 \\ 0 & 1 & 0 \\ 0 & 0 & 0 \end{bmatrix}, \quad S^{-1}P_4S = \begin{bmatrix} 0 & 0 & 0 \\ 0 & 0 & 0 \\ 0 & 0 & 1 \end{bmatrix},$$

which were used in constructing the split flux of eq. (3.7a), with

$$(3.33) \qquad F_1 = \frac{(\Gamma-1)}{\Gamma}\rho \begin{bmatrix} 1 \\ u \\ v \\ E - \frac{a^2}{\Gamma(\Gamma-1)} \end{bmatrix}, \quad F_{3,4} = \frac{\rho}{2\Gamma} \begin{bmatrix} 1 \\ u \pm a \\ v \\ H \pm ua \end{bmatrix},$$

$\lambda_i^{\pm}$ defined by eqs. (3.6b), (3.7c), and (3.29), and Γ defined by eq. (3.30).

3.2 *Van Leer Flux-Vector Splitting*

Van Leer [23] developed a perfect gas flux-vector splitting for the one-dimensional Euler equations with the conditions that:

(i) $F(Q) = F^{+}(Q) + F^{-}(Q)$,

(ii) $\frac{\partial F^{+}}{\partial Q}$ must have all eigenvalues ≥ 0,

(iii) $\frac{\partial F^{-}}{\partial Q}$ must have all eigenvalues ≤ 0,

under the restrictions that:

(1) $F^{\pm}(Q)$ must be continuous, with

$F^{+}(Q) \equiv F(Q)$ for $M \geq 1$,

$F^{-}(Q) \equiv F(Q)$ for $M \leq -1$,

(2) The components of F^{+} and F^{-} must mimic the symmetry of F with respect to M (all other state quantities held constant), i.e.

$F_k^{\pm}(M) = \pm F_k^{\mp}(-M)$ if $F_k(M) = \pm F_k(-M)$,

(3) $\frac{\partial F^{\pm}}{\partial Q}$ must be continuous,

(4) $\frac{\partial F^{\pm}}{\partial Q}$ must have one eigenvalue vanish for $|M| < 1$,

(5) $F^{\pm}(M)$, like $F(M)$, must be a polynomial in M, and of lowest possible degree.

Van Leer notes that restriction 1 ensures that the flux-vector splitting leads to standard upwind differencing in supersonic regions, Restriction 4 makes it possi-

ble to form stationary shock structures with a maximum of two interior zones, and that restriction 5 guarantees the uniqueness of the splitting.

In terms of the density ρ, the Mach number, M, and the sound speed a, the full flux F can be written as

$$F = F(\rho,a,\mathrm{M}) = \begin{bmatrix} f_1 \\ f_2 \\ f_3 \end{bmatrix} = \begin{bmatrix} \rho a \mathrm{M} \\ \rho a^2(\mathrm{M}^2 + \frac{1}{\gamma}) \\ \rho a^3 \mathrm{M}(\frac{\mathrm{M}^2}{2} + \frac{1}{\gamma - 1}) \end{bmatrix} , \tag{3.34}$$

where γ is the constant ratio of specific heats and a is defined by eq. (3.5). Applying restrictions 1, 3, and 5, Van Leer concluded that F^+ must include a factor $(\mathrm{M} + 1)^2$ while F^- must include a factor $(-\mathrm{M} + 1)^2$, resulting in the mass flux splitting

$$f_1^{\pm} \equiv \pm \frac{\rho a}{4}(\mathrm{M} \pm 1)^2 , \qquad |\mathrm{M}| < 1 , \tag{3.35}$$

the momentum flux splitting

$$f_2^{\pm} \equiv f_1^{\pm}[u - (u \mp 2a)/\gamma] , \qquad |\mathrm{M}| < 1 , \tag{3.36}$$

and the energy flux splitting

$$f_3^{\pm} \equiv \frac{\gamma^2}{2(\gamma - 1)} \frac{(f_2^{\pm})^2}{f_1^{\pm}} , \qquad |\mathrm{M}| < 1 . \tag{3.37}$$

Van Leer concludes the derivation by proving that for $|M| \leq 1$, the non-zero eigenvalues of $\frac{\partial F^+}{\partial Q}$ are both positive while the non-zero eigenvalues of $\frac{\partial F^-}{\partial Q}$ are both negative for the range $1 \leq \gamma \leq 3$.

3.2.1 *VL1 - Splitting by Grossman and Walters*

Utilizing the equivalent sound speed $\tilde{a}$, defined by eq. (3.15), the procedures given above were extended directly to real gases [6,25], with the full flux F now given as:

$$F = F(\rho, \tilde{a}, \tilde{M}) = \begin{bmatrix} f_1 \\ f_2 \\ f_3 \\ f_4 \end{bmatrix} = \begin{bmatrix} \rho\tilde{a}\tilde{M} \\ \rho\tilde{a}^2(\tilde{M}^2 + \frac{1}{\tilde{\gamma}}) \\ \rho v\tilde{a}\tilde{M} \\ \rho\tilde{a}^3\tilde{M}(\frac{\tilde{M}^2}{2} + \frac{1}{\tilde{\gamma} - 1}) \end{bmatrix}, \tag{3.38}$$

where $\tilde{\gamma}$ is given by eq. (3.10) and $\tilde{M}$, the "equivalent Mach number", is defined as:

$$\tilde{M} = \frac{u}{\tilde{a}} \quad . \tag{3.39}$$

Since the flux vector F is in a form equivalent to the perfect gas form of eq. (3.34), the flux-vector splitting for a real gas becomes:

$$F^{\pm} = \begin{bmatrix} f_1^{\pm} \\ f_2^{\pm} \\ f_3^{\pm} \\ f_4^{\pm} \end{bmatrix} = \begin{bmatrix} \pm \frac{\rho\tilde{a}}{4}\left(\tilde{\mathrm{M}} \pm 1\right)^2 \\ f_1^{\pm}[u - (u \mp 2\tilde{a})/\tilde{\gamma}] \\ f_1^{\pm} v \\ f_1^{\pm}\left\{ \frac{[(\tilde{\gamma}-1)u \pm 2\tilde{a}]^2}{2(\tilde{\gamma}^2-1)} + \frac{1}{2}v^2 \right\} \end{bmatrix} . \tag{3.40}$$

3.2.2 *VL2 - Splitting by Liou, Van Leer, and Shuen*

Liou et al. [26] present a derivation for a family of flux choices that are both independent of the equation of state and do not require the use of the approximate wave speeds, eq. (3.14). As in the perfect gas case, the mass flux splitting is defined:

$$f_1^{\pm} = \pm \frac{\rho a}{4}(\mathrm{M} \pm 1)^2 \ , \tag{3.41}$$

where a, the true sound speed, is given by eq. (3.22a). The authors note that since $f_1^{\pm}$ is quadratic in $(\mathrm{M} \pm 1)^2$, its slope vanishes as $\mathrm{M} \to \mp 1$, resulting in smooth switching in sonic regions (Fig. 2), unlike the Steger-Warming splitting (Fig. 3). Consequently, the rest of the fluxes are derived in terms of $f_1^{\pm}$. The x-momentum flux f_2 can be expressed as:

$$f_2 = \rho u^2 + p = u\rho a\mathrm{M} + p \ . \tag{3.42}$$

Since the first term on the RHS is already in terms of f_1, all that is needed is to find an expression for p in terms of $(M+1)^2$ and $(M-1)^2$. The authors proposed the function:

$$p = x[(M+1)^2 - (M-1)^2] + y[(M+1)^2 + (M-1)^2] \tag{3.43}$$
$$= 4xM + 2y(M^2+1) \ .$$

Letting $M=0$, they obtained:

$$y = \frac{1}{2}p \ ,$$
$$x = -\frac{1}{4}pM \ .$$

Thus, p can be expressed as:

$$p = \frac{p}{\rho a^2}[f_1^+(-u+2a) + f_1^-(-u-2a)] \ . \tag{3.44}$$

Substitution into eq. (3.42) yields the $f_2^{\pm}$ splitting

$$f_2^{\pm} = f_1^{\pm}[u - \frac{p}{\rho a^2}(u \mp 2a)] \tag{3.45}$$
$$= f_1^{\pm}[u - (u \mp 2a)/\Gamma] \ ,$$

where Γ is defined:

$$\Gamma = \frac{\rho a^2}{p} \ . \tag{3.46}$$

The y-momentum flux f_3, expressed as:

(3.47) $$f_3 = \rho uv = v\rho a\mathrm{M} \quad ,$$

can be split directly from eq. (3.41) such that:

(3.48) $$f_3^{\pm} = f_1^{\pm} v \quad .$$

The energy flux f_4 can be expressed as:

(3.49) $$f_4 = \rho uE + pu = \rho aE\mathrm{M} + pu \quad .$$

Liou et al. assumed a quadratic function in u for pu that, because of symmetry, has the form:

(3.50) $$\begin{aligned} pu &= f_1^{+}(lu^2 + 2mua + na^2) + f_1^{-}(lu^2 - 2mua + na^2) \\ &= (l+m)\rho u^3 + (m+n)\rho u a^2 \quad . \end{aligned}$$

They chose to eliminate ρu^3 by letting:

$$m + n = \frac{p}{\rho a^2} \quad ,$$

resulting in the $f_4^{\pm}$ splitting:

(3.51) $$f_4^{\pm} = f_1^{\pm}[H - m(u \mp a)^2] \quad ,$$

which actually defines a family of splittings determined by the parameter m . The Van Leer splitting was obtained by requiring that the terms in the brackets of eq. (3.51) form a perfect square, resulting in the following expression for m :

(3.52) $$m = \frac{\frac{h}{a^2}}{1 + 2\frac{h}{a^2}} \quad .$$

3.2.3 *VL3 - Splitting by Vinokur and Liu*

In compliance with the restrictions stated in section 3.2, Vinokur and Liu [27] obtained relations for the split fluxes $f_1^{\pm}$, $f_2^{\pm}$, and $f_3^{\pm}$ that were identical to those of Liou et al., e.g. eqs. (3.41), (3.45), and (3.48), with Γ defined by eq. (3.30). The choice for the energy flux, based on satisfying conditions of continuity and symmetry, was defined as:

(3.53) $$f_4^{\pm} = f_1^{\pm}\left\{ \frac{[(\Gamma - 1)u \pm 2a]^2}{2(\Gamma^2 - 1)} + \frac{1}{2}v^2 + e - \frac{a^2}{\Gamma(\Gamma - 1)} \right\} ,$$

with a defined by eq. (3.29). This represents a choice of $m = \frac{1}{\Gamma + 1}$ in eq. (3.50).

3.3 *Roe's Approximate Rieman Solver*

The one-dimensional Euler equations, i.e.

$$\frac{\partial Q}{\partial t} + \frac{\partial F}{\partial x} = 0 \,, \tag{3.54}$$

$$Q = \begin{bmatrix} \rho \\ \rho u \\ \rho E \end{bmatrix}, \qquad F = \begin{bmatrix} \rho u \\ \rho u^2 + p \\ u(\rho E + p) \end{bmatrix},$$

can be linearized:

$$\frac{\partial Q}{\partial t} + \frac{\partial F}{\partial Q}\frac{\partial Q}{\partial x} = \frac{\partial Q}{\partial t} + A\frac{\partial Q}{\partial x} = 0 \,. \tag{3.55}$$

Roe [21] developed a perfect gas flux-difference splitting for eq. (3.54) by approximating the linearization of eq. (3.55) as:

$$\frac{\partial Q}{\partial t} + \hat{A}\frac{\partial Q}{\partial x} = 0 \,, \tag{3.56}$$

where the matrix A has been replaced with a locally constant matrix $\hat{A}$, determined by satisfying the conditions:

(i) The mapping from vector space Q to vector space f is linear,

(ii) As $Q_L \to Q_R \to Q$, $\hat{A}(Q_L, Q_R) \to A(Q)$, where $A = \partial F/\partial Q$,

(iii) For any Q_L, Q_R, $\hat{A}(Q_L, Q_R) \times (Q_L - Q_R) = F_L - F_R$,

(iv) The eigenvectors of $\hat{A}$ are linearly independent,

with the subscripts L and R indicating left and right fluid states, respectively. Roe notes that condition (ii) maintains consistency with the governing differential equation, while condition (iii) ensures that $\hat{A}$ satisfies the Rankine-Hugoniot shock jump condition. The Roe-averaged matrix $\hat{A}$ is defined as:

$$\hat{A} = \begin{bmatrix} 0 & 1 & 0 \\ (\gamma-3)\frac{\hat{u}^2}{2} & (3-\gamma)\hat{u} & \gamma-1 \\ -\frac{\hat{u}\hat{a}^2}{\gamma-1} + (\gamma-2)\frac{\hat{u}^3}{2} & \frac{\hat{a}^2}{\gamma-1} + (3-2\gamma)\frac{\hat{u}^2}{2} & \gamma\hat{u} \end{bmatrix}, \tag{3.57}$$

where the hats imply evaluation at a Roe-averaged state. Since conditions (i) and (iv) ensure that the matrix $\hat{A}$ has three independent eigenvalues, the matrix $\hat{A}$ can be diagonalized:

$$\hat{A} = \hat{S}\,\hat{\Lambda}\,\hat{S}^{-1}, \tag{3.58a}$$

with $\hat{\Lambda}$, the diagonal matrix of wave speeds, given by:

$$\hat{\Lambda} = \begin{bmatrix} \hat{u}-\hat{a} & 0 & 0 \\ 0 & \hat{u} & 0 \\ 0 & 0 & \hat{u}+\hat{a} \end{bmatrix}, \tag{3.58b}$$

and $\hat{S}$ and $\hat{S}^{-1}$, the right and left eigenvectors of $\hat{A}$, respectively given by:

$$(3.58c) \qquad \hat{S} = \begin{bmatrix} 1 & 1 & 1 \\ \hat{u} - \hat{a} & \hat{u} & \hat{u} + \hat{a} \\ \frac{\hat{a}^2}{\gamma - 1} + \hat{u}\left(\frac{\hat{u}}{2} - \hat{a}\right) & \frac{\hat{u}^2}{2} & \frac{\hat{a}^2}{\gamma - 1} + \hat{u}\left(\frac{\hat{u}}{2} + \hat{a}\right) \end{bmatrix},$$

$$\hat{S}^{-1} = \begin{bmatrix} \frac{\hat{u}}{2\hat{a}}\left(1 + \frac{\gamma - 1}{2}\frac{\hat{u}}{\hat{a}}\right) & -\frac{1}{2\hat{a}}\left(1 + (\gamma - 1)\frac{\hat{u}}{\hat{a}}\right) & \frac{\gamma - 1}{2\hat{a}^2} \\ 1 - \frac{\gamma - 1}{2}\frac{\hat{u}^2}{\hat{a}^2} & (\gamma - 1)\frac{\hat{u}}{\hat{a}^2} & -\frac{(\gamma - 1)}{\hat{a}^2} \\ -\frac{\hat{u}}{2\hat{a}}\left(1 - \frac{\gamma - 1}{2}\frac{\hat{u}}{\hat{a}}\right) & \frac{1}{2\hat{a}}\left(1 - (\gamma - 1)\frac{\hat{u}}{\hat{a}}\right) & \frac{\gamma - 1}{2\hat{a}^2} \end{bmatrix}.$$

By using parameter vectors, Roe determined an appropriate averaging that assured that the linearized solver would satisfy conditions (i)-(iv). The only condition not satisfied by a simple algebraic averaging of the left and right states is (iii), the Rankine-Hugoniot shock jump condition. By expanding the matrix equations of condition (iii), Roe was able to directly solve the resulting algebraic equations for the appropriate averages. Multiplying $\hat{A}$ by $\Delta(Q)$, where

$$(3.59) \qquad \Delta(\bullet) = (\bullet)_R - (\bullet)_L \ ,$$

the first two equations can be written as:

$$(3.60) \qquad \Delta(\rho u) = \hat{\rho}\Delta u + \hat{u}\Delta\rho \ ,$$

$$(3.61) \qquad \Delta(\rho u^2) = 2\hat{\rho}\hat{u}\Delta u + \hat{u}^2\Delta\rho \ .$$

Substituting $\hat{\rho}$ from equation (3.60) into equation (3.61) results in a quadratic equation for $\hat{u}$:

$$\hat{u}^2\Delta\rho - 2\hat{u}\Delta(\rho u) + \Delta(\rho u^2) = 0 \ . \tag{3.62}$$

Solving for the negative root of $\hat{u}$ by expanding the $\Delta(\bullet)$ terms yields:

$$\hat{u} = \frac{\rho_L^{1/2}u_L + \rho_R^{1/2}u_R}{\rho_L^{1/2} + \rho_R^{1/2}} \ . \tag{3.63}$$

Substituting equation (3.63) back into equation (3.60) and solving for $\hat{\rho}$ yields:

$$\hat{\rho} = (\rho_L\rho_R)^{1/2} \ . \tag{3.64}$$

The third equation that results from multiplying $\hat{A}\Delta Q$ is essentially an expression for the Roe-averaged speed of sound. Substituting eqs. (3.60) and (3.61) into the third equation gives:

$$\hat{\rho}\hat{a}^2\Delta u = \gamma[\Delta up - \hat{u}\Delta p] + \frac{(\gamma-1)}{2}\left[\Delta\rho u^3 - \hat{u}^3\Delta\rho - 3\hat{\rho}\hat{u}^2\Delta u\right] \ . \tag{3.65}$$

Expanding the right hand side of eq. (3.65) using the ideal gas law and eqs. (3.60) and (3.61) yields:

$$\rho_L\rho_R\hat{a}^2 = \gamma\frac{\rho_L p_R + \rho_R p_L}{\rho_L + \rho_R} + \frac{\gamma-1}{2}\frac{\rho_L^2\rho_R^2(u_R-u_L)^2}{(\rho_L+\rho_R)^2} \ . \tag{3.66}$$

Eq. (3.66) can be simplified considerably by introducing a Roe-averaged total enthalpy defined as:

(3.67) $$\hat{H} = \frac{\hat{a}^2}{\gamma - 1} + \frac{\hat{u}^2}{2} \quad .$$

Substituting $\hat{a}$ from equation (3.66) into (3.67) yields:

(3.68) $$\hat{H} = \frac{\rho_L^{1/2} H_L + \rho_R^{1/2} H_R}{\rho_L^{1/2} + \rho_R^{1/2}} \quad .$$

with the stagnation enthalpy defined as:

$$H = \frac{a^2}{\gamma - 1} + \frac{u^2}{2} \quad ,$$

The Roe-averaged speed of sound, $\hat{a}$, is then found from eq. (3.67) as:

(3.69) $$\hat{a}^2 = (\gamma - 1)\left(\hat{H} - \frac{\hat{u}^2}{2}\right) .$$

Once the Roe-averaged conditions are known, the flux can be obtained from either the left or right fluid states such that:

(3.70*a*) $$F(Q_L, Q_R) = F_L + \hat{S}\,\hat{\Lambda}^{(-)}\,\hat{S}^{-1}\,\Delta Q \quad ,$$

(3.70*b*) $$F(Q_L, Q_R) = F_R - \hat{S}\,\hat{\Lambda}^{(+)}\,\hat{S}^{-1}\,\Delta Q \quad ,$$

where $\Lambda^{(-)}$ and $\Lambda^{(+)}$ are given by:

(3.71) $$\hat{\Lambda}^{(+)} = \frac{\hat{\Lambda} + |\hat{\Lambda}|}{2} \quad , \qquad \hat{\Lambda}^{(-)} = \frac{\hat{\Lambda} - |\hat{\Lambda}|}{2} \quad .$$

Equivalently, by averaging eqs. (3.70a) and (3.70b), the flux at the interface between two Riemann states can be expressed as:

$$F(Q_L, Q_R) = \frac{1}{2}\left(F_L + F_R - \hat{S}\left|\hat{\Lambda}\right|\hat{S}^{-1}\,\Delta Q\right)$$
$$= \frac{1}{2}\left(F_L + F_R - \sum_{i=1}^{3}\left|\Delta\hat{F}_i\right|\right), \tag{3.72a}$$

where

$$\left|\Delta\hat{F}_1\right| = |\hat{u}|\begin{bmatrix} \Delta\rho - \dfrac{\Delta p}{\hat{a}^2} \\ \hat{u}\left(\Delta\rho - \dfrac{\Delta p}{\hat{a}^2}\right) \\ \dfrac{\hat{u}}{2}\left(\Delta\rho - \dfrac{\Delta p}{\hat{a}^2}\right) \end{bmatrix}$$

$$\left|\Delta\hat{F}_{2,3}\right| = |\hat{u} \pm \hat{a}|\left\{\frac{\Delta p \pm \hat{\rho}\hat{a}\Delta u}{2\hat{a}^2}\right\}\begin{bmatrix} 1 \\ \hat{u} \pm \hat{a} \\ \hat{H} \pm \hat{u}\hat{a} \end{bmatrix}. \tag{3.72b}$$

In a numerical scheme, $F(Q_L,Q_R)$ is used to represent the flux found at the interface between grid cells, while the volume-averaged flow variables extrapolated to the cell faces from the left or right side represent the Riemann states. It should be noted that the cell centered values obtained from the above relations are only accurate to first order.

Although Roe's approximate solution to the Riemann problem is strictly valid only for the one-dimensional case, it has been extended to multi-dimensions by

assuming that conserved quantities in grid cells are only affected by waves propagating normal to the cell interfaces. Thus, velocities parallel to the cell interface are ignored and any difference in the parallel component is assumed to take place across the contact surface. The resulting two-dimensional flux-difference splitting, $\Delta\hat{F}_i$, is given by:

$$
\left|\Delta\hat{F}_1\right| = |\hat{u}| \begin{bmatrix} \Delta\rho - \dfrac{\Delta p}{\hat{a}^2} \\ \hat{u}\left(\Delta\rho - \dfrac{\Delta p}{\hat{a}^2}\right) \\ \hat{v}\left(\Delta\rho - \dfrac{\Delta p}{\hat{a}^2}\right) + \hat{\rho}\Delta v \\ \left(\dfrac{\hat{u}^2+\hat{v}^2}{2}\right)\left(\Delta\rho - \dfrac{\Delta p}{\hat{a}^2}\right) + \hat{\rho}\hat{v}\Delta v \end{bmatrix} \tag{3.73}
$$

$$
\left|\Delta\hat{F}_{2,3}\right| = |\hat{u} \pm \hat{a}| \left\{ \frac{\Delta p \pm \hat{\rho}\hat{a}\Delta u}{2\hat{a}^2} \right\} \begin{bmatrix} 1 \\ \hat{u} \pm \hat{a} \\ \hat{v} \\ \hat{H} \pm \hat{u}\hat{a} \end{bmatrix},
$$

with

$$
\hat{\rho} = (\rho_L \rho_R)^{1/2} , \tag{3.74a}
$$

$$
\hat{u} = \frac{\rho_L^{1/2} u_L + \rho_R^{1/2} u_R}{\rho_L^{1/2} + \rho_R^{1/2}} , \tag{3.74b}
$$

$$
\hat{v} = \frac{\rho_L^{1/2} v_L + \rho_R^{1/2} v_R}{\rho_L^{1/2} + \rho_R^{1/2}} , \tag{3.74c}
$$

(3.74*d*)
$$\hat{H} = \frac{\rho_L^{1/2} H_L + \rho_R^{1/2} H_R}{\rho_L^{1/2} + \rho_R^{1/2}} \quad ,$$

$$H = \frac{a^2}{\gamma - 1} + \frac{u^2 + v^2}{2} \quad ,$$

(3.74*e*)
$$\hat{a}^2 = (\gamma - 1)\left(\hat{H} - \frac{\hat{u}^2 + \hat{v}^2}{2} \right) .$$

3.3.1 Roe1 - Splitting by Grossman and Walters

Grossman and Walters [6,25] developed a one-dimensional, real gas, flux-difference splitting based on the parameter vector approach taken by Roe [21] for a perfect gas. In one space dimension, the parameter vector is given by

(3.75)
$$W = \begin{bmatrix} w_1 \\ w_2 \\ w_3 \end{bmatrix} = \rho^{1/2} \begin{bmatrix} 1 \\ u \\ H \end{bmatrix} .$$

The parameter vector W is used to obtain the Roe averaged matrix $\hat{A}$ by first finding intermediate matrices $\hat{B}$ and $\hat{C}$, which satisfy

(3.76)
$$\Delta Q = \hat{B} \Delta W \quad \text{and} \quad \Delta F = \hat{C} \Delta W \ ,$$

and then eliminating ΔW to obtain

(3.77) $$\hat{A} = \hat{C}\hat{B}^{-1} ,$$

which satifies

(3.78) $$\Delta F = \hat{A}\Delta Q ,$$

where $\Delta(\bullet)$ is defined by eq. (3.59).

They note that for a perfect gas, Q and F are quadratic in terms of the components of W. This will not be the case for a real gas, however, since the absence of an analytical equation of state prohibits the expression of the pressure solely in terms of the components of W, as can be seen by again introducing an equivalent $\tilde{\gamma}$, defined by eq. (3.10) such that:

(3.79) $$\begin{aligned} p &= \frac{\tilde{\gamma}-1}{\tilde{\gamma}}\left(\rho H - \frac{\rho u^2}{2}\right) \\ &= \frac{\tilde{\gamma}-1}{\tilde{\gamma}}\left(w_1 w_3 - \frac{w_2^2}{2}\right) . \end{aligned}$$

The appearance of $\tilde{\gamma}$ in the expression for p complicates the use of the parameter vector in obtaining the matrices $\hat{B}$ and $\hat{C}$, which require the calculation of the jump in p, Δp, and thus the jump in $\tilde{\gamma}$, $\Delta\tilde{\gamma}$. By assuming that the jumps in $\tilde{\gamma}$ will always be relatively small, they obtain the relation:

$$\Delta p = \frac{\hat{\gamma}-1}{\hat{\gamma}}\left(\hat{w}_3\Delta w_1 - \hat{w}_2\Delta w_2 + \hat{w}_1\Delta w_3\right) + \frac{1}{\hat{\gamma}(\hat{\gamma}-1)}\hat{p}\Delta\tilde{\gamma} + O(\Delta\tilde{\gamma})^2 \quad , \tag{3.80}$$

which still requires an approximation for the term $\Delta\tilde{\gamma}$.

This was achieved by approximating the differential equation for $\tilde{\gamma}$,

$$d\tilde{\gamma} = (\tilde{\gamma}-1)\left[1-\frac{\hat{\gamma}}{\hat{\Gamma}}\right]\frac{dp}{\hat{p}} \quad , \tag{3.81}$$

developed by Colella and Glaz [34] for the isentropic flow of a real gas, by

$$\Delta\tilde{\gamma} = (\tilde{\gamma}-1)\left[1-\frac{\hat{\gamma}}{\hat{\Gamma}}\right]\frac{\Delta p}{\hat{p}} \quad , \tag{3.82}$$

where $\hat{\gamma}$ and $\hat{\Gamma}$ are the arithmetic averages

$$\hat{\gamma} = \frac{\tilde{\gamma}_L+\tilde{\gamma}_R}{2} \quad , \qquad \hat{\Gamma} = \frac{\Gamma_L+\Gamma_R}{2} \quad , \tag{3.83}$$

and Γ is again defined by:

$$\Gamma = \frac{\rho a^2}{p} \quad , \tag{3.84}$$

where a is the true sound speed defined in eq. (3.11). They further assume that $\hat{\gamma}$ is nearly equal to $\hat{\Gamma}$, such that a small parameter ε can be introduced as:

$$\varepsilon = \left(\frac{\hat{\gamma}}{\hat{\Gamma}} - 1 \right) \frac{1}{\hat{\gamma}} \quad , \tag{3.85}$$

resulting in the expression:

$$\Delta p = \frac{\hat{\gamma} - 1}{\hat{\gamma}} (1 - \varepsilon)(\hat{w}_3 \Delta w_1 - \hat{w}_2 \Delta w_2 + \hat{w}_1 \Delta w_3) \ . \tag{3.86}$$

Utilizing this definition for Δp, they obtained expressions for $\hat{B}$ and $\hat{C}$, which upon substitution into eq. (3.77) yield:

(3.87)

$$\hat{A} = \begin{bmatrix} 0 & 1 & 0 \\ [\hat{\gamma} - 3 - \varepsilon\hat{\gamma}(\hat{\gamma} - 1)] \frac{\hat{u}^2}{2} & [3 - \hat{\gamma} + \varepsilon\hat{\gamma}(\hat{\gamma} - 1)]\hat{u} & (\hat{\gamma} - 1)(1 - \varepsilon\hat{\gamma}) \\ (\hat{\gamma} - 1)(1 - \varepsilon\hat{\gamma}) \frac{\hat{u}^3}{2} - \hat{H}\hat{u} & \hat{H} - (\hat{\gamma} - 1)(1 - \varepsilon\hat{\gamma})\hat{u}^2 & [1 - \varepsilon(\hat{\gamma} - 1)]\hat{\gamma}\hat{u} \end{bmatrix} ,$$

where $\hat{u}$ and $\hat{H}$ are the usual Roe averages, defined in eqs. (3.63) and (3.68). The eigenvalues and eigenvectors of $\hat{A}$ were found to be:

$$\hat{\lambda}_{1,2,3} = \hat{u} - \hat{a} \ , \ \hat{u} \ , \ \hat{u} + \hat{a} \ , \tag{3.88}$$

and

$$\hat{e}_{1,2,3} = \begin{bmatrix} 1 \\ \hat{u} - \hat{a} \\ \hat{H} - \hat{u}\hat{a} \end{bmatrix}, \quad \begin{bmatrix} 1 \\ \hat{u} \\ \frac{\hat{u}^2}{2} \end{bmatrix}, \quad \begin{bmatrix} 1 \\ \hat{u} + \hat{a} \\ \hat{H} + \hat{u}\hat{a} \end{bmatrix}, \tag{3.89}$$

with $\hat{a}$ defined as:

$$\begin{aligned} \hat{a}^2 &= (\hat{\gamma} - 1)(1 - \varepsilon\hat{\gamma})\left(\hat{H} - \frac{\hat{u}^2}{2}\right) \\ &= \frac{(\hat{\gamma} - 1)\hat{\Gamma}}{\hat{\gamma}}\left(\hat{H} - \frac{\hat{u}^2}{2}\right). \end{aligned} \tag{3.90}$$

This formulation degenerates to the original results of Roe for the case of a perfect gas, in which $\hat{\gamma} = \hat{\Gamma} = \gamma$.

To complete the derivation of Roe's approximate Riemann solver, ΔF must be projected onto the eigenvectors of $\hat{A}$ such that

$$\Delta F = \sum_{i=1}^{3} \hat{\lambda}_i \hat{\alpha}_i \hat{e}_i , \tag{3.91}$$

where the $\hat{\alpha}_i{}'s$ are the strengths of the waves travelling with speeds $\hat{\lambda}_i$. The $\hat{\alpha}_i{}'s$, found by diagonalizing $\hat{A}$ with eqs. (3.58a), (3.58b), (3.89), and (3.90), are given by:

$$\hat{\alpha}_{1,3} = \frac{1}{2\hat{a}^2}\left[\Delta p \mp \hat{\rho}\hat{a}\Delta u\right] ,$$
$$\hat{\alpha}_2 = \frac{1}{\hat{a}^2}\left[\hat{a}^2\Delta\rho - \Delta p\right] . \tag{3.92}$$

Since this formulation corresponds to the original developement of Roe, the interface fluxes can be computed from eqs. (3.72a) and (3.73)-(3.74d), with the exception that $\hat{a}$ must be computed from eq. (3.90) rather than eq. (3.74e).

3.3.2 Roe2 - Splitting by Liou, Van Leer, and Shuen

Liou et al. [26] determined Roe's flux-difference splitting for the one-dimensional Euler equations by satisfying

$$\Delta F = \hat{A}\Delta Q , \tag{3.93a}$$

$$\hat{A} = A(\hat{Q}) , \tag{3.93b}$$

$$\hat{Q} = \hat{Q}(Q_L , Q_R) , \tag{3.93c}$$

where $\Delta(\bullet)$ is defined by eq. (3.59) and the flux Jacobian A is given by eq. (3.8). To define the matrix $\hat{A}$, they sought expressions for the independent averages $\hat{\rho}$, $\hat{u}$, $\hat{e}$, $\hat{H}$, $\hat{p}_e$, and $\hat{p}_\rho$. Noting that the mass-flux equation in (3.93a) is auto-

matically satisfied for any average state, they chose to satisfy the momentum-flux equation with:

$$\Delta\rho u = \hat{\rho}\Delta u + \hat{u}\Delta\rho \ , \tag{3.94}$$

$$\Delta\rho u^2 = 2\hat{\rho}\hat{u}\Delta u + \hat{u}^2\Delta\rho \ . \tag{3.95}$$

These two equations can only be satisfied with the averages $\hat{u}$ and $\hat{\rho}$ previously defined by eqs. (3.63) and (3.64), respectively. By assuming that

$$\Delta\rho e = \hat{\rho}\Delta e + \hat{e}\Delta\rho \ , \tag{3.96}$$

which is satisfied by:

$$\hat{e} = \frac{\rho_L^{1/2} e_L + \rho_R^{1/2} e_R}{\rho_L^{1/2} + \rho_R^{1/2}} \ , \tag{3.97}$$

the second equation of (3.93a) becomes:

$$RHS = \Delta\rho u^2 + (\hat{p}_e \Delta e + \hat{p}_\rho \Delta\rho) \ ,$$
$$LHS = \Delta\rho u^2 + \Delta p \ ,$$

which leads to the expression:

$$\Delta p = \hat{p}_e \Delta e + \hat{p}_\rho \Delta\rho \ . \tag{3.98}$$

The third equation of (3.93a) is satisfied by setting:

$$\Delta\rho u H = \hat{p}\hat{H}\Delta u + \hat{u}\Delta\rho H \ , \tag{3.99}$$

with $\hat{H}$ defined by eq. (3.68).

Liou et al. note that while the relation of total enthalpy H to the other flow quantities holds pointwise, it does not necessarily hold for the average state quantities. Similarily, while $p = p(\rho , e)$, it does not necessarily follow that $\hat{p} = \hat{p}(\hat{\rho} , \hat{e})$. Likewise, $\hat{p}_e$ and $\hat{p}_\rho$ must be defined separately from p_e and p_ρ. They proposed a formula that used derivative information at the average state $(\hat{\rho} , \hat{e})$ by introducing the intermediate states:

$$\bar{p}_\rho = p_\rho(\hat{\rho} , \hat{e}) , \qquad \bar{p}_e = p_e(\hat{\rho} , \hat{e}) , \tag{3.100}$$

and dividing the residual of (3.98), i.e.

$$\delta p = \Delta p - \bar{p}\rho\Delta\rho - \bar{p}e\Delta e ,$$

equally over the terms $\hat{p}_e$ and $\hat{p}_\rho$ such that:

$$\begin{aligned} \hat{p}_\rho\Delta\rho &= \bar{p}_\rho\Delta\rho + 0.5\delta p \\ \hat{p}_e\Delta\rho &= \bar{p}_e\Delta e + 0.5\delta p . \end{aligned}$$

This results in the expressions:

$$\begin{aligned} \hat{p}_e &= \frac{1}{2}\left[\frac{(\Delta p - \bar{p}_\rho\Delta\rho)}{\Delta e} + \bar{p}_e \right] , \\ \hat{p}_\rho &= \frac{1}{2}\left[\frac{(\Delta p - \bar{p}_e\Delta e)}{\Delta\rho} + \bar{p}_\rho \right] , \end{aligned} \tag{3.101a}$$

when $\Delta e \neq 0$, $\Delta\rho \neq 0$, respectively, and

(3.101*b*)

$$\hat{p}_e = \overline{p}_e \ ,$$
$$\hat{p}_\rho = \overline{p}_\rho \ ,$$

when $\Delta e = 0$, $\Delta\rho = 0$, respectively. The choices for $\hat{p}_e$ and $\hat{p}_\rho$ were made by this author, as no such provision was made in ref. [26].

Although explicit definitions for $\hat{p}$ and $\hat{a}$ are not needed to obtain the averages $\hat{\rho}$, $\hat{u}$, $\hat{e}$, $\hat{H}$, $\hat{p}_e$, and $\hat{p}_\rho$, used to evaluate the average flux Jacobian matrix $\hat{A}$, they are needed for its diagonalization. Using eqs (3.117) and (3.118e) to define $\hat{a}$ and $\hat{p}$, respectively, the flux-difference splitting by Liou et al. was found to be exactly the same as Glaister's, e.g. eq. (3.122), with the exception that $\hat{p}_e$ and $\hat{p}_\rho$ are now defined by eqs. (3.101a) and (3.101b).

3.3.3 Roe3 - Splitting by Vinokur and Liu

Vinokur and Liu [27] developed their flux-difference splitting by also seeking appropriate averages that would satisfy eqs. (3.93a)-(3.93c). As a result, they obtained the relationships of eqs (3.74a)-(3.74d) for $\hat{\rho}$, $\hat{u}$, $\hat{v}$, and $\hat{H}$, respectively. However, by defining their equation of state with eq. (3.27a) rather than eq. (2.2), they obtained the following expressions for the Roe-average sound speed, $\hat{a}$ such that:

(3.102) $$\hat{a}^2 = \hat{\chi} + \hat{\kappa}\hat{h} \ ,$$

and the jump in p, Δp such that:

(3.103) $$\Delta p = \hat{\chi}\Delta\rho + \hat{\kappa}\Delta \epsilon \ .$$

Although these expressions appear simple enough, the formation of the averages $\hat{\chi}$, $\hat{\kappa}$, and $\hat{h}$ are quite cumbersome. Utilizing the definitions of eqs. (3.74b) and (3.74d), $\hat{h}$ is readily found to be:

(3.104) $$\hat{h} = \frac{\rho_L^{1/2} h_L + \rho_R^{1/2} h_R}{\rho_L^{1/2} + \rho_R^{1/2}} + \frac{1}{2} \frac{\hat{\rho}(\Delta u)^2}{\rho_L + 2\hat{\rho} + \rho_R} \ .$$

Vinokur and Liu note that $\hat{h}$ could lie outside the range of h_L and h_R if Δu is sufficiently large. The values of $\hat{\chi}$ and $\hat{\kappa}$ were obtained by projecting the average state given by R and L onto the straight line defined by eq. (3.103), which yields:

(3.105*a*) $$\frac{1}{\hat{\kappa}} = \frac{D\Delta\rho + \Delta \epsilon \Delta p}{\Delta p^2 + \bar{a}^4 \Delta\rho^2} \ ,$$

where the arithmetically averaged sound speed, $\bar{a}$, is defined as:

(3.105*b*) $$\bar{a}^2 = \frac{1}{2}\left(a_L^2 + a_R^2\right) \ ,$$

and the coefficient D as:

$$(3.105c) \qquad D = \frac{1}{2}\left(\frac{\chi_L}{\kappa_L} + \frac{\chi_R}{\kappa_R}\right)\Delta p + \frac{1}{2}\left(\frac{1}{\kappa_L} + \frac{1}{\kappa_R}\right)\bar{a}^4\Delta\rho \ .$$

Since eq. (3.105a) becomes indeterminate for $\Delta\rho,\ \Delta p \to 0$, as is the case for the freestream, the roe-averages for $\hat{\kappa}$ and $\hat{\chi}$ were formed by evaluating eqs. (3.27b) and (3.27c) at the left states.

3.3.4 Roe4 - Splitting by Glaister

Glaister [28], following a similar course of reasoning as that used by Roe and Pike [36] for an ideal gas, developed an approximate Riemann solver for the one-dimensional Euler equations with a general convex equation of state, i.e. eq. (2.4). The one-dimensional flux Jacobian A was defined:

$$(3.106) \quad A = \begin{bmatrix} 0 & 1 & 0 \\ a^2 - u^2 - \frac{p_e}{\rho}(H - u^2) & 2u - \frac{up_e}{\rho} & \frac{p_e}{\rho} \\ u(a^2 - H) - \frac{up_e}{\rho}(H - u^2) & H - \frac{u^2 p_e}{\rho} & u(1 + \frac{p_e}{\rho}) \end{bmatrix} ,$$

with eigenvalues λ_i such that:

$$(3.107) \qquad \lambda_{1,2,3} = u + a,\ u - a,\ u \ ,$$

and right eigenvectors e_i:

$$(3.108)\qquad e_1 = \begin{bmatrix} 1 \\ u+a \\ H+ua \end{bmatrix}, \quad e_2 = \begin{bmatrix} 1 \\ u-a \\ H-ua \end{bmatrix}, \quad e_3 = \begin{bmatrix} 1 \\ u \\ H-\dfrac{\rho a^2}{p_e} \end{bmatrix},$$

where a is defined by eq. (3.22a) and p_e , p_ρ are defined by eq. (3.9).

As in the work by Roe and Pike, Glaister sought coefficients α_1 , α_2 , and α_3 such that for states Q_L , Q_R close to an average state Q, the relation:

$$(3.109)\qquad \Delta Q = \sum_{j=1}^{3} \alpha_j e_j$$

would be accurate within $O(\Delta^2)$, where $\Delta(\bullet)$ is defined by eq. (3.59). Expanding eq. (3.109) yields the following algebraic relations:

$$(3.110a)\qquad \Delta\rho = \alpha_1 + \alpha_2 + \alpha_3 ,$$

$$(3.110b)\qquad \Delta(\rho u) = \alpha_1(u+a) + \alpha_2(u-a) + \alpha_3 u ,$$

$$(3.110c)\qquad \Delta(\rho E) = \alpha_1(H+au) + \alpha_2(H-au) + \alpha_3(H-\frac{\rho a^2}{p_e}) .$$

Utilizing eq. (3.22a), eqs. (3.110a)-(3.110c) can be solved simultaneously such that:

$$(3.111a)\qquad \alpha_1 = \frac{1}{2a^2}(\Delta p + \rho a \Delta u) ,$$

(3.111*b*)
$$\alpha_2 = \frac{1}{2a^2}(\Delta p - \rho a \Delta u) \ ,$$

(3.111*c*)
$$\alpha_3 = \Delta\rho - \frac{\Delta p}{a^2} \ .$$

It can easily be verified that these α_i also satisfy:

(3.112)
$$\Delta F = \sum_{i=1}^{3} \lambda_i \alpha_i e_i \ .$$

For the general case of two arbitrary states Q_L , Q_R that are not necessarily close, Glaister found averages $\hat{\rho}$, $\hat{u}$, $\hat{e}$, $\hat{p}$, $\hat{p}_\rho$, $\hat{p}_e$ in terms of the states Q_L , Q_R that satisfied the relations:

(3.113*a*)
$$\Delta Q = \sum_{j=1}^{3} \hat{\alpha}_j \hat{e}_j \ ,$$

(3.113*b*)
$$\Delta F = \sum_{i=1}^{3} \hat{\lambda}_i \hat{\alpha}_i \hat{e}_i \ ,$$

where

(3.114)
$$\hat{\lambda}_{1,2,3} = \hat{u} + \hat{a} \ , \ \hat{u} - \hat{a} \ , \ \hat{u} \ ,$$

$$\hat{e}_{1,2,3} = \begin{bmatrix} 1 \\ \hat{u} + \hat{a} \\ \hat{H} + \hat{u}\hat{a} \end{bmatrix}, \begin{bmatrix} 1 \\ \hat{u} - \hat{a} \\ \hat{H} - \hat{u}\hat{a} \end{bmatrix}, \begin{bmatrix} 1 \\ \hat{u} \\ \hat{H} - \frac{\hat{\rho}\hat{a}^2}{\hat{p}_e} \end{bmatrix}, \tag{3.115}$$

$$\hat{\alpha}_1 = \frac{1}{2a^2}(\Delta p + \hat{\rho}\hat{a}\Delta u) , \tag{3.116a}$$

$$\hat{\alpha}_2 = \frac{1}{2a^2}(\Delta p - \hat{\rho}\hat{a}\Delta u) , \tag{3.116b}$$

$$\hat{\alpha}_3 = \Delta\rho - \frac{\Delta p}{\hat{a}^2} , \tag{3.116c}$$

and

$$\hat{a}^2 = \frac{\hat{p}\hat{p}_e}{\hat{\rho}^2} + \hat{p}_\rho . \tag{3.117}$$

With sufficient algebraic manipulation of eqs. (3.113a) and (3.113b), the following averages are obtained:

$$\hat{\rho} = (\rho_L \rho_R)^{1/2} , \tag{3.118a}$$

$$\hat{u} = \frac{\rho_L^{1/2} u_L + \rho_R^{1/2} u_R}{\rho_L^{1/2} + \rho_R^{1/2}} , \tag{3.118b}$$

$$\hat{e} = \frac{\rho_L^{1/2} e_L + \rho_R^{1/2} e_R}{\rho_L^{1/2} + \rho_R^{1/2}} , \tag{3.118c}$$

(3.118*d*)
$$\hat{H} = \frac{\rho_L^{1/2} H_L + \rho_R^{1/2} H_R}{\rho_L^{1/2} + \rho_R^{1/2}} \ ,$$

(3.118*e*)
$$\hat{p} = \hat{\rho}\left(\hat{H} - \hat{e} - \frac{1}{2}\hat{u}^2\right) \ ,$$

with the jump in p defined:

(3.119)
$$\Delta p \ = \ \hat{p}_e \Delta e + \hat{p}_\rho \Delta \rho \ .$$

Thus, the only differences between Glaister's and the perfect gas approximate Riemann solver are the presence of the terms $\hat{p}_e$ and $\hat{p}_\rho$, which he chose to approximate by:

(3.120*a*)
$$\begin{aligned} \hat{p}_e \ &= \ \frac{1}{\Delta e}\left(\frac{1}{2}\left[p(\rho_R\,, e_R) + p(\rho_L\,, e_R)\right] - \frac{1}{2}\left[p(\rho_R\,, e_L) + p(\rho_L\,, e_L)\right]\right) \\ \hat{p}_\rho \ &= \ \frac{1}{\Delta \rho}\left(\frac{1}{2}\left[p(\rho_R\,, e_R) + p(\rho_R\,, e_L)\right] - \frac{1}{2}\left[p(\rho_L\,, e_R) + p(\rho_L\,, e_L)\right]\right) \ , \end{aligned}$$

if $\Delta e \neq 0$, $\Delta \rho \neq 0$, respectively, and

(3.120*b*)
$$\begin{aligned} \hat{p}_e \ &= \ \frac{1}{2}\left[p_e(\rho_L\,, e) + p_e(\rho_R\,, e)\right] \\ \hat{p}_\rho \ &= \ \frac{1}{2}\left[p_\rho(\rho\,, e_L) + p_\rho(\rho\,, e_R)\right] \ , \end{aligned}$$

if $\Delta e = 0$, $\Delta \rho = 0$, respectively.

Glaister notes that if the equation of state can be separated into a series of terms such that $p = R(\rho)\mathrm{E}(e)$ where R, E depend soley on ρ, e, respectively, then eqs. (3.120a) and (3.120b) become

$$\hat{p}_e = \begin{cases} \overline{R}\,\dfrac{\Delta \mathrm{E}}{\Delta e} & \text{if } \Delta e \neq 0 \\ \overline{R}\mathrm{E}'(e) & \text{if } \Delta e = 0 \ , \end{cases} \tag{3.121a}$$

$$\hat{p}_\rho = \begin{cases} \overline{\mathrm{E}}\,\dfrac{\Delta R}{\Delta \rho} & \text{if } \Delta \rho \neq 0 \\ \overline{\mathrm{E}}R'(\rho) & \text{if } \Delta \rho = 0 \ , \end{cases} \tag{3.121b}$$

where $\Delta(\bullet) = (\bullet)_R - (\bullet)_L$, as before, and $(\bar{\bullet}) = \dfrac{1}{2}[(\bullet)_L + (\bullet)_R]$, the arithmetic mean.

With the averages of eqs. (3.116a)-(3.121b), the full flux can be obtained from eqs. (3.)-(3.) with the two-dimensional flux-difference splitting, $\Delta\hat{F}_i$, now given by:

$$
\left|\Delta\hat{F}_1\right| = |\hat{u}| \begin{bmatrix} \Delta\rho - \dfrac{\Delta p}{\hat{a}^2} \\ \hat{u}\left(\Delta\rho - \dfrac{\Delta p}{\hat{a}^2}\right) \\ \hat{v}\left(\Delta\rho - \dfrac{\Delta p}{\hat{a}^2}\right) + \hat{\rho}\Delta v \\ \left(\Delta\rho - \dfrac{\Delta p}{\hat{a}^2}\right)\left(\hat{H} - \dfrac{\hat{\rho}\hat{a}^2}{\hat{p}_e}\right) + \hat{\rho}\hat{v}\Delta v \end{bmatrix}
$$

(3.122)

$$
\left|\Delta\hat{F}_{2,3}\right| = |\hat{u} \pm \hat{a}| \left\{ \frac{\Delta p \pm \hat{\rho}\hat{a}\Delta u}{2\hat{a}^2} \right\} \begin{bmatrix} 1 \\ \hat{u} \pm \hat{a} \\ \hat{v} \\ \hat{H} \pm \hat{u}\hat{a} \end{bmatrix},
$$

with $\hat{v}$ given by eq. (3.74c).

3.4 Extension to Generalized Coordinates - An Example

The extension to generalized coordinates is easily obtained by incorporating the results of section 2.4 with the various flux-splittings detailed in sections 3.1.1 through 3.3.4. For an example, the Van Leer flux-vector splitting of Grossman and Walters (VL1) is considered.

Noting that eq (3.38) is in a form similar to eq. (2.24), eq. (2.29) can be applied directly to eq. (3.40), yielding the result:

$$(3.123a) \qquad F^{*\pm} = \frac{\left|\vec{\nabla}\xi\right|}{J}\begin{bmatrix} f_1^{\pm} \\ f_1^{\pm}[(\tilde{\gamma}-1)\bar{u} \pm 2\tilde{a}]/\tilde{\gamma} \\ f_1^{\pm} v^{*} \\ f_1^{\pm}\left\{ \dfrac{[(\tilde{\gamma}-1)\bar{u} \pm 2\tilde{a}]^2}{2(\tilde{\gamma}^2-1)} + \dfrac{1}{2} v^2 \right\} \end{bmatrix},$$

with

$$(3.123b) \qquad f_1^{\pm} = \pm \frac{\rho \tilde{a}}{4}\left(\frac{\bar{u}}{\tilde{a}} \pm 1\right)^2 .$$

Utilizing eqs. (2.32) and (2.23), the split flux $\bar{f}_2^{\pm}$ can be expressed as:

$$(3.124) \qquad \bar{f}_2^{\pm} = \frac{\left|\vec{\nabla}\xi\right|}{J} f_1^{\pm}\left\{ \frac{[(\tilde{\gamma}-1)\bar{u} \pm 2\tilde{a}]}{\tilde{\gamma}} \bar{\xi}_x - v^{*}\bar{\xi}_y \right\} .$$

Substituting $\bar{u}$ and v^{*} from eqs. (2.12a) and (2.25) into eq. (3.124) yields:

(3.125*a*)

$$\bar{f}_2^{\pm} = \frac{\left|\vec{\nabla}\xi\right|}{J} f_1^{\pm}\left\{ \left(\frac{-\bar{u} \pm 2\tilde{a}}{\tilde{\gamma}} \right)\bar{\xi}_x + (u\bar{\xi}_x + v\bar{\xi}_y)\bar{\xi}_x - (-u\bar{\xi}_y + v\bar{\xi}_x)\bar{\xi}_y \right\} ,$$

which can be simplified to obtain:

(3.125c)
$$\bar{f}_2^{\pm} = \frac{|\vec{\nabla}\xi|}{J} f_1^{\pm}\left[\frac{-\bar{u} \pm 2\tilde{a}}{\tilde{\gamma}}\bar{\xi}_x + u\right].$$

Similarily, the split flux $\bar{f}_3^{\pm}$ can be expressed as:

(3.126a)
$$\bar{f}_2^{\pm} = \frac{|\vec{\nabla}\xi|}{J} f_1^{\pm}\left\{\left(\frac{-\bar{u} \pm 2\tilde{a}}{\tilde{\gamma}}\right)\bar{\xi}_y + (u\bar{\xi}_x + v\bar{\xi}_y)\bar{\xi}_y - (-u\bar{\xi}_y + v\bar{\xi}_x)\bar{\xi}_x\right\},$$

which can also be simplified to obtain:

(3.126b)
$$\bar{f}_2^{\pm} = \frac{|\vec{\nabla}\xi|}{J} f_1^{\pm}\left[\frac{-\bar{u} \pm 2\tilde{a}}{\tilde{\gamma}}\bar{\xi}_y + v\right].$$

Thus the generalized split-flux is expressed as:

(3.127)
$$\bar{F}^{\pm} = \frac{|\vec{\nabla}\xi|}{J}\begin{bmatrix} f_1^{\pm} \\ f_1^{\pm}[u + \left(\frac{-\bar{u} \pm 2\tilde{a}}{\tilde{\gamma}}\right)\bar{\xi}_x] \\ f_1^{\pm}[v + \left(\frac{-\bar{u} \pm 2\tilde{a}}{\tilde{\gamma}}\right)\bar{\xi}_y] \\ f_1^{\pm}\left\{\frac{[(\tilde{\gamma}-1)\bar{u} \pm 2\tilde{a}]^2}{2(\tilde{\gamma}^2-1)} + \frac{v^2}{2}\right\} \end{bmatrix},$$

which contains none of the rotation tensor terms, e.g. v^* or η^*.

IV. RESULTS AND DISCUSSION

4.1 Solution Algorithm

The various flux algorithms were implemented in a general, two-dimensional finite volume, flux split computer code called ANSERS, developed at V.P.I. & S.U. by Prof. R. W. Walters. Originally, the code only contained perfect gas versions of Van Leer's [23] and Roe's [21] flux-splitting algorithms. Included in the code are various time integration and relaxation schemes, such as vertical/horizontal line Gauss-Seidel (VLGS/HLGS), Runge-Kutta, Approximate Factorization (AF), and a space-marching algorithm based on line Gauss-Seidel iteration. All of the algorithms in the code are in a cell-centered, finite volume formulation in general curvilinear coordinates.

The flux calculations at cell faces were computed using MUSCL differencing, i.e. the conserved variables Q were extrapolated to the cell interfaces , in an upwind

or upwind biased direction, prior to calculating the fluxes, as opposed to non-MUSCL differencing in which the fluxes themselves must be extrapolated. Values of the conserved variables at the cell faces were obtained by extrapolating the variable $\overline{Q}_e = [\rho,\ \rho u,\ \rho v,\ p,\ \tilde{\gamma},\ \Gamma]^T$ from the cell centers to the cell faces, as in refs. [6, 25], by the use of:

$$
\begin{aligned}
[Q_e^-]_{i+1/2,\,j} &= \left\{ I + \frac{1}{4}[(1-\sigma)\nabla + (1+\sigma)\Delta] \right\} Q_{e_{i,\,j}} \\
[Q_e^+]_{i+1/2,\,j} &= \left\{ I - \frac{1}{4}[(1+\sigma)\nabla + (1-\sigma)\Delta] \right\} Q_{e_{i+1,\,j}} ,
\end{aligned}
\tag{4.1}
$$

where

$$
\begin{aligned}
\Delta Q_{e_{i,\,j}} &= Q_{e_{i+1,\,j}} - Q_{e_{i,\,j}} \\
\nabla Q_{e_{i,\,j}} &= Q_{e_{i,\,j}} - Q_{e_{i-1,\,j}} ,
\end{aligned}
\tag{4.2}
$$

and σ controls the spatial accuracy of the scheme.

The flux-splitting in the ξ – direction is based on the testing of the Mach number:

$$
\overline{\mathrm{M}}_\xi = \frac{\bar{u}}{a} ,
\tag{4.4}
$$

where $\bar{u}$ is the contravariant velocity component at the cell face normal to a line of constant ξ, defined in eq. (2.7a), and a is the sound speed associated with a given splitting, i.e. SW1, VL1, etc. A similar relation holds for the η – direction.

The partial derivatives p_e and p_ρ, required by several of the flux algorithms, were obtained by analytically differentiating the pressure curve fit of reference [30].

4.2 Supersonic Inlet Problem

Initially, the flux-splitting algorithms were tested on a high temperature internal flow through a simple inlet, which consisted of a 10° compression followed by a 10° expansion, both of which were symmetric with respect to the centerline. The lower half of the symmetry plane was modeled with a grid that contained 201 points in the axial direction and 51 points in the normal direction. The grid was exponentially stretched near the compression and expansion corners in the axial direction and was clustered near the wall in the normal direction, as shown in Fig. 4, in order to more accurately resolve the oblique shock and the expansion fan. At the inflow boundary, all thermodynamic properties were held fixed at the reference conditions of $M_\infty = 5$, $p_\infty = 1$atm., and $T_\infty = 3573$°K. Since the outflow is supersonic, no conditions were required, and all properties were extrapolated from the interior. On the surface, wall tangency was imposed along with requiring that the values of enthalpy, pressure, and entropy be set equal to the first cell-centered value off the wall. Along the grid centerline, symmetry conditions were enforced. In the axial direction, second order upwind MUSCL differencing ($\sigma = -1$) was used to extrapolate the variable Q_e from the cell centers to the cell faces, while third-order upwind biased MUSCL differencing ($\sigma = 1/3$)

was used in the normal direction for all cases. A so-called *catastrophic* limiter was used to reduce the spurious oscillations associated with higher-order shock capturing schemes. This limiter reduced the accuracy of the scheme to first order in space in regions of large gradients, when a higher accuracy would result in a negative pressure.

Since the flow remains supersonic throughout the inlet, the solution was obtained using the space-marching algorithm contained in ANSERS. This algorithm would take an incremental step in the axial direction and perform VLGS until a specified convergence was achieved before taking the next axial step. The convergence criteria for all cases was that the normalized residual be reduced to at least 5.E-03. All ten algorithms exhibited similar convergence rates, in terms of the number of iterations required per station. On average, 9 iterations were required per axial station.

The surface temperature distribution is plotted in Fig. 5 for the Steger-Warming-type flux-vector split scheme, the Van Leer-type flux-vector split scheme, and the Roe-type flux-difference split scheme, all from Grossman and Walters [25]. All solutions show excellent agreement with respect to the exact equilibrium air solution shock and expansion locations, and good agreement with regard to the post-shock and post-expansion temperature levels. Only small variations in the solutions from these methods are distinguishable. The post-shock region of Fig. 5 is shown on an expanded temperature scale and an expanded axial scale in Fig. 6. The axial scale is expanded by plotting versus station num-

ber rather than x/L, thereby increasing the spacing at the compression and expansion corners, where the grid was stretched exponentially. Although the differences in the solution are not significant, it is interesting to note that the Steger-Warming-type and the Van Leer-type flux-vector splitting results are very similar. Between similar splitting types, the differences between the temperature solutions are nearly indistinguishable. The surface temperature distributions for the three different Steger-Warming type schemes, SW1, SW2, and SW3, are plotted in Fig. 7. The results from the three different Van Leer-type schemes, VL1, VL2, and VL3, are presented in Fig. 8, and the results from the four Roe-type flux-difference schemes are given in Fig. 9. Similar results are obtained for the other flow variables, as can be seen in the plot of surface pressure distribution, Fig. 10, for the three schemes SW1, VL1, and Roe1 by Grossman and Walters [25]. The temperature contour for the supersonic inlet problem is given in Fig. 11 while the pressure contour is given in Fig. 12. In summary, no significant variations between the various splittings are discernable for this problem.

4.2 Hypersonic Blunt Body Problem

Since very little difference was observed in the solutions for a completely supersonic flow, the test case of hypersonic flow over a cylindrical nose followed by a 5° compression ramp was considered since it would contain a subsonic flow re-

gion. The inclusion of a subsonic region prohibited using the space-marching algorithm. Consequently the global iteration strategy of VLGS, which requires considerablly more computations, was utilized to test the flux-splitting algorithms. As a result, a relatively coarse grid of 81 points tangent to the surface and 41 points normal to the surface, as shown in Fig. 13, was used. The grid was slightly clustered near the surface. On the inflow boundary, all thermodynamic properties were held fixed at the reference conditions of $M_\infty = 24.5$, $p_\infty = 52.63$ pa., and $T_\infty = 268.57°K$. Along the symmetry line and on the surface, wall tangency was imposed along with requiring that the values of enthalpy, pressure, and entropy be set equal to the first cell-centered value off the wall. Again, since the outflow boundary is supersonic, all properties were extrapolated from the interior. In both the normal and tangential directions, first-order MUSCL differencing was utilized to extrapolate the variable Q_e from the cell centers to the cell faces for all cases. Attempts were made to obtain a third-order spatially-accurate solution on the grid in Fig. 13 by using converged first-order solutions for initial conditions. However, the normalized residual would rise and then sporadically increase and decrease, with no set pattern. Other authors [37] have noted that solutions to extremely high Mach number flows are extremely difficult to obtain. Although not presented, solutions were obtained for both first-order and third-order upwind biased MUSCL differencing for the test case with freestream conditions of $M_\infty = 15.0$, $p_\infty = 52.63$pa., and $T_\infty = 268.57°K$. Since freestream conditions were specified everywhere for initial conditions, the initial time step was restricted

to a value of 0.0005. Larger time steps immediately produced negative pressures. This restriction resulted in a drastic increase in the number of iterations required for convergence, which was on the order of 6000 for VL1. As such, it was decided to use a converged solution from VL1 as the initial condition for all of the other algorithms. It was determined that a time step of 0.0005 could be used to start both a Steger-Warming-type scheme and a Roe-type scheme from freestream conditions. All the comparisons of the methods for this $M_\infty = 24.5$ hypersonic blunt body problem were done with first-order spatial accuracy. It is expected that the conclusions regarding the comparison of the methods will also hold for higher spatial accuracies.

The symmetry line temperature distribution is plotted in Fig. 14 the Stéger-Warming-type flux-vector split scheme, the Van Leer-type flux-vector split scheme, and the Roe-type flux-difference split scheme, all by Grossman and Walters [25]. The results of Fig. 14 indicate a crisply captured bow shock. In Fig. 19, the surface temperature distribution is plotted for the Steger-Warming-type flux-vector split scheme, the Van Leer-type flux-vector split scheme, and the Roe-type flux-difference split scheme, all by Grossman and Walters [25]. Again, no significant differences are observed between the three different schemes, other than the appearance of a *glitch* in the temperature distribution in the Steger-Warming type solution of Fig. 19 at sonic conditions, a previously documented result [14]. It should be noted that in order to compute this case with the Roe-type splitting, a form of artificial viscosity had to be incorporated in the form of

adding a small number ε to the wave speeds λ_i [38]. Thus, the values $|\hat{u}|$ and $|\hat{u} \pm \hat{a}|$ in eqs. (3.72b), (3.73), and (3.122) were actually defined as:

$$
\begin{aligned}
|\lambda_1| &= |\hat{u}| + \varepsilon \\
|\lambda_{2,3}| &= |\hat{u} \pm \hat{a}| + \varepsilon
\end{aligned}
\tag{4.5}
$$

The surface temperature distribution, determined using the Roe1 algorithm, is plotted in Fig. 24 for the values of $\varepsilon = 0.05,\ 0.10,$ and 0.15 . Although from this plot it is evident that the choice of $\varepsilon = 0.05$ exhibits the least amount of dissipation, it aslo exhibits an undesired jump. Thus, the choice of $\varepsilon = 0.1$ was used to modify all of the Roe-type flux-difference schemes. The results from the three Steger-Warming-type schemes, SW1, SW2, and SW3, are plotted in Fig. 15 for the symmetry line temperature distribution and in Fig. 20 for the surface temperature distribution. The results from the three Van Leer-type schemes, VL1, VL2, and VL3, are plotted in Fig. 16 for the symmetry line temperature distribution and in Fig. 21 for the surface temperature distribution. The results from the four Roe-type schemes, Roe1, Roe2, Roe3, and Roe4, are plotted in Fig. 17 for the symmetry line temperature distribution and in Fig. 22 for the surface temperature distribution. Again, very little variation is seen between solutions of the same splitting type. The same conclusion of little variation in solution can be made for the other flow variables, as indicated by the plots of symmetry line pressure distribution, Fig. 18, and surface pressure distribution, Fig. 23, for the three schemes SW1, VL1, and Roe1 by Grossman and Walters [25]. The tem-

perature contour for the hypersonic blunt body problem is given in Fig. 25 while the pressure contour is given in Fig. 26.

V. CONCLUSIONS

Of the ten algorithms tested, no significant variations were observed between the the various solutions, other than the presence of a *glitch* at sonic points for all of the Steger-Warming-type flux-vector splittings. With regard to programming ease and efficiency, the algorithms of Grossman and Walters [25] are clearly superior, as indicated in the derivations of chapter 3 for the following reasons:

(i) They do not require the additional calculation of the variables p_e and p_ρ, which are utilized in all of the other flux-splitting algorithms.

(ii) Their formulation of the Roe-type flux difference scheme is the only one that does not require separate evaluations for cases when $\Delta\rho$ or Δe are near zero.

(iii) All of their splittings are formulated exactly like the perfect gas versions, with the real gas effects being incorporated by the the use of a variable ratio of specific heats, $\tilde{\gamma}$, and an equivalent

sound speed, $\tilde{a}$. A concern of some of the references [26-28] was that the splittings of Grossman and Walters [6,25], based on an equivalent Mach number, would inaccurately split the flux. The comparisons of figs. 7-9, 13-15, and 18-20 indicate that this is not the case.

With regard to the Steger-Warming-type flux-vector split schemes, the most cumbersome formulation was SW2 by Liou et al., in which the pseudo flux-splitting of $F^{\pm} = F_h^{\pm} + 0.5F'$ was utilized. The SW3 splitting of Vinokur and liu was very similar to the SW1 splitting of Grossman and Walters, the main differences being the definition of the ratio of specific heats, the sound speed, and the energy flux associated with the wave speed $\lambda_1 = u$.

In regard to the Van Leer-type flux-vector splitting schemes, the only differences between the three algorithms occurred in the formulation of the energy flux and again the definitions of the sound speed and the ratio of specific heats.

The greatest variation among algorithms of the same type occurred for the Roe-type flux-difference splitting. All of the algorithms except Roe1 by Grossman and Walters required Roe-averaged partial derivatives of the pressure with respect to density and energy, i.e. $\hat{p}_\rho$ and $\hat{p}_e$. The most complicated of these averagings was that of Vinokur and Liu, due partially to their choice of the state equation as $p = p(\rho,\ \rho e)$ rather than $p = p(\rho,\ e)$. All of the proposed averages require a "fix" when $\Delta\rho$ or $\Delta e \to 0$ Vinokur and Liu [27] stated that their method was valid when either Δe or $\Delta\rho \to 0$. However, if $\Delta\rho,\ \Delta p \to 0$ at the same time,

as in the freestream, their choice for $\hat{\kappa}$ becomes undefined. A similar problem occurs for the choice of $\hat{p}_e$ when $\Delta e \to 0$ and $\hat{p}_\rho$ when $\Delta\rho \to 0$ in the definitions by Liou et al. [26]. The only author that recognized this problem and included his own fix was Glaister [28], who proposed arithmetic averaging of the derivatives after evaluation at the left and right states. However, his computations for p_ρ and p_e required the greatest number of calls to the thermodynamic curve fits, and thus the greatest amount of CPU time.

For future consideration, these methods should be compared on a viscous test problem. Also, they should be tested with other equilibrium chemistry models.

APPENDIX A

The flux Jacobian A is defined as:

$$(A.1) \qquad A = \frac{\partial F}{\partial Q} = \begin{bmatrix} \frac{\partial f_1}{\partial q_1} & \frac{\partial f_2}{\partial q_1} & \frac{\partial f_3}{\partial q_1} & \frac{\partial f_4}{\partial q_1} \\ \frac{\partial f_1}{\partial q_2} & \frac{\partial f_2}{\partial q_2} & \frac{\partial f_3}{\partial q_2} & \frac{\partial f_4}{\partial q_2} \\ \frac{\partial f_1}{\partial q_3} & \frac{\partial f_2}{\partial q_3} & \frac{\partial f_3}{\partial q_3} & \frac{\partial f_4}{\partial q_3} \\ \frac{\partial f_1}{\partial q_4} & \frac{\partial f_2}{\partial q_4} & \frac{\partial f_3}{\partial q_4} & \frac{\partial f_4}{\partial q_4} \end{bmatrix},$$

where

$$(A.2) \qquad Q = \begin{bmatrix} q_1 \\ q_2 \\ q_3 \\ q_4 \end{bmatrix} = \begin{bmatrix} \rho \\ \rho u \\ \rho v \\ \rho E \end{bmatrix}$$

and

$$(A.3) \qquad F = \begin{bmatrix} f_1 \\ f_2 \\ f_3 \\ f_4 \end{bmatrix} = \begin{bmatrix} \rho u \\ \rho u^2 + p \\ \rho uv \\ u(\rho E + p) \end{bmatrix} = \begin{bmatrix} q_2 \\ \dfrac{q_2^2}{q_1} + p \\ \dfrac{q_2 q_3}{q_1} \\ \dfrac{q_2(q_4 + p)}{q_1} \end{bmatrix} ,$$

with

$$(A.4) \qquad E = e + \frac{u^2 + v^2}{2}$$

and

$$(A.5) \qquad p = p(\rho, e) .$$

Inspection of eq. (A.4) indicates that:

$$(A.6) \qquad e = \frac{q_4}{q_1} - \frac{q_2 + q_3}{2{q_1}^2} ,$$

and consequently that:

$$(A.7) \qquad p = p[\rho(q_1), e(q_1, q_2, q_3, q_4)] .$$

Hence, the partial derivatives of p with respect to q_i can be expressed as:

$$(A.8) \qquad \frac{\partial p}{\partial q_1} = \frac{\partial p}{\partial \rho} + \frac{\partial e}{\partial \rho} = p_\rho + \frac{1}{\rho}\left(\frac{u^2 + v^2}{2} - e\right)p_e$$

$$\frac{\partial p}{\partial q_2} = \frac{\partial p}{\partial e}\frac{\partial e}{\partial(\rho u)} = -\frac{u}{\rho}p_e \tag{A.9}$$

$$\frac{\partial p}{\partial q_3} = \frac{\partial p}{\partial e}\frac{\partial e}{\partial(\rho v)} = -\frac{v}{\rho}p_e \tag{A.10}$$

$$\frac{\partial p}{\partial q_3} = \frac{\partial p}{\partial e}\frac{\partial e}{\partial(\rho E)} = \frac{1}{\rho}p_e \tag{A.11}$$

where

$$p_e = \frac{\partial p}{\partial e}\Big|_\rho \quad \text{and} \quad p_\rho = \frac{\partial p}{\partial \rho}\Big|_e \,. \tag{A.12}$$

Evaluation of the flux Jacobian, eq. (A.1), yields:

$$A = \begin{bmatrix} 0 & 1 & 0 & 0 \\ p_\rho - u^2 + \frac{p_e}{\rho}\left(\frac{q^2}{2} - e\right) & u\left(2 - \frac{p_e}{\rho}\right) & -v\frac{p_e}{\rho} & \frac{p_e}{\rho} \\ -uv & v & u & 0 \\ u\left[p_\rho - H + \frac{p_e}{\rho}\left(\frac{q^2}{2} - e\right)\right] & H - u^2\frac{p_e}{\rho} & -uv\frac{p_e}{\rho} & u\left(1 + \frac{p_e}{\rho}\right) \end{bmatrix}. \tag{A.13}$$

REFERENCES

1. Jameson, A., "Successes and Challenges in Computational Aerodynamics," AIAA Paper 87-1184, June 1987.

2. Anderson, J. D., "A Survey of Modern Research in Hypersonic Aerodynamics," AIAA Paper 84-1578, June 1984.

3. Lax, Peter D., "Weak Solutions of Nonlinear Hyperbolic Equations and Their Numerical Computation," *Communications on Pure and Applied Mathematics*, Vol. 7, pp.159-193, 1954.

4. Roe, P.L., "Characteristic Based Schemes for the Euler Equations," *Annual Review of Fluid Mechanics*, Vol. 18, pp. 337-365, 1986.

5. MacCormack, R.W., "The Effect of Viscosity in Hypervelocity Impact Cratering," Technical Paper AIAA-69-354, 1969.

6. Grossman, B. and Walters, R. W., "Flux-Split Algorithms for the Multi-Dimensional Euler Equations with Real Gases," *Computers and Fluids*, Vol. 17, No. 1, pp. 99-112, 1989.

7. Moretti, G., Grossman, B., Marconi, F., "A Complete Numerical Technique for the Calculation of Three-Dimensional Inviscid Supersonic Flows," AIAA Paper No. 72-192, Jan. 1972.

8. Kutler, P., Reinhardt, W.A., and Warming, R.F., "Multishocked, Three-Dimensional Supersonic Flowfields with Real Gas Effects," *AIAA J.*, Vol. 11, No. 4, pp.657-664, 1973.

9. Warming, R.F. and Beam, R.M., "Upwind Second-Order Difference Schemes and Applications in Aerodynamic Flows," *AIAA Journal*, Vol. 14, No. 9, pp.1241-1249, September 1976.

10. Moretti, G., "Computation of Flows with Shocks," *Ann. Rev. of Fluid Mech.*, Vol. 19, pp. 313-37, 1987.

11. Walters, R.W. and Thomas, J.L., "Advances in Upwind Relaxation Methods," *State of the Art Surveys in Computational Mechanics*, Chapter 4, ASME special publication, A.K. Noor, Ed., 1987.

12. Lax, Peter D., "Hyperbolic Systems of Conservation Laws and the Mathematical Theory of Shock Waves," Regional Conference Series in Applied Mathematics, Courant Institute of Mathematical Sciences, New York University, 1973.

13. Steger, J.L. and Warming, R.F., "Flux Vector Splitting of the Inviscid Gas Dynamics Equations with Applications to Finite Difference Methods," *Journal of Computational Physics*, Vol. 40, pp. 263-293, 1981.

14. Van Leer, B., Thomas, J.L., Roe, P.L., and Newsome, R.W., "A Comparison of Numerical Flux Formulas for the Euler and Navier-Stokes Equations," AIAA Paper 87-1104, June 1987.

15. Godunov, S.K., "Finite-Difference Method for Numerical Computation of Discontinuous Solutions of the Equations of Fluid Dynamics," *Mat. Sbornik*, Vol. 47, pp. 271-306, 1959. (In Russian).

16. Osher, S., "Riemann Solvers, the Entropy Condition and Difference Approximations," *SIAM J. of Num. Anal.*, Vol. 21, pp. 217-235, 1984.

17. Harten, A., Lax, P.D., and Van Leer, B., "On Upstream Differencing and Godunov-Type Schemes for Hyperbolic Conservation Laws," *SIAM Review*, Vol 25., pp. 35-61, 1983.

18. Van Leer, B., "On the Relation Between the Upwind-Differencing Schemes of Godunov, Engquist-Osher, and Roe," *SIAM J. of Scientific and Statistical Computations*, Vol. 5, No. 1, March 1984.

19. Roe, P.L., "Approximate Riemann Solvers, Parameter Vectors and Difference Schemes," *Journal of Computational Physics*, Vol. 43, pp. 357-372, 1981.

20. Roe, P.L., "A Basis for Upwind Differencing of the Two-Dimensional Unsteady Euler Equations," Proceedings of CFD Conference, Reading University, April 1985.

21. Colella, P. and Woodward, P.R., "The Piecewise Parabolic Method (PPM) for Gas-Dynamical Simulations," *J. of Comp. Physics*, Vol. 54, pp. 174-201, 1984.

22. Chakravarthy, S.R., "Relaxation Methods for Unfactored Implicit Upwind Schemes," AIAA Paper 84-0165, Jan. 1984.

23. Van Leer, B., "Flux-Vector Splitting for the Euler Equations," ICASE Report 82-30, September 1982, also in *Lecture Notes in Physics*, Vol. 170, pp. 507-512, 1982.

24. Anderson, W.K., Thomas, J.L. and Van Leer, B., "A Comparison of Finite Volume Flux Vector Splittings for the Euler Equations", AIAA Paper 85-0122, January 1985.

25. Grossman, B. and Walters, R. W., "An Analysis of Flux-Split Algorithms for Euler's Equations with Real Gases," AIAA Paper 87-1117-CP, June 1987.

26. Liou, M.S., Van Leer, B. and Shuen, J.S., "Splitting of Inviscid Fluxes for Real Gases," NASA TM 100856, April 1988.

27. Vinokur, M. and Liu, Y., "Equilibrium Gas Flow Computations II: An Analysis of Numerical Formulations of Conservation Laws," AIAA Paper 88-0127, January 1988.

28. Glaister, P., "An Approximate Linearised Riemann Solver for the Euler Equations for Real Gases," *J. Comp. Phys.*, Vol. 74, 1988, pp. 382-408.

29. Montagne, J.L., "Use of an Upwinded Scheme for Simulating Non Viscous Flows of Real Gas at Equilibrium," La Recherche Aerospatiale, Dec. 1986.

30. Srinivasan, S., Tannehill, J.C. and Weilmuenster, K.J., "Simplified Curve Fits for the Thermodynamic Properties of Equilibrium Air," NASA Ref. Pub. 1181, August 1987.

31. Gordon, S. and McBride, B.J., "Computer Program for Calculation of Complex Chemical Equilibrium Compositions, Rocket Performance, Incident and Reflected Shocks, and Chapman-Jouget Detonations," NASA SP-273, 1971.

32. Viviand, H., "Conservation Forms of Gas Dynamic Equations," *La Recherche Aerospatiale*, No. 1, pp. 65-68, Jan.-Feb., 1974.

33. Thomas, J.L., Van Leer, B. and Walters, R.W., "Implicit Flux-Split Schemes for the Euler Equations," AIAA Paper No. 85-1680, July 1985.

34. Colella, P. and Glaz, H., "Efficient Solution Algorithm for the Riemann Problem for Real Gases," *J. Comp. Phys.*, Vol. 59, pp. 264-289, 1985.

35. Vinokur, M., "An Analysis of Finite-Difference and Finite-Volume Formulations of Conservation Laws," NASA CR-177416, June 1986.

36. Roe, P., and Pike, J., "Efficient Construction and Utilisation of Approximate Riemann Solutions," in *Computing Methods in Applied Science and Engineering VI*, edited by R. Glowinski and J.-L. Lions (North-Holland, Amsterdam, 1984), p.499.

37. Hanel, D. and Schwane, R., "An Implicit Flux-Vector Splitting Scheme for the Computation of Viscous Hypersonic Flow," AIAA Paper 89-0274, January, 1989.

38. Harten, A., "High Resolution Schemes for Hyperbolic Conservation Laws," *J. Comput. Phys.*, Vol. 50, p.235, 1983.

FIGURES

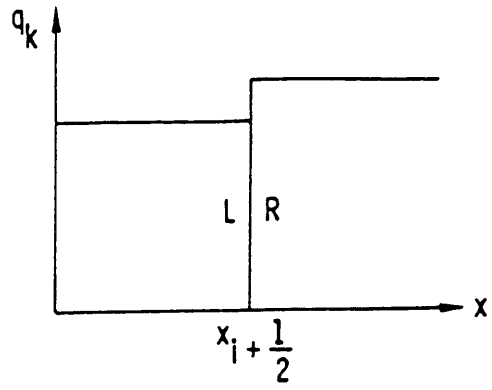

a) Uniform left and right states

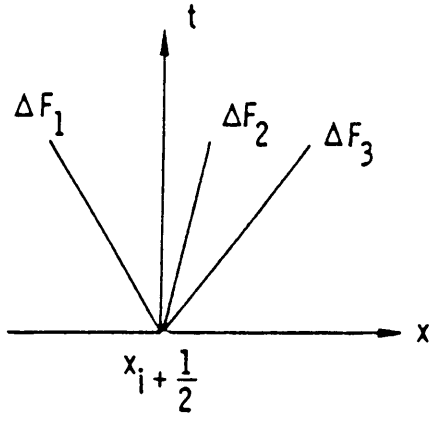

b) Waves resulting from the breakup of the discontinuity

Figure 1. Schematic of the Riemann problem

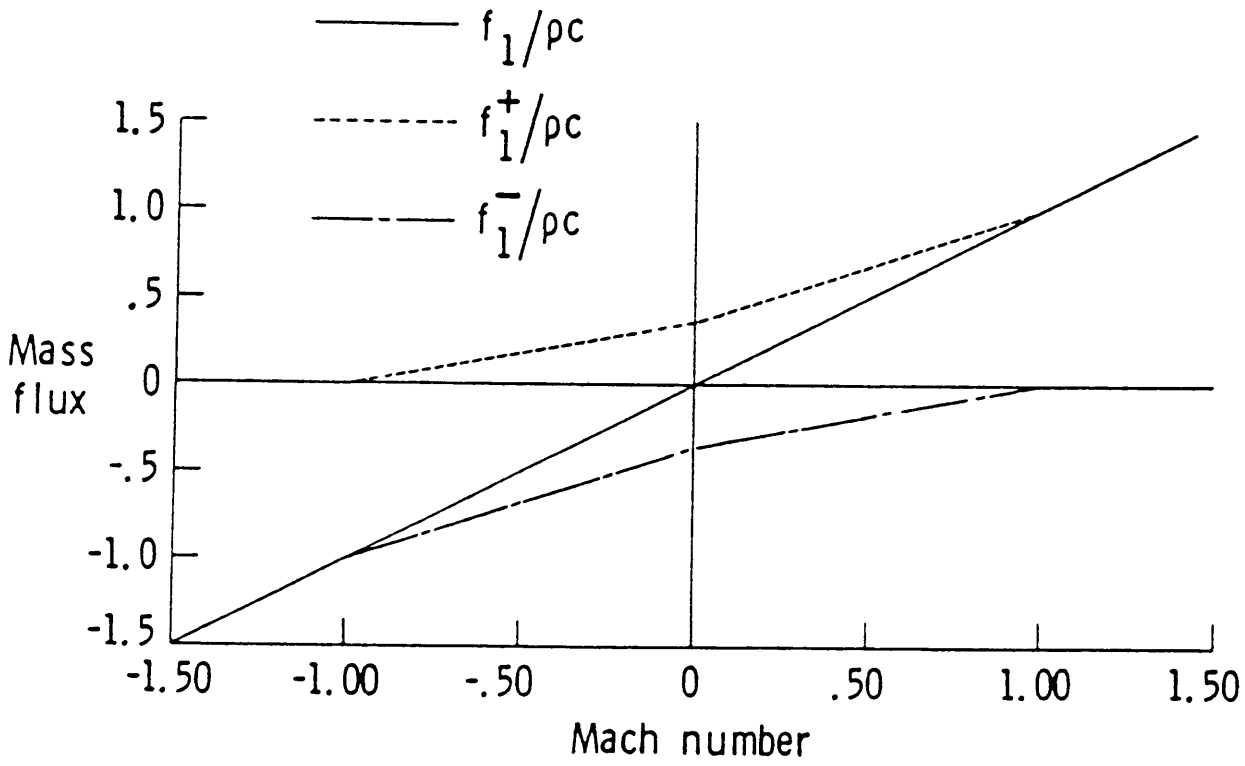

Figure 2. Variation of Steger-Warming split mass flux with Mach number

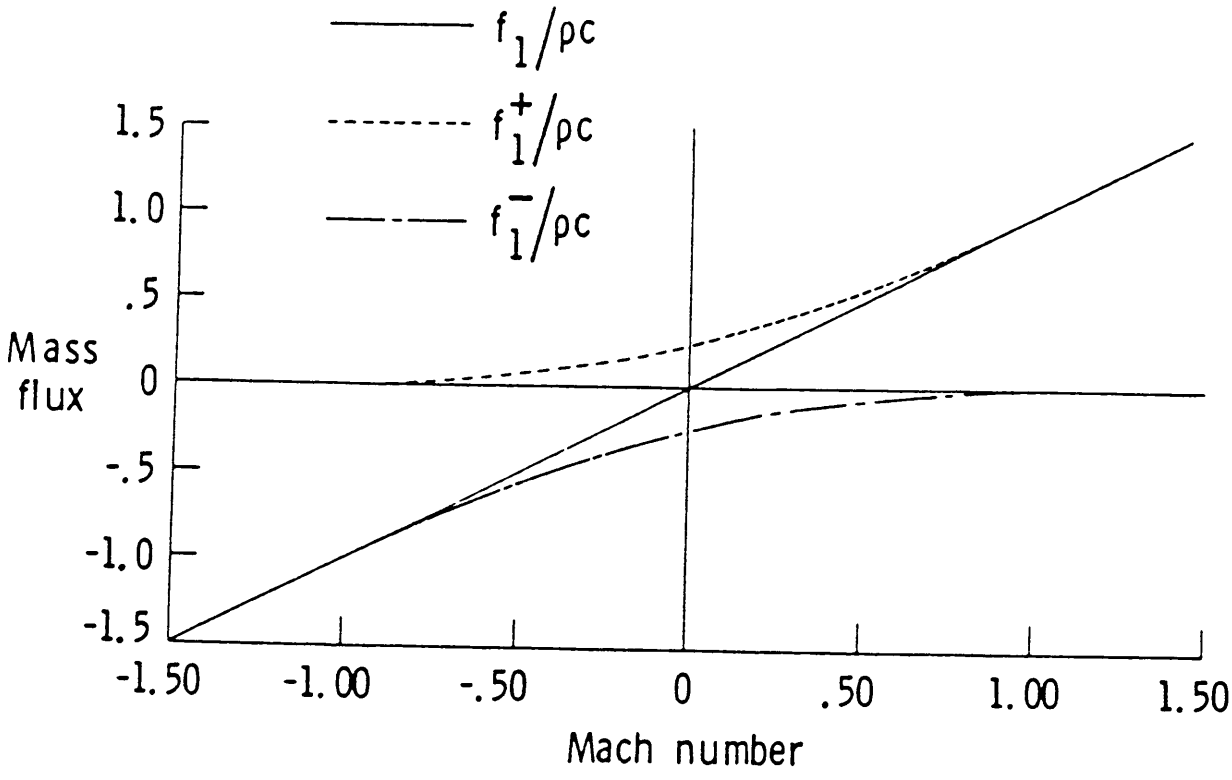

Figure 3. Variation of Van Leer split mass flux with Mach number

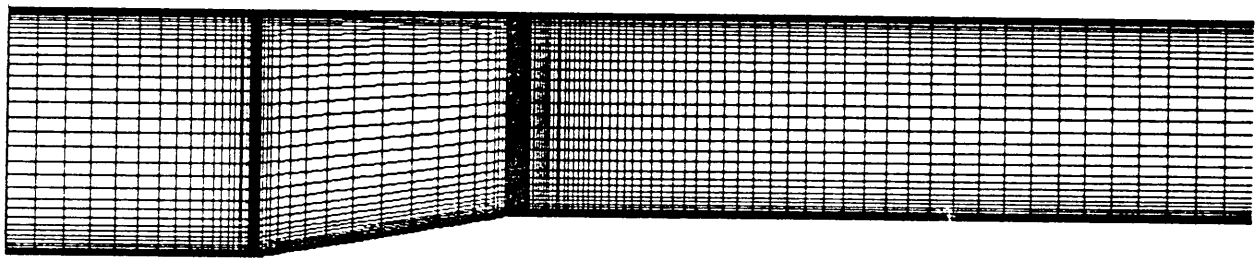

Figure 4. Structured mesh for the supersonic inlet problem: 10° compression followed by a 10° expansion. 201 grid points in the axial direction, 51 grid points in the normal direction.

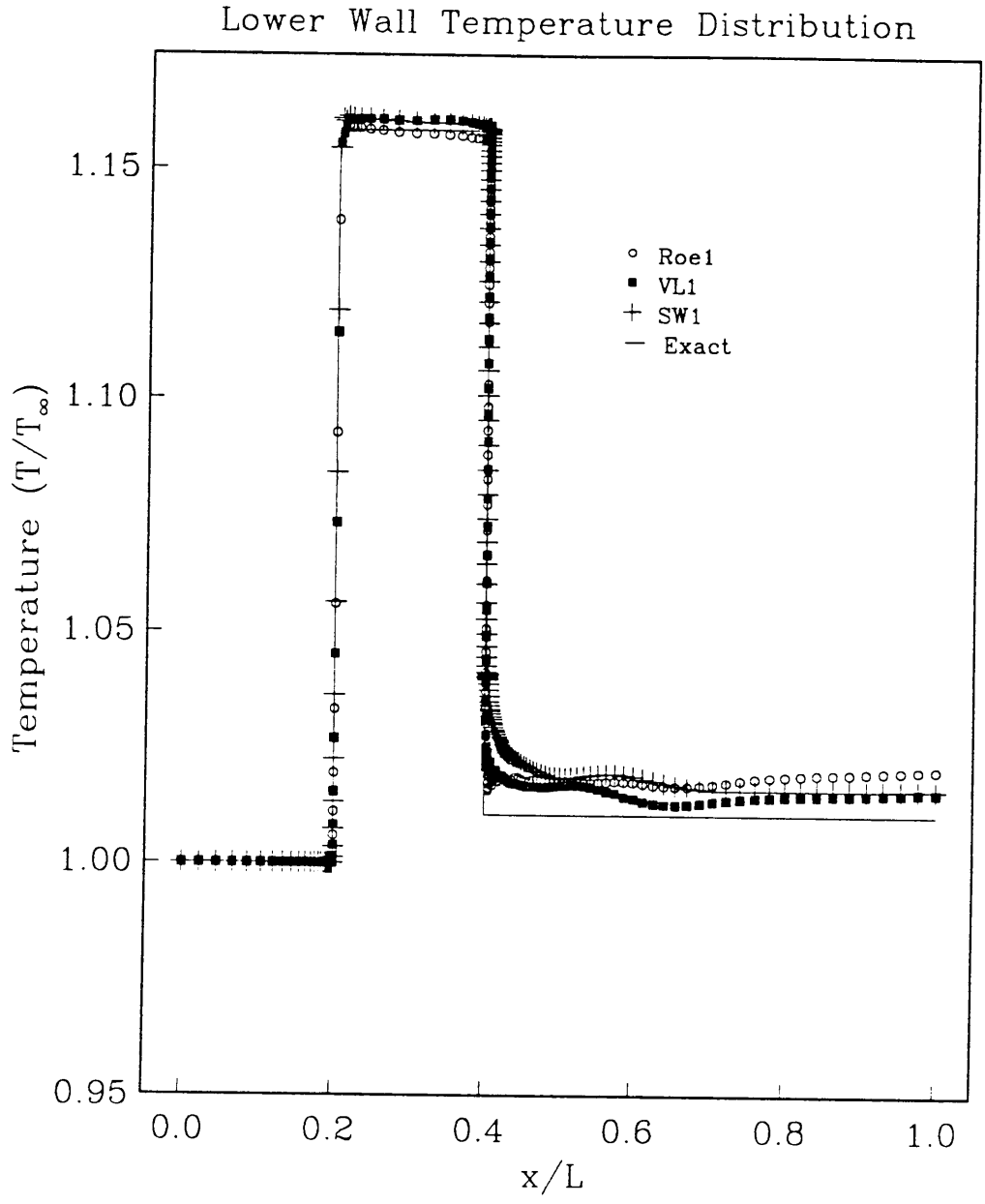

Figure 5. Surface temperature distribution for the supersonic inlet problem: The inlet conditions are $M_\infty = 5.0$, $p_\infty = 1$atm., and $T_\infty = 3573°K$. Comparison of the Steger-Warming-type flux-vector split scheme, the Van Leer-type flux-vector split scheme, and the Roe-type flux-difference split scheme of Grossman and Walters [25].

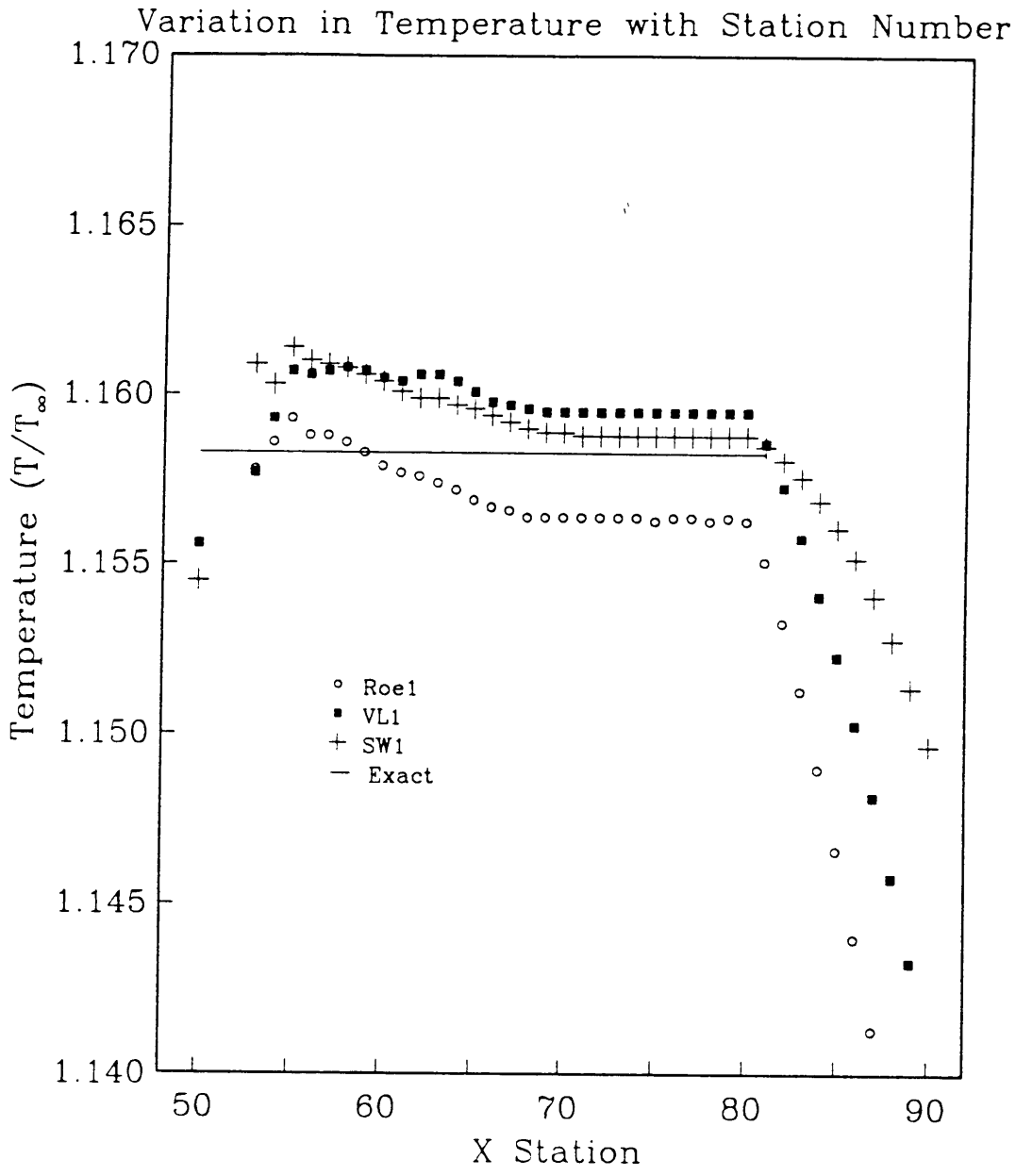

Figure 6. Compression surface temperature distribution for the supersonic inlet problem in Fig. 5 using expanded scales.

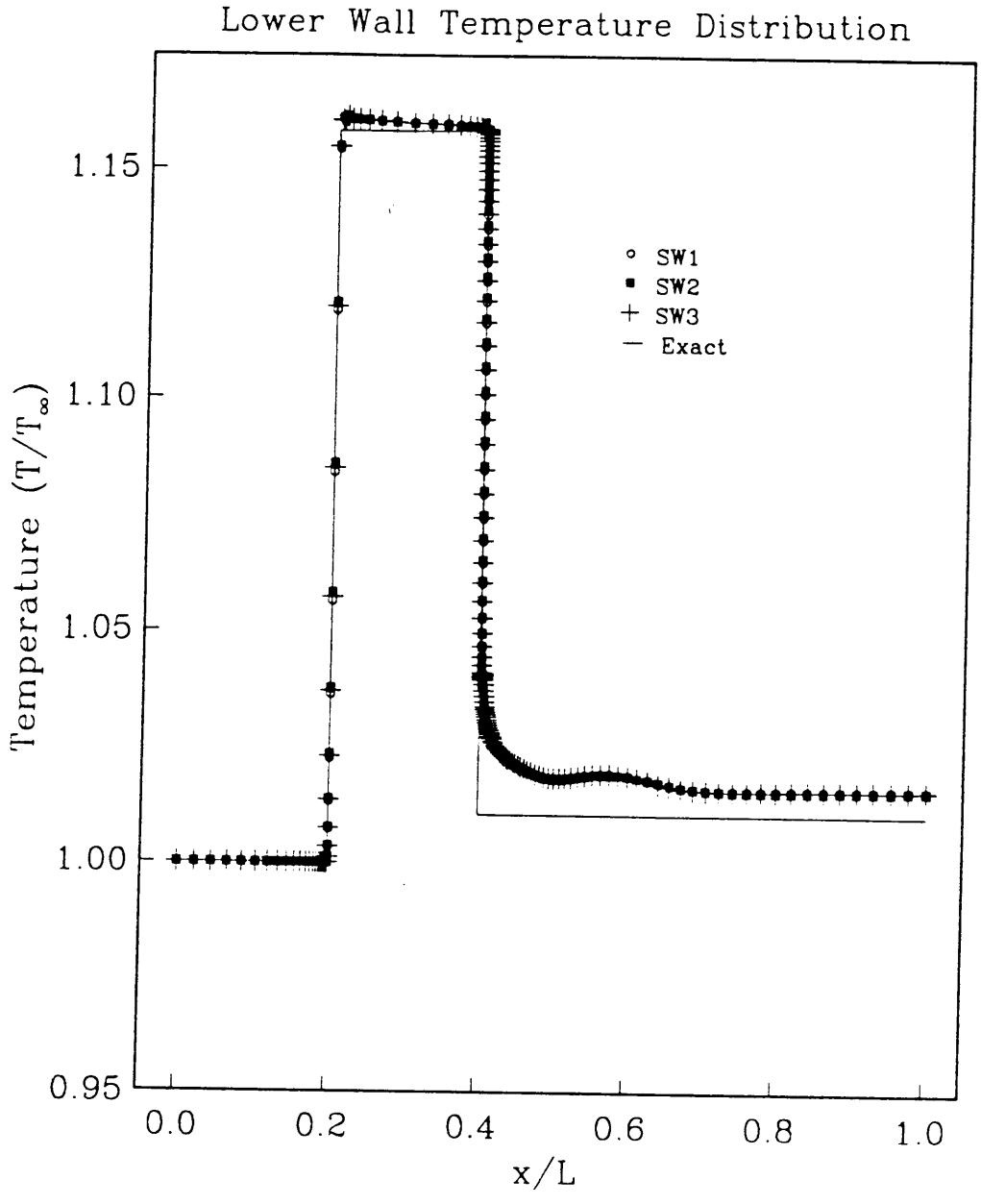

Figure 7. Surface temperature distribution for the supersonic inlet problem in Fig. 5 comparing various Steger-Warming-type flux-vector split schemes: SW1: Grossman and Walters [25], SW2: Liou, Van Leer, and Shuen [26], SW3: Vinokur and Liu [27].

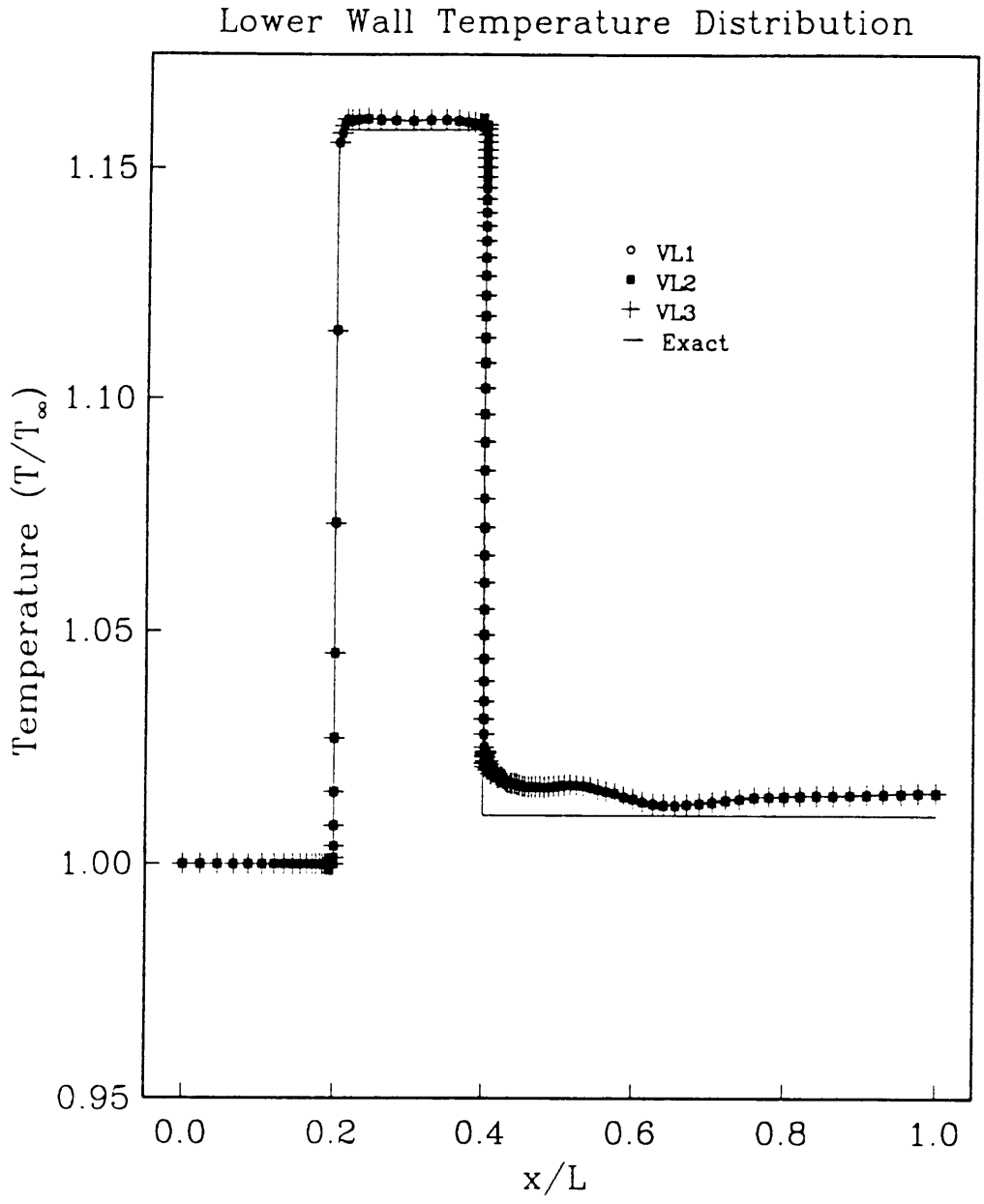

Figure 8. Surface temperature distribution for the supersonic inlet problem in Fig. 5 comparing various Van Leer-type flux-vector split schemes: VL1: Grossman and Walters [25], VL2: Liou, Van Leer, and Shuen [26], VL3: Vinokur and Liu [27].

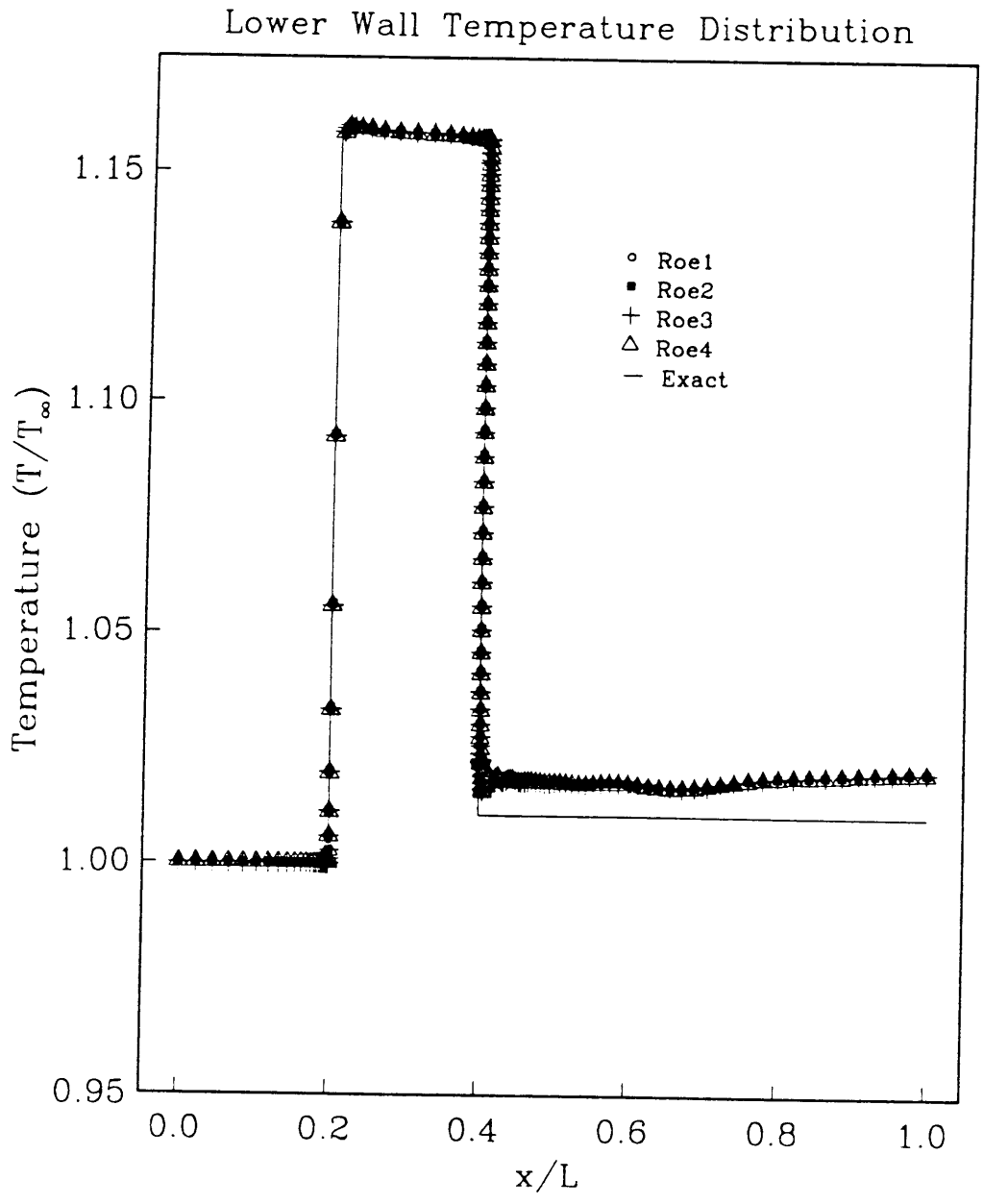

Figure 9. Surface temperature distribution for the supersonic inlet problem in Fig. 5 comparing various Roe-type flux-difference split schemes: Roe1: Grossman and Walters [25], Roe2: Liou, Van Leer, and Shuen [26], Roe3: Vinokur and Liu [27], Roe4: Glaister [28].

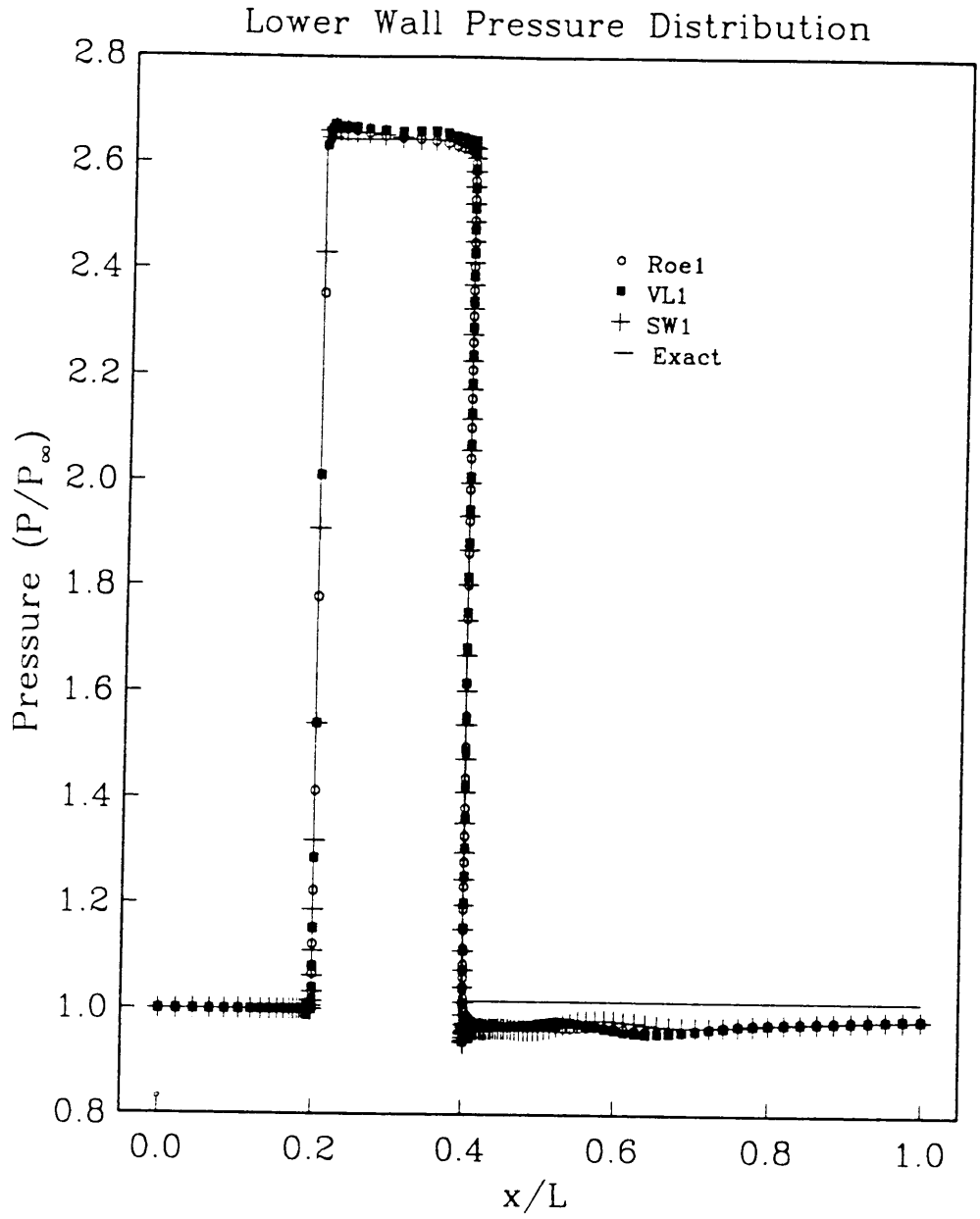

Figure 10. Surface pressure distribution for the supersonic inlet problem: The inlet conditions are $M_\infty = 5.0$, $p_\infty = 1$atm., and $T_\infty = 3573°K$. Comparison of the Steger-Warming-type flux-vector split scheme, the Van Leer-type flux-vector split scheme, and the Roe-type flux-difference split scheme of Grossman and Walters [25].

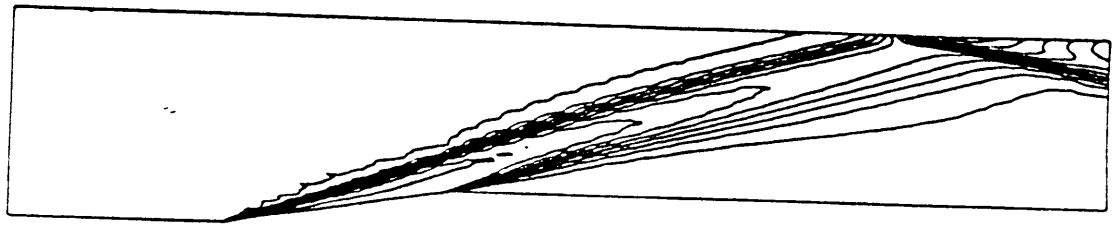

Figure 11. Temperature contour for the supersonic inlet problem in Fig. 5

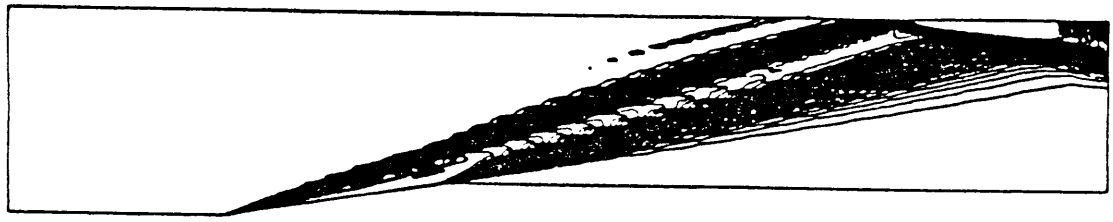

Figure 12. Pressure contour for the supersonic inlet problem in Fig. 5

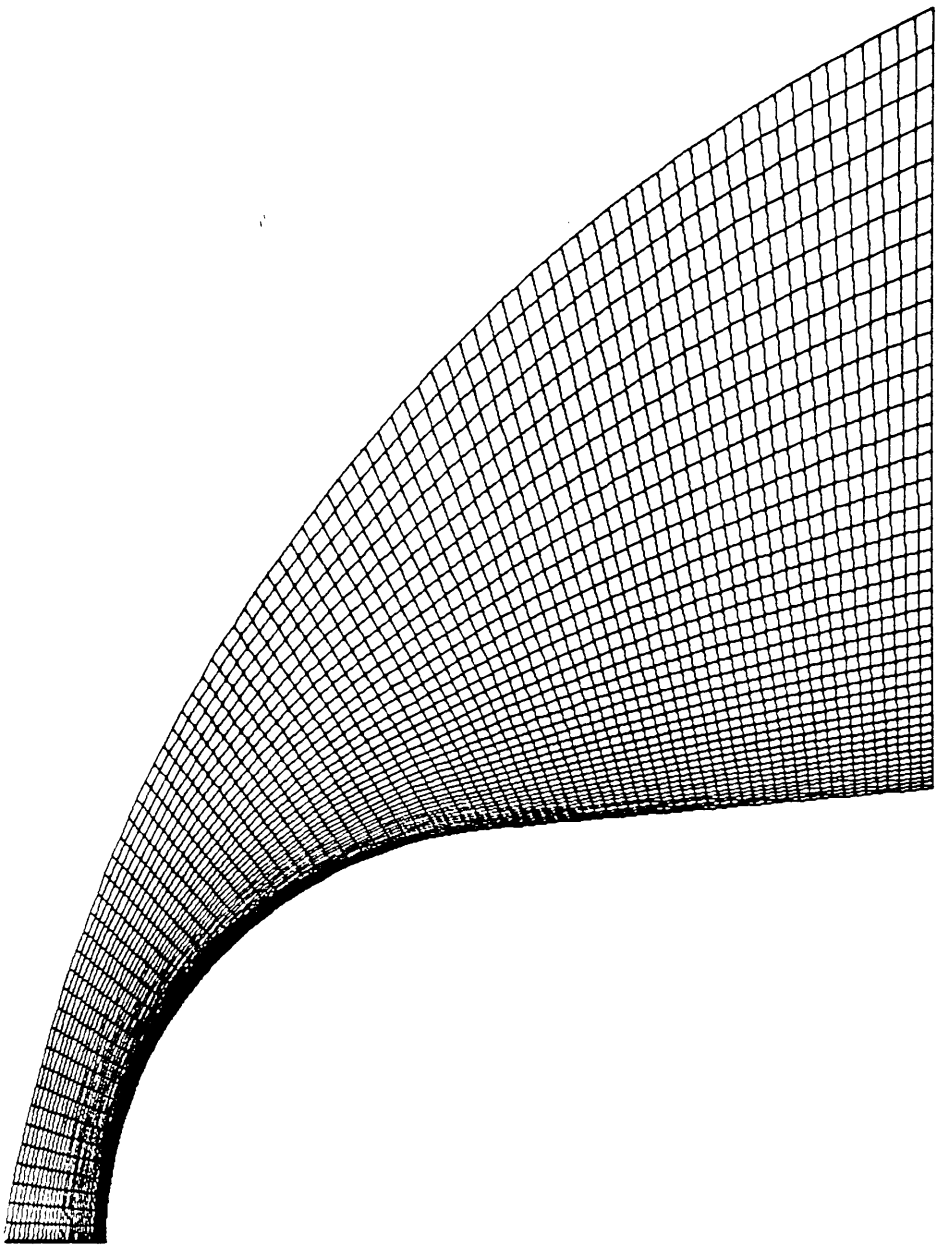

Figure 13. Structured mesh for the hypersonic blunt body problem: Cylindrical nose followed by a 5° compression ramp. 81 grid points parallel and 41 grid points normal to the body.

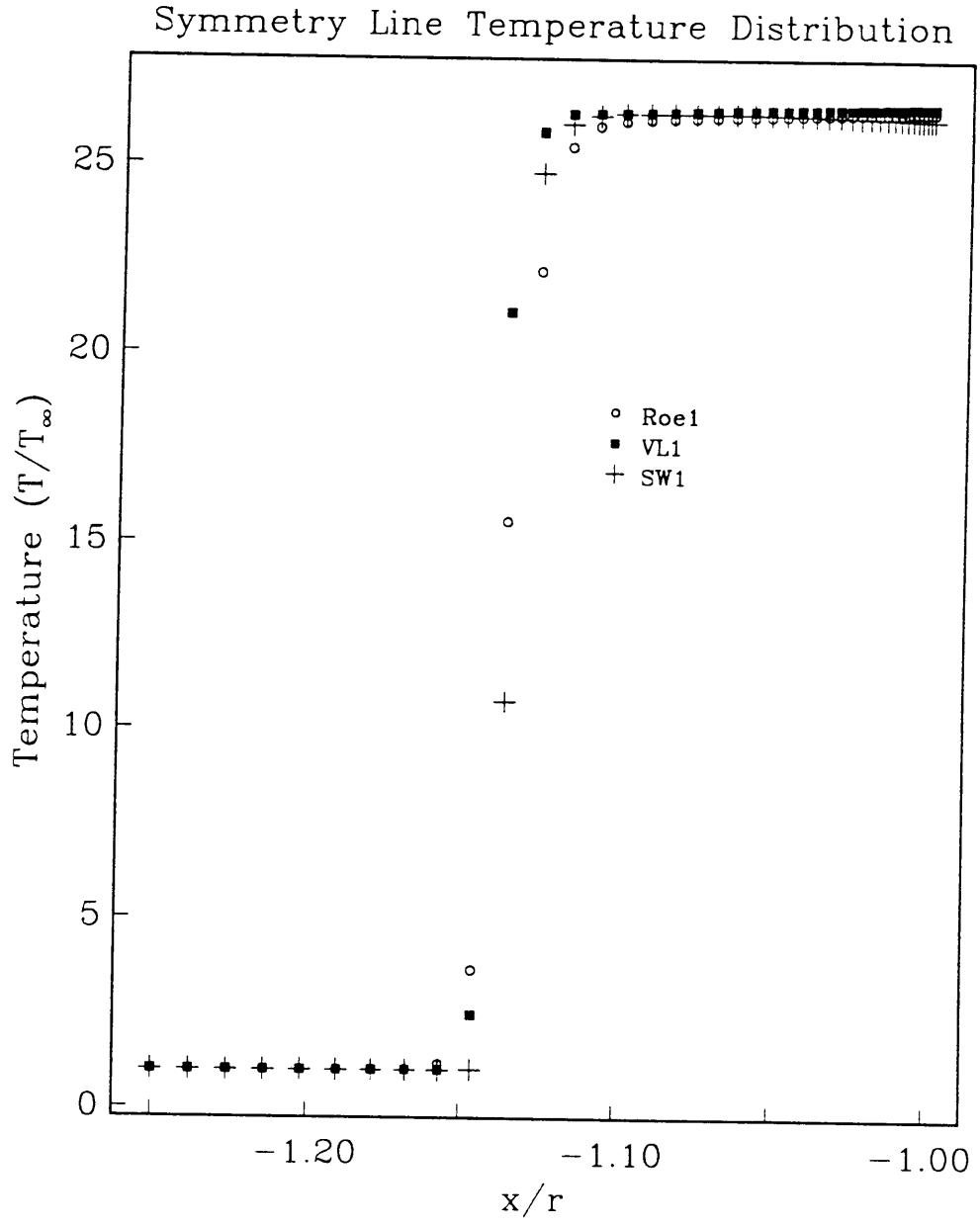

Figure 14. Symmetry line temperature distribution for the hypersonic blunt body problem: The inlet conditions are $M_\infty = 24.5$, $p_\infty = 51.63$pa., and $T_\infty = 268.57$°K. Comparison of the Steger-Warming-type flux-vector split scheme, the Van Leer-type flux-vector split scheme, and the Roe-type flux-difference split scheme of Grossman and Walters [25].

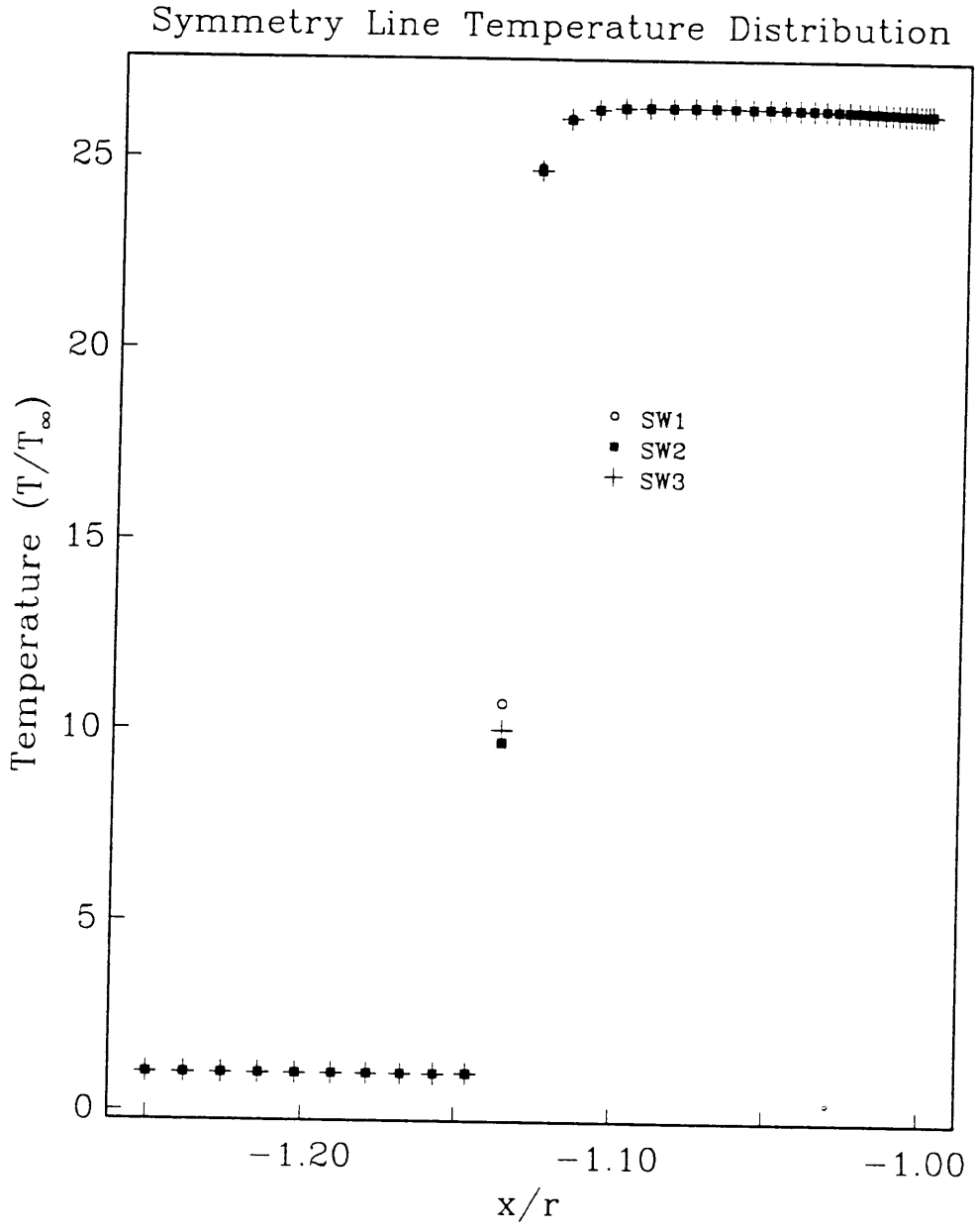

Figure 15. Symmetry line temperature distribution for the hypersonic blunt body problem in Fig. 14 comparing various Steger-Warming-type flux-vector split schemes: SW1: Grossman and Walters [25], SW2: Liou, Van Leer, and Shuen [26], SW3: Vinokur and Liu [27].

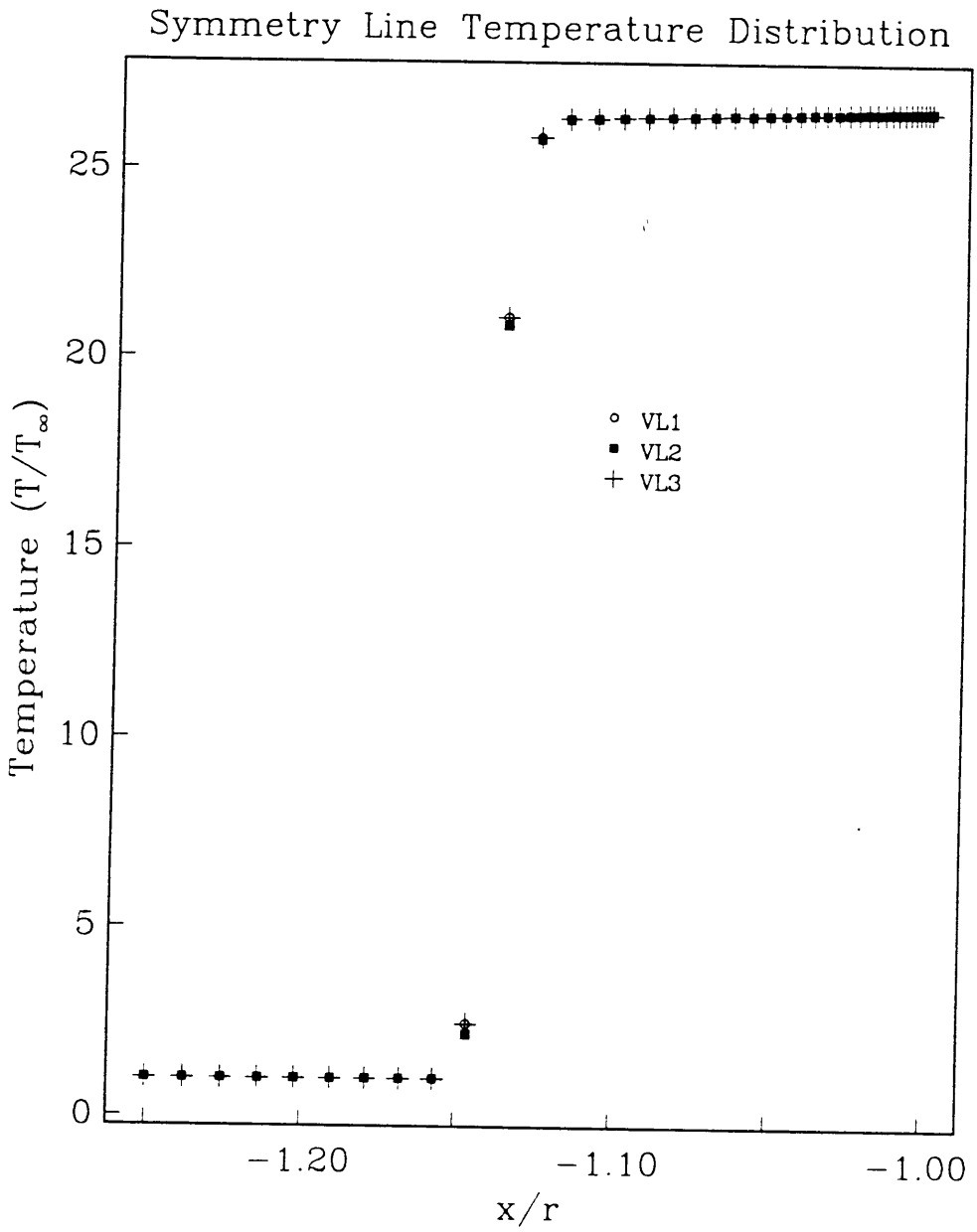

Figure 16. Symmetry line temperature distribution for the hypersonic blunt body problem in Fig. 14 comparing various Van Leer-type flux-vector split schemes: VL1: Grossman and Walters [25], VL2: Liou, Van Leer, and Shuen [26], VL3: Vinokur and Liu [27].

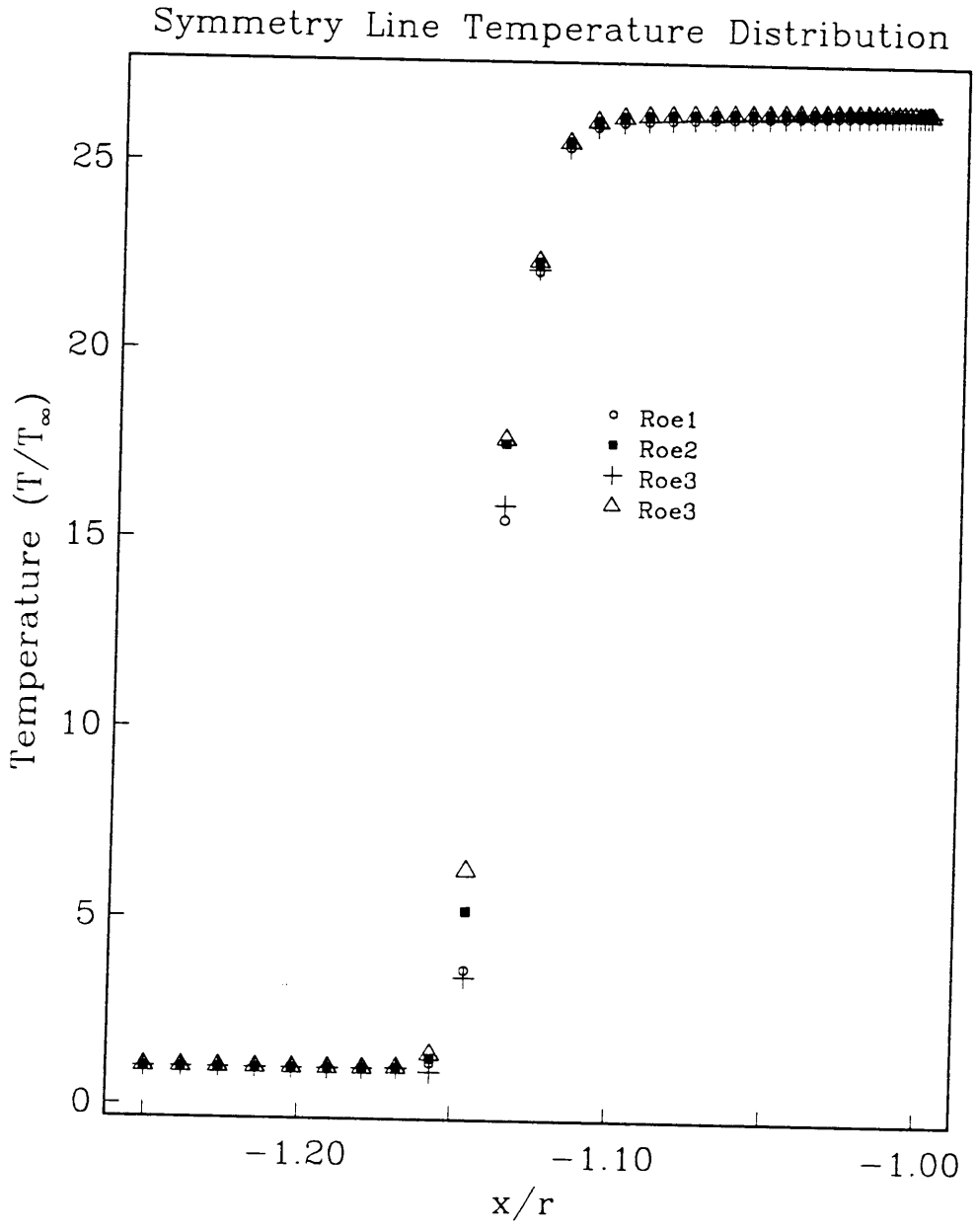

Figure 17. Symmetry line temperature distribution for the hypersonic blunt body problem in Fig. 14 comparing various Roe-type flux-difference split schemes: Roe1: Grossman and Walters [25], Roe2: Liou, Van Leer, and Shuen [26], Roe3: Vinokur and Liu [27], Roe4: Glaister [28].

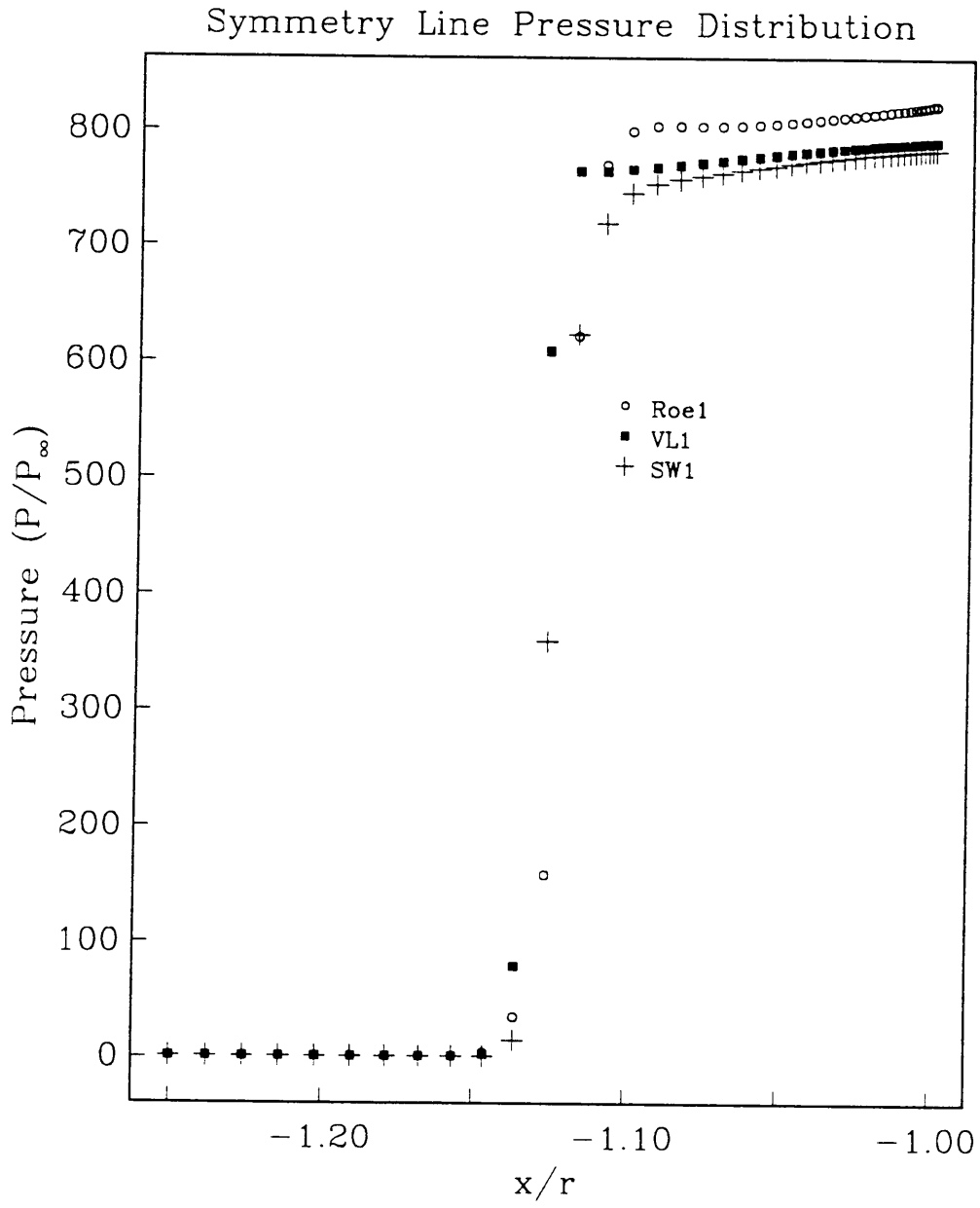

Figure 18. Symmetry line pressure distribution for the hypersonic blunt body problem: The inlet conditions are $M_\infty = 24.5$, $p_\infty = 51.63$pa., and $T_\infty = 268.57$°K. Comparison of the Steger-Warming-type flux-vector split scheme, the Van Leer-type flux-vector split scheme, and the Roe-type flux-difference split scheme of Grossman and Walters [25].

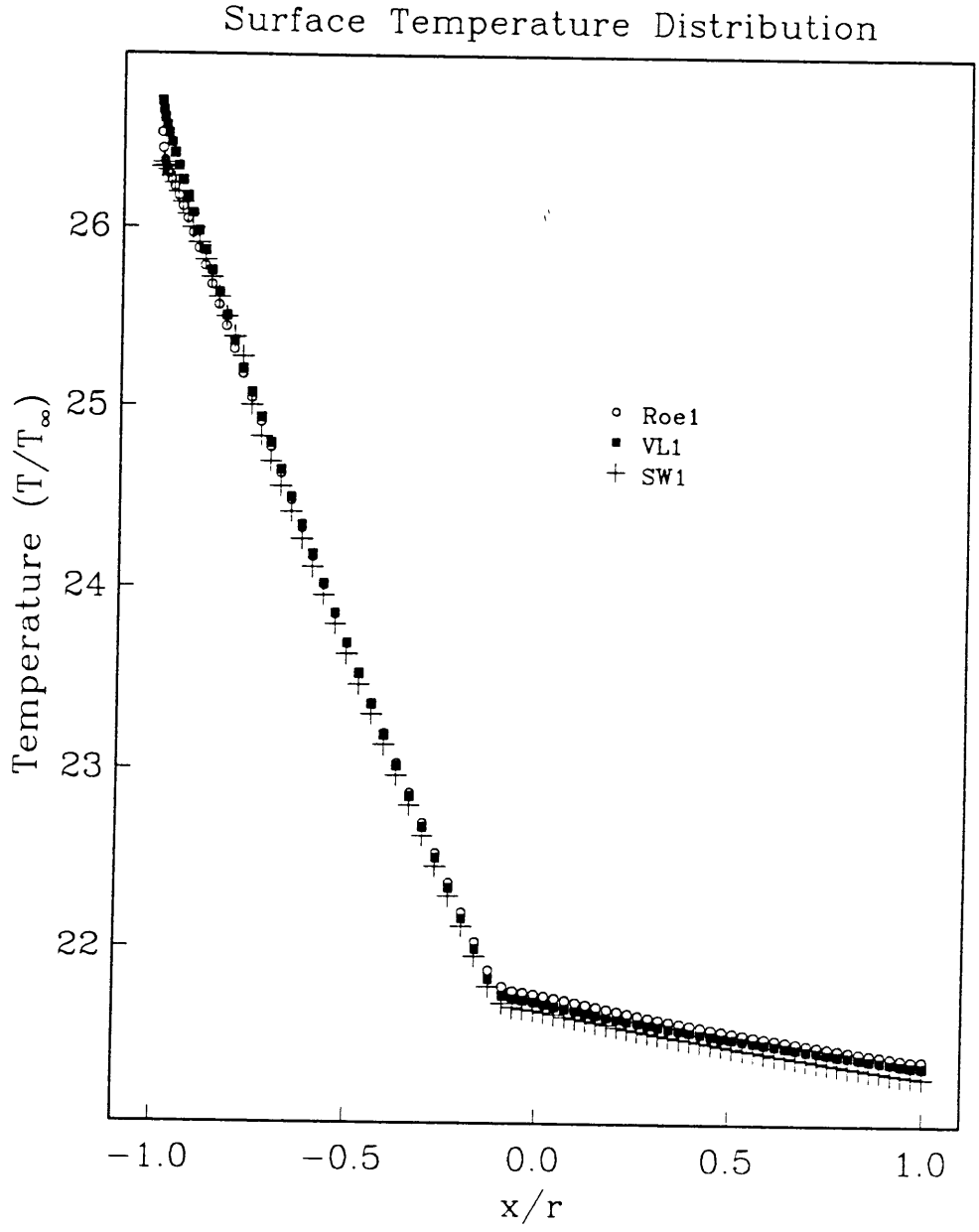

Figure 19. Surface temperature distribution for the hypersonic blunt body problem: The inlet conditions are $M_\infty = 24.5$, $p_\infty = 51.63$pa., and $T_\infty = 268.57$°K. Comparison of the Steger-Warming-type flux-vector split scheme, the Van Leer-type flux-vector split scheme, and the Roe-type flux-difference split scheme of Grossman and Walters [25].

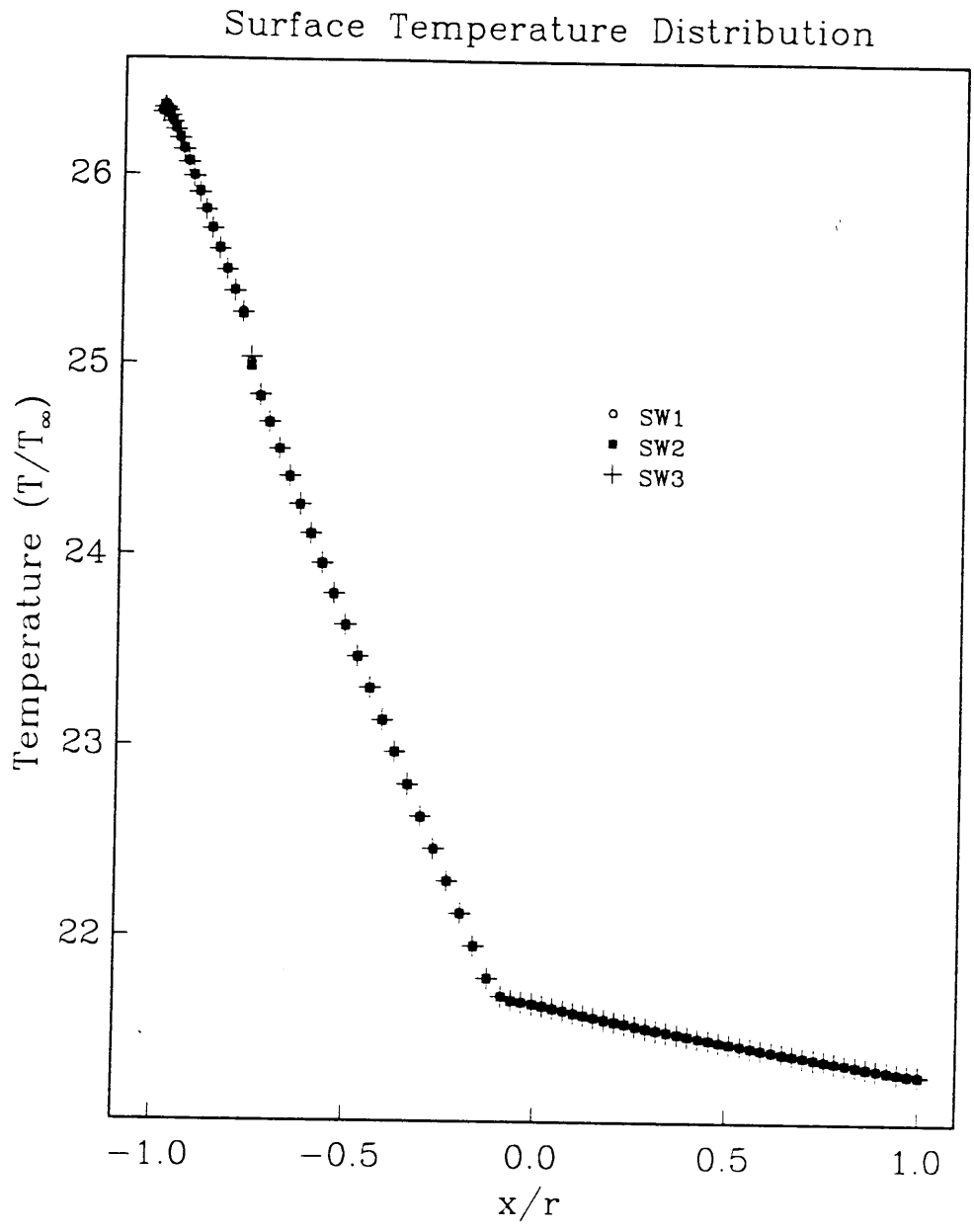

Figure 20. Surface temperature distribution for the hypersonic blunt body problem in Fig. 19 comparing various Steger-Warming-type flux-vector split schemes: SW1: Grossman and Walters [25], SW2: Liou, Van Leer, and Shuen [26], SW3: Vinokur and Liu [27].

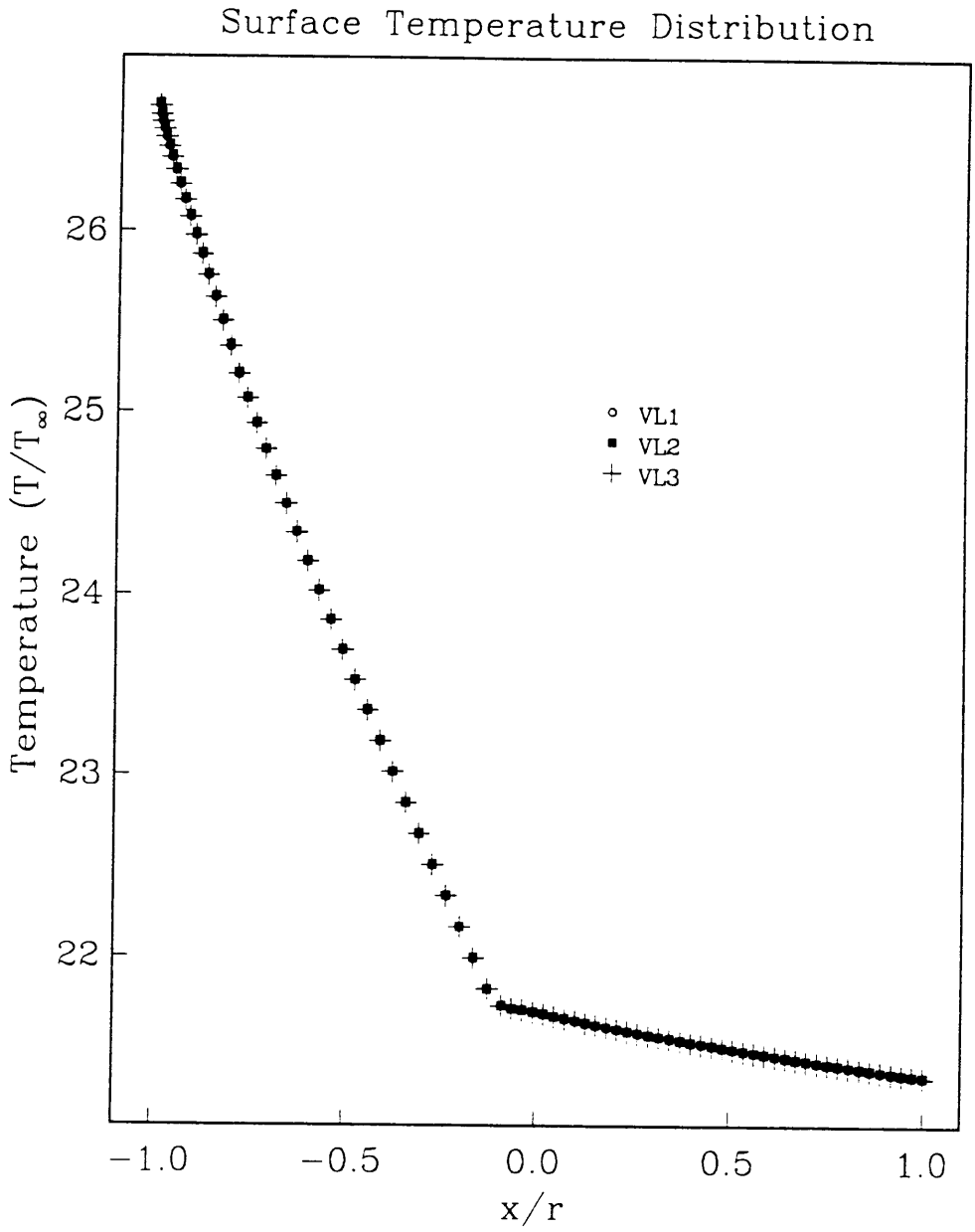

Figure 21. Surface temperature distribution for the hypersonic blunt body problem in Fig. 19 comparing various Van Leer-type flux-vector split schemes: VL1: Grossman and Walters [25], VL2: Liou, Van Leer, and Shuen [26], VL3: Vinokur and Liu [27].

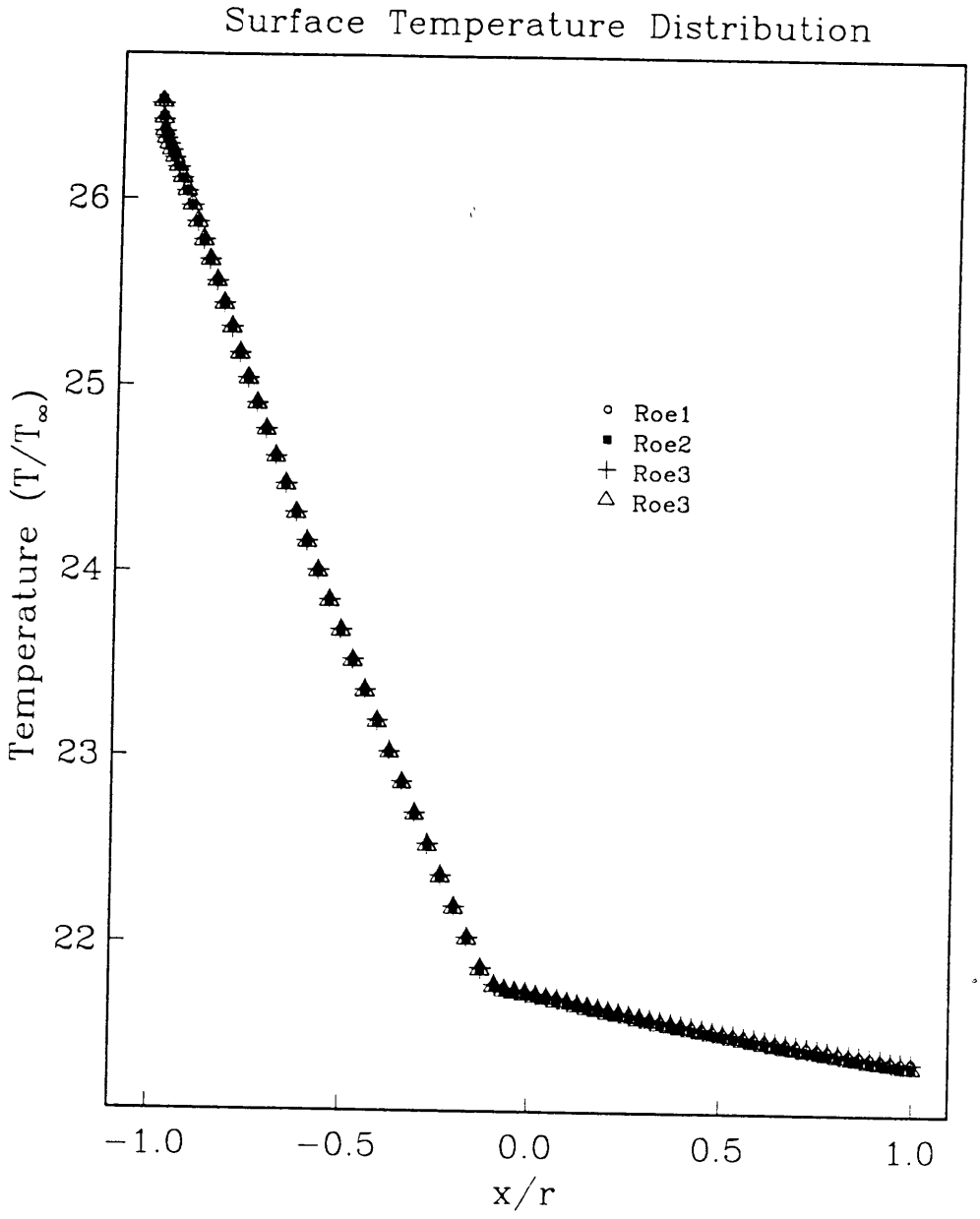

Figure 22. Surface temperature distribution for the hypersonic blunt body problem in Fig. 19 comparing various Roe-type flux-difference split schemes: Roe1: Grossman and Walters [25], Roe2: Liou, Van Leer, and Shuen [26], Roe3: Vinokur and Liu [27], Roe4: Glaister [28].

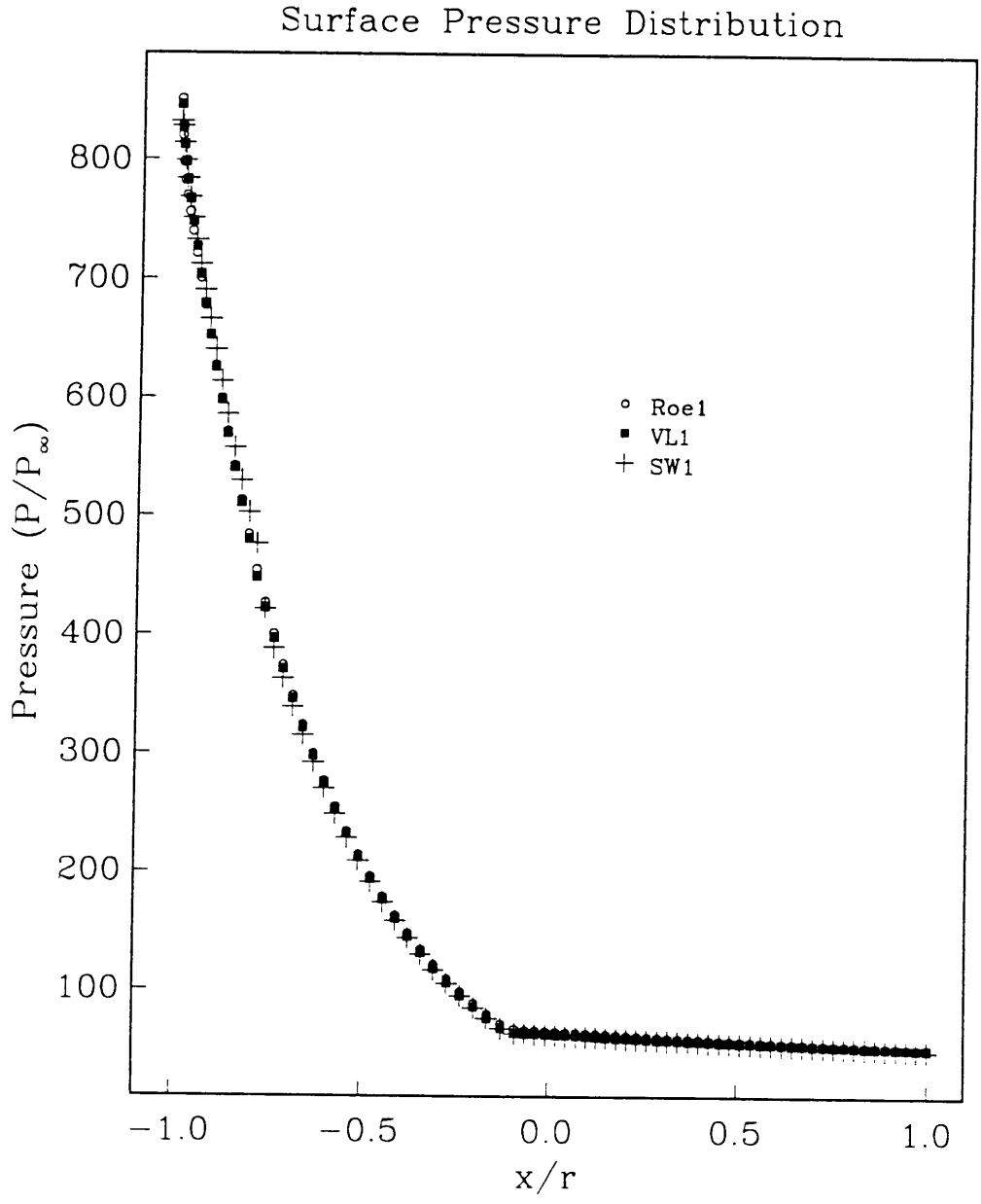

Figure 23. Surface pressure distribution for the hypersonic blunt body problem: The inlet conditions are $M_\infty = 24.5$, $p_\infty = 51.63$pa., and $T_\infty = 268.57$°K. Comparison of the Steger-Warming-type flux-vector split scheme, the Van Leer-type flux-vector split scheme, and the Roe-type flux-difference split scheme of Grossman and Walters [25].

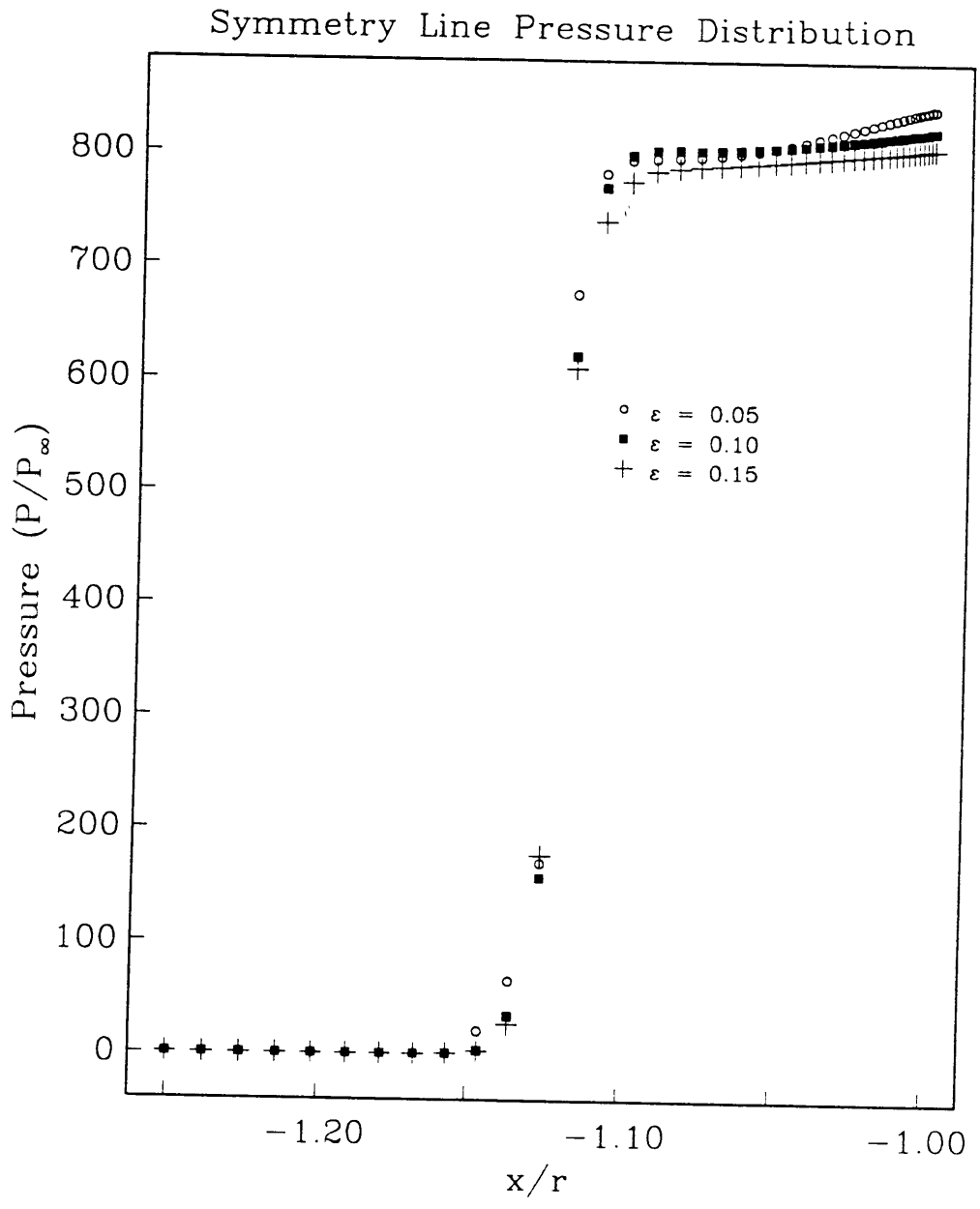

Figure 24. Symmetry line pressure distribution for the hypersonic blunt body problem in Fig. 19 comparing three values of epsilon for the Roe1 scheme [6,25]

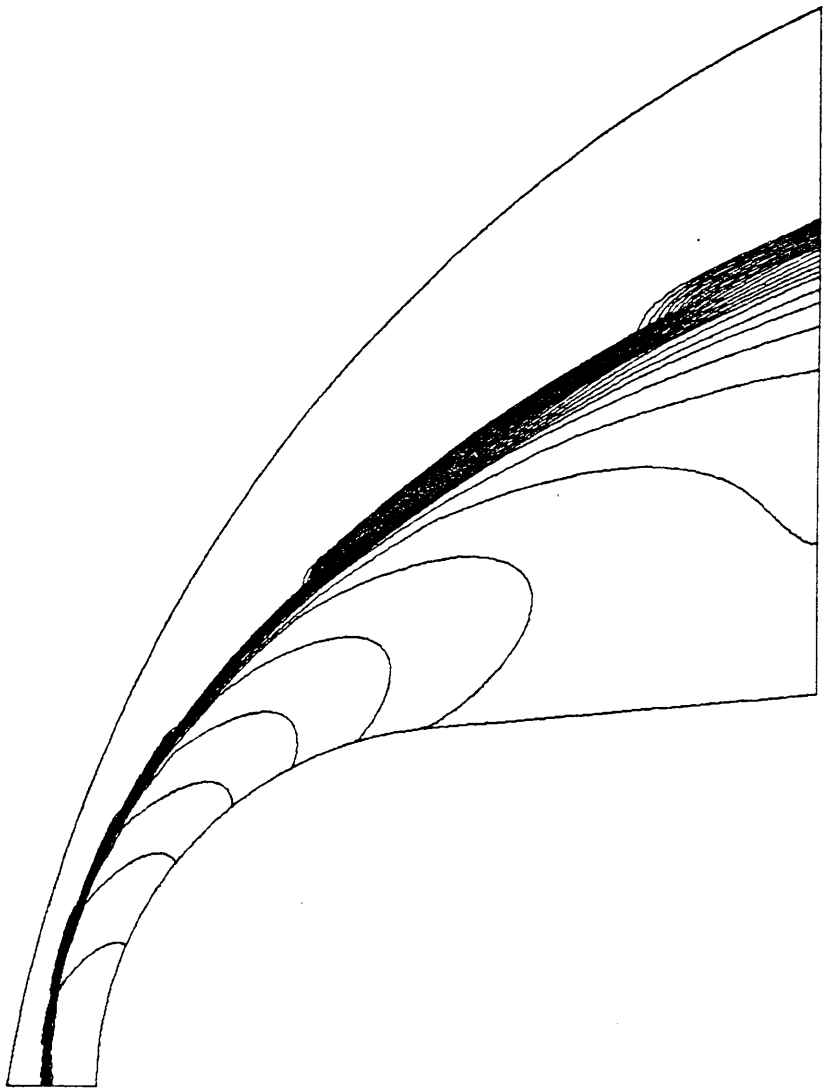

Figure 25. Temperature contour for the hypersonic blunt body problem in Fig. 14

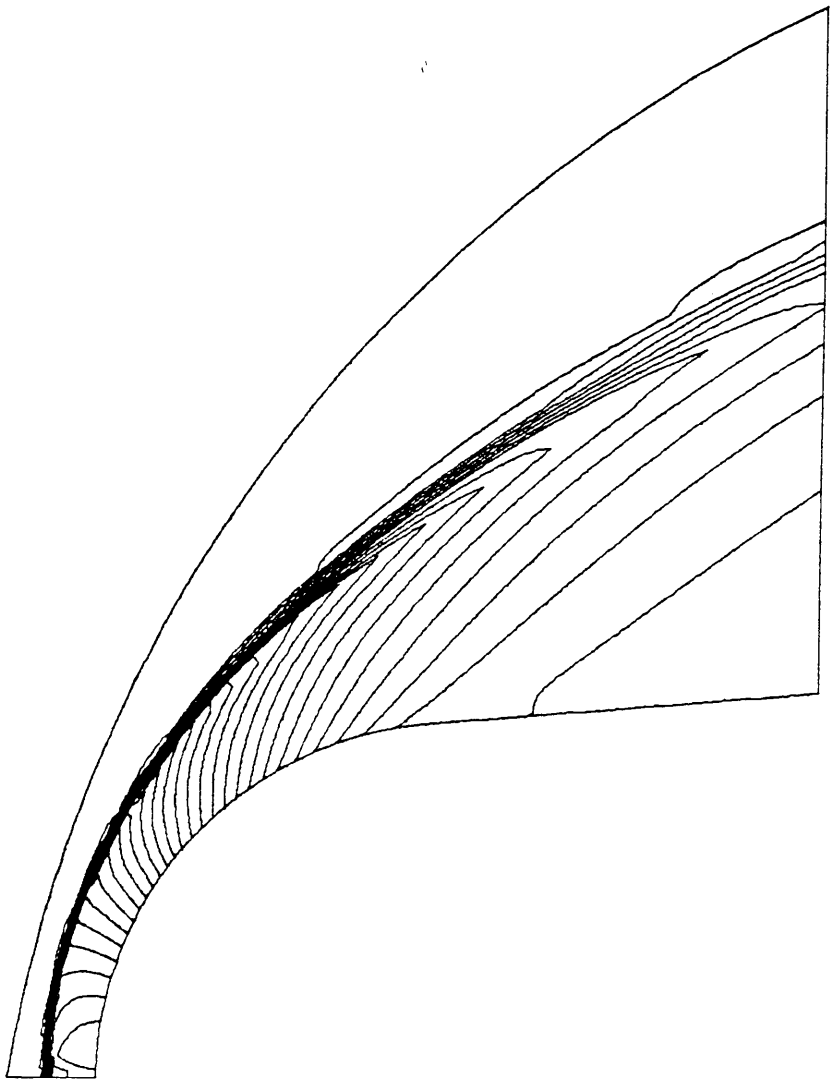

Figure 26. Pressure contour for the hypersonic blunt body problem in Fig. 14

The vita has been removed from the scanned document